1-1-2013

Squeeze Flow of Highly Concentrated Suspensions

Mohsen Nikkhoo
University of South Carolina - Columbia

SQUEEZE FLOW OF HIGHLY CONCENTRATED SUSPENSIONS

by

Mohsen Nikkhoo

Bachelor of Science
Sharif University of Technology, 2004

Master of Science
Sharif University of Technology, 2007

Submitted in Partial Fulfillment of the Requirements

For the Degree of Doctor of Philosophy in

Chemical Engineering

College of Engineering and Computing

University of South Carolina

2013

Accepted by:

Francis Gadala-Maria, Major Professor

Jamil Khan, Committee Member

Harry Ploehn, Committee Member

John Weidner, Committee Member

Lacy Ford, Vice Provost and Dean of Graduate Studies

DEDICATION

This dissertation is lovingly dedicated to my wife, Anahita. Her support, encouragement, and constant love have sustained me through my life.

ACKNOWLEDGEMENTS

I would like to gratefully and sincerely thank first my advisor, Professor Francis Gadala-Maria for guiding, teaching, and inspiring the research in this dissertation. I appreciate all his contributions of time and ideas to make my Ph.D. experience productive and stimulating.

I would like to thank my committee members, Dr. Harry Ploehn, Dr. Jamil Khan, and Dr. John Weidner for all their time, attention, and guidance.

Special thanks to my dear wife, Anahita, who was always available with endless support, unlimited encouragement, and great love. Many thanks to my parents, Nahid and Hassan, who raised an independent, driven child, and never doubted my abilities. Also, I thank Anahita's parents, Aghdas and Akbar, whose love and acceptance allowed me to believe in myself.

Each and everyone listed above and others who have not been named directly, but whose friendship remains important to me, deserve my gratitude and my admiration for supporting me through this stage of my life and career.

ABSTRACT

In this thesis we investigated through experiment and model, the anomalous normal stress distribution during constant-force squeeze flow of highly concentrated suspensions. Using pressure-sensitive films the normal stress distribution is measured in suspensions of glass spheres in a Newtonian liquid undergoing constant-force squeeze flow. At volume fractions of solids up to 0.55, the normal stress distribution is independent of volume fraction and almost identical to the parabolic pressure distribution expected for Newtonian fluids. However, at higher volume fractions, the normal stresses become an order of magnitude larger near the center and very low beyond that region. At these high volume fractions, the normal stresses decrease in the outer regions and increase in the inner regions as the squeezing proceeds. The normal stress distribution that results when the glass spheres without any fluid are subjected to squeeze flow is very similar to that for suspensions with volume fractions above 0.55, suggesting that the cause for the drastic changes in the normal stress distribution is the jamming of the particles in the suspension.

The drastic changes in the normal stress distribution are explained in terms of the radial flow migration of the liquid phase away from the center of the sample and of the jamming that results from it. Experimental measurements show that changes in the volume fraction of solids due to liquid-phase migration are found to depend on the initial volume fraction of solids, the viscosity of the suspending fluid, and the size of the particles. Under some conditions, the volume fraction of solids remains essentially

constant during the squeeze test, indicating that liquid-phase migration does not take place to any significant degree; however, under other conditions, the volume fraction of solids increases throughout the sample as the squeezing proceeds and liquid is expelled from the test region in preference to the solids. In these latter cases the concentration increases are largest toward the center of the samples. Criteria for the occurrence of liquid-phase migration in suspensions undergoing squeeze flow are discussed in terms of dimensionless groups.

Liquid-phase migration is modeled numerically by taking into account the time and position dependence of the rheological properties of the material due to the change in the volume fraction of solids. This is done by coupling the equation of motion for a non-Newtonian material that approximates a Bingham plastic with a continuity equation that includes diffusive flux. The developed model is first validated with experimental data and then used to study the effect of various parameters on pressure-induced phase separation. Changes in the volume fraction of solids within the squeezed suspensions due to liquid-phase migration were found to depend on the degree of slip at the surfaces and on the applied force as well as on the material properties.

TABLE OF CONTENTS

LIST OF TABLES

LIST OF FIGURES

CHAPTER 1

INTRODUCTION

Suspensions of solid particles in liquids are ubiquitous in industry and nature. The rheological characterization of highly concentrated suspensions and pastes is useful in predicting the processing characteristics of solder pastes, concrete, paving asphalt, bulk molding compounds, ceramic pastes, and other industrial materials. Sometimes, the final product itself is a concentrated suspension or paste, and its rheological characteristics affect its performance. Such is the case for tooth paste, diaper cream, modeling clay, etc. The rheological behavior of these suspensions depends on the particle shape, size and size distribution, volume fraction of particles, particle-particle and particle-fluid interactions, and measurement conditions such as temperature and shear rate (Gulmus and Yilmazer 2005).

The multi-phase nature of highly concentrated suspensions gives rise to complex rheological behavior as a result of particle contacts, jamming, liquid-phase migration, and shear localization (Mascia and Wilson 2007). The heterogeneities and anisotropy induced by the flow may affect the mechanical, thermal, and electrical properties of the final product (Collomb et al. 2004).

Rotational viscometers are, in general, inadequate to characterize these materials, mainly because of slip at the surfaces and exudation of the sample during testing. Squeeze flow, one of the few tests capable of generating useful rheological data for these materials, is now more frequently used. In squeeze flow the material is deformed between

two surfaces approaching each other at either a controlled velocity or under the influence of a controlled force. Figure 1.1 presents a schematic and the coordinate system for our squeeze flow tests. We denote the distance between the plates by *H* and the half-distance by *h* and use a coordinate system with the origin of the *z*-axis placed at the symmetry plane.

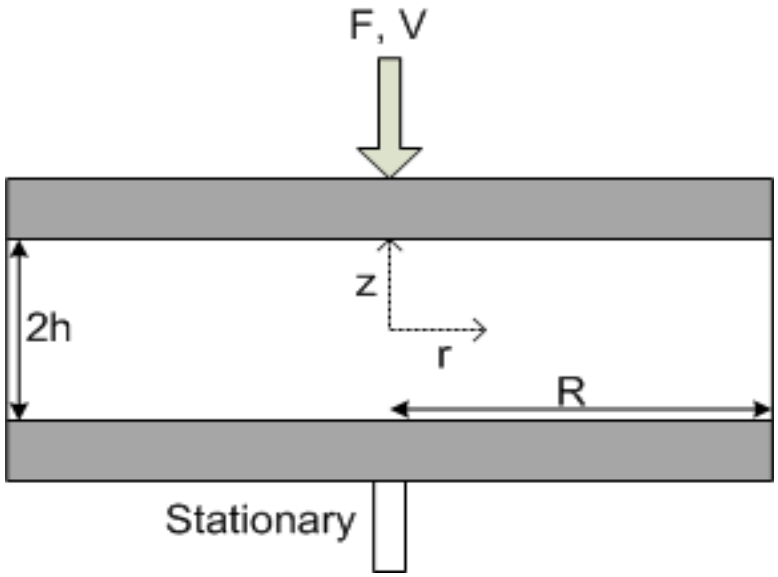

Figure 1.1 Schematic and coordinate system for the squeeze tests

The review paper by Engmann et al. (2005) summarizes the various aspects of squeeze flow rheometry. When highly concentrated suspensions are subjected to constant-velocity squeeze flow two main flow regimes can be identified (see, for example, Delhaye et al. 2000). In the first regime, when the surfaces approach each other at relatively high velocities, the suspension remains fairly homogeneous as it squeezed, and the applied force at a given gap increases with increasing approach velocity. In the second regime, the fluid filters through the particle network as the material is squeezed, and the applied force at a given gap decreases with increasing approach velocity. Two regimes are also observed in constant-force experiments depending on the magnitude of the applied

squeeze force (Meeten 2007). Sherwood (2002) used the relation describing the uniaxial compaction of suspensions in the lubrication analysis of the squeeze flow of a plastic material with slip at the walls. He thus derived the governing equations for the solid content within the suspension as a function of time and radial position. These equations predict that if the squeeze velocity is sufficiently small, the solid volume fraction within the suspension will be non-uniform, with higher volume fractions near the axis of plates.

A constitutive model by Poitou and Racineux (2001) compares the time scale of the deformation of the suspension to the time scale of the filtration, due to a pressure gradient, of the liquid phase through the solid particle network. At high squeeze velocities the deformation time scale is much smaller than the filtration time scale, and filtration is not important; on the other hand, at low squeeze velocities the opposite is true, and filtration cannot be neglected. This model has been used to describe the rheological behavior of ceramic pastes (Poitou and Racineux 2001), sewage sludge (Chaari et al. 2003), and suspensions of hard spheres in Newtonian fluids (Delhaye et al. 2000) and shear thinning fluids (Collomb et al. 2004). When low approach velocities are used, the concentration of solids in the squeezed samples is larger towards the center of the plate; in some cases (Poitou and Racineux 2001) the material at the center is obviously drier than the rest. Roussel and Lanos (2004) studied squeeze flow of dense clay suspension and proposed a model that allows prediction of the solid volume fraction through the squeeze test in terms of the sample's rheological parameters but in their model the average permeability and the yield stress value are not depending upon the average solid volume fraction.

Boundary conditions also play an important role in squeeze flow because, unless there is perfect slip at the plates, the shear stress at the surface is transmitted to the bulk of the sample. Achieving perfect-slip boundary conditions for any material is very difficult in experiments (Meeten 2004) although Mascia and Wilson (2007) studied purely biaxial extensional strain by using Teflon to eliminate the friction from the plates together and by using large initial sample height (the initial gap was the same order of magnitude as the radius of the plate). They also found that the effect of lubricating the plates was negligible at large sample heights and the difference was only apparent at heights below 40% of the initial height. Experiments by Estellé et al. (2006) with smaller initial height showed that the squeeze flow boundary condition is divided into two zones: a small circular central zone where the sample sticks to the plates, and the region beyond that zone, where friction causes the sample to partially slip at the plates. Smyrnaios and Tsamopoulos (2001) showed that when a Bingham plastic undergoes squeeze flow between parallel disks approaching each other at a constant velocity, there is a region around the center of each plate that undergoes no deformation. The unyielded region on the top plate does not connect with the unyielded region on the bottom plate. As the plates approach each other these unyielded regions become smaller. Previously, for the same setup, O'Donovan and Tanner (1984) had shown that regions of almost unyielded material would be expected around the flow stagnation points (the centers of the top and bottom plates) for a material that approximates a Bingham plastic by having a very large viscosity at low shear rates and a shear stress that varies linearly with shear rate at larger shear rates.

Navier and Sur (1827) first proposed a partial slip condition by relating the tangential velocity (slip velocity) to the local tangential shear stress for rough surfaces. If the shear viscosity of the fluid comprising the apparent slip is Newtonian then the relation between slip velocity and shear stress is linear. Laun et al. (1999) provided analytical solution for squeeze flow of Newtonian and power-law fluids by using the lubrication approximation and partial wall slip which slip velocity increases linearly with radial position. For yield stress materials, the tangential stress at the interfaces is usually assumed to be constant and is expressed as a fraction of the yield stress of the material (Engmann et. al 2005). Sherwood and Durban (1998) provided analytical solution for Herschel-Bulkley material by using this method.

Using a grid array of miniature pressure sensors distributed over the face of one of the plates, Yates et al. (2001) measured the pressure profile in a Newtonian fluid and in some food pastes undergoing the constant-velocity squeeze flow. The results for the Newtonian fluid were in good agreement with the theoretical predictions and the data for the pastes was fitted to the predictions for pseudoplastic fluids.

The relation between applied velocity and force in squeeze flow for most types of homogeneous materials has been studied before (see, for example, the review paper by Engmann et al. 2005), but any model which takes into account liquid-phase migration is necessarily more complicated than those that assume the test material is homogeneous. Lipscomb and Denn (1984), using the constitutive equation for a Bingham plastic and assuming no slip at surfaces, showed that on the central plane (between the two approaching surfaces) the shear stress is zero and predicted unyielded material in that plane. However, the velocity field predicted for this case by lubrication theory implies

extensional straining of the material in the central plane. There is, therefore, an inconsistency in their analysis. Sherwood and Durban (1996 and 1998) resolved this inconsistency by the adoption of a constant shear stress as a boundary condition at the wall.

Sherwood (2002) used the relation describing the uniaxial compaction of suspensions when applying lubrication theory to the squeeze flow of a Herschel-Bulkley material between parallel disks with slip at the walls. He thus derived the governing equations for the solid content within the suspension as a function of time and radial position.

For a Herschel-Bulkley material, Chan and Baird (2002) estimated that the error involved in the lubrication approximation could be large when the ratio of the distance between two plates to the radius of plate is large, so that numerical calculation is needed for a general case.

O'Donovan and Tanner (1984) and Smyrnaios and Tsamopoulos (2001) predicted numerically that when a Bingham plastic undergoes squeeze flow between parallel disks approaching each other at a constant velocity, there is a region at the center of each disk that undergoes no deformation. The unyielded region on the top disk does not connect with the unyielded region on the bottom disk. They approximated the behavior of the Bingham plastic with that of a material with a very high viscosity at low shear rates and a linear dependence of shear stress on shear rate at higher shear rates. Yang and Zhu (2006) used the same approximation and assumed a linear relation between shear stress and slip velocity at the wall to obtain analytical solutions of the velocity profile for a Bingham plastic undergoing constant-velocity squeeze flow.

Kaci et al. (2011) observed during the constant-velocity squeeze flow of a highly concentrated suspension that the squeeze force as a function of the gap between the plates becomes almost independent of the velocity below a certain gap size. They believed that they had reached a transition to solid-like behavior and that the slope of the force curves provided the elastic modulus of the granular skeleton.

Depending on the industrial application, it is sometimes important to either hinder or promote liquid-phase migration. Phase separation in constant-velocity squeeze flow has been investigated in ceramic pastes (Poitou and Racineux 2001), clay (Roussel and Lanos 2004), sewage sludge (Chaari et al. 2003), suspensions of hard spheres in Newtonian fluids (Delhaye et al. 2000), suspensions of hard spheres in shear thinning fluids (Collomb et al. 2004), and highly concentrated microcrystalline cellulose suspensions (Mascia and Wilson 2007). Mascia and Wilson (2008) proposed a modified Herschel-Bulkley model for constant-velocity squeeze flow with perfect slip at the surfaces. They also observed liquid-phase migration at slow approach velocities.

Delhaye et al. (2000) argued that the concentration heterogeneity cannot be attributed to the well studied shear-induced particle migration in non-homogeneous shear flow (Leighton and Acrivos 1987) because shear-induced migration is a diffusive phenomenon that occurs on time scales much larger than those involved in typical squeeze flow experiments.

Ramachandran and Leighton (2010) studied the constant-volume squeeze flow of a concentrated suspension between two parallel disks. Under certain conditions, they observed the formation of a highly packed layer of particles at the advancing front of the suspension, with the concentration in the rest of the suspension remaining unaffected.

They attributed the accumulation of particles at the advancing front to shear-induced migration (Leighton and Acrivos 1987) and developed criteria to predict when this phenomenon would occur. Using their criteria, this effect should be absent from our experiments even if they had been performed at constant volume. In constant-area squeeze flow, the method we used in our measurements, there is no advancing front because the gap between the plates is always full and suspension is being expelled from the edge as the disks approach one another. Therefore, we expect that the phenomenon observed by Ramachandran and Leighton did not affect our experiments.

Meeten (2007) investigated the behavior of several soft solids undergoing constant-force squeeze flow. His results showed that samples that readily lost liquid when placed on filter paper also deviated from the behavior predicted for Herschel-Bulkley materials. He attributed the deviation to the radial filtration of the liquid during the squeeze flow. A few milliliters of the material held in a cylindrical tube of radius a, were placed in contact with filter paper of thickness, porosity. Capillary suction drew the liquid out of the material and the radius of the wetting front was measured as a function of time. Patel et al. (2007) verified the existence of liquid-phase migration experimentally and developed a model that predicted this phenomenon for highly concentrated suspensions of glass spheres in Newtonian fluid undergoing extrusion.

According to Meeten and Smeulders (1995) the desorptivity is proportional to the square root of the ratio of the permeability of the material's solid matrix to the viscosity of the liquid. Meeten (2007) found that materials for which porosity is larger than 2 $\mu m \cdot s^{-1/2}$ deviated from the behavior predicted for Herschel-Bulkley materials and thus were presumed to exhibit radial filtration of the liquid during the squeeze flow. This

criterion for the prediction of liquid-phase migration in squeeze flow does not account for the possible effect of the squeezing conditions. For example, for constant-force squeeze flow, a material may exhibit liquid-phase migration when squeezed with a small force but not when squeezed with a large force. Similarly, under constant-velocity squeeze flow, a material may exhibit liquid-phase migration when squeezed slowly but not when squeezed rapidly.

Yield stress is another phenomena commonly observed in highly concentrated suspensions (Barnes 1999). Heymann et al. (2002) present evidence for an elastic component of deformation at high particle concentrations and conclude that, at low shear stress, particles interact as an elastic network, which breaks up when the yield stress is reached. They found that the yield stress is a function of the particle volume fraction and is larger for smaller spheres because of the greater density of particle-particle interactions, which gives rise to a more robust particle network. They found that the network deforms elastically in response to an applied stress, which is transmitted through the network via direct particle-particle contact. The yield stress is reached when the applied stress is sufficient to cause the network to break up, beyond which point the suspension flows. It appeared that by carefully controlling the experimental conditions of the squeeze test one can obtain yield stress values that agree with the common rheological measurements (Rabideau et al. 2009).

As the solid volume fraction of a concentrated suspension approaches its maximum value, the rheology changes from Newtonian to pseudo-plastic behavior (Mueller et al. 2010). Moreover, potential of the particle migration (see for example Leighton and Acrivos 1987) and liquid phase redistribution make the mechanics of these systems more

complicated. Therefore, a numerical modeling that takes into account time and position dependence of the rheological properties of the material is needed.

Mascia and Wilson (2008) performed a constant-velocity squeeze flow of highly concentrated suspension of glass powder in Newtonian liquid between lubricated plates. Measuring solid content showed uniform radial concentration of solid at high squeeze velocity and non-uniform solid profile at low squeeze velocity. Kaci et al. (2011) reported an experimental study of concentrated suspension undergoing constant-force squeeze flow. By measuring the squeeze forces at constant velocity versus the sample thickness, they concluded that the suspension experiences squeeze-induced heterogeneities, and eventually jamming under certain conditions. Liquid-phase migration have also reported in cement-based materials (Toutou et al. 2005), microcrystalline cellulose pastes (Mascia et al. 2006), sewage sludge (Chaari et al. 2003), titanium oxide particle in an acidic binder (Poitou and Racineux 2001), and clay (Roussel and Lanos 2004) at constant-velocity slow squeezing and for soft solids (Meeten 2007) at constant-force squeeze flow.

Suspensions can be studied from a microscopic or macroscopic pinot of view (Ritz et al. 2000). In the microscopic, or particle-based, point of view, despite the limitation in the amount of computing, the characterization of interactions appearing at the scale of particles can applied to describe flow behavior in the scale of suspension. On the other hand, macroscopic approach considers the suspension as a continuum phase modeled through a rheological law which is a function of the local values of macroscopic quantities such as shear rate and concentration.

In most studies on the squeeze flow, the tested material is assumed to remain homogeneous through the test although there is evidence that complex materials like suspensions became heterogeneous when undergoing squeeze flow. Poitou and Racineux (2001) showed that in a constant-velocity squeezing flow of suspensions, liquid-phase migration occurs in the suspension as long as the squeeze velocity does not exceed a critical value. Roussel and Lanos (2004) proposed a simplified model in order to take into account the drainage of water during the constant-velocity squeezing the clay. Their results showed that the heterogeneity is induced by slow compression and their model predicted of the average void ratio evolution through the squeeze test in terms of parameters that can be identified on high speed squeezing test.

Boundary conditions also play an important role in the squeeze flow of suspensions. Meeten (2004) experimental study on Newtonian fluids and soft solids showed that achieving perfect-slip boundary conditions for any material is very difficult. On the other hand, achieving perfect no-slip boundary condition is difficult for highly concentrated suspensions too because the local particle concentration of the suspension is depleted at a boundary such that the suspension's rheological properties differ from those in the bulk then apparent wall slip may occur (Barnes 1995). Gulmus and Yilmazer (2005) observed that as the volume fraction of particles increased, the wall slip velocity increased and as the particle size increased, the wall slip velocity decreased. Navier and Sur (1827) first proposed a partial slip condition by relating the slip velocity to the local tangential shear stress for rough surfaces. If the shear viscosity of the fluid comprising the apparent slip is Newtonian then the relation between slip velocity and shear stress is linear. Laun et al. (1999) provided an analytical solution for the squeeze flow of Newtonian and power-law

fluids by using the lubrication approximation and partial wall slip which slip velocity increases linearly with the radial position. For materials with yield stress, the tangential stress at the interfaces is usually assumed to be constant and is expressed as a fraction of the yield stress of the material (Engmann 2005). Sherwood and Durban (1998) provided an analytical solution for Herschel-Bulkley materials by using this method. Slip tests on suspensions with high concentrations showed that the squeeze flow boundary condition is not uniform and the boundary condition on the surface of the plates was intermediate between perfect slip and no slip and slip at the surfaces promoted by increasing the solid volume fraction. Slip can affect the liquid phase migration in squeeze flow of suspensions; theoretical work by Ayadi (2011) on the squeeze flow of Bingham plastics showed that the radial pressure gradient increases when there is no slip at the plates, and this boosts the liquid filtration process.

In this thesis we investigated through experiment and model, the normal stress distribution during constant-force squeeze flow of highly concentrated suspensions. In chapter 2, the results of using pressure-sensitive films to measure the normal stress distribution in suspensions of glass spheres in a Newtonian liquid are presented. In order to validate the use of the pressure-sensitive films, the normal stress distribution for a Newtonian fluid was measured and compared to the theoretical predictions. The changes in the normal stress distribution were also investigated as the squeezing proceeded by changing the pressure-sensitive film.

In chapter 3, the results of measuring the solid volume fraction distribution throughout the suspension undergoing the squeeze flow are presented. The influence of rheological and process parameters on the liquid phase migration was investigated and criteria for the

occurrence of liquid-phase migration in suspensions undergoing squeeze flow are discussed in terms of dimensionless groups.

In chapter 4, the result of developing a model to predict the behavior of highly concentrated suspensions in squeeze flow is introduced. We compare the model's predictions with our previous experimental results on the constant-force squeeze flow of highly concentrated suspensions. The model is then used to study the effect of process parameters (such as slip and applied force) and material properties (such as the viscosity of the suspending fluid, the yield stress, and the particle size) on the migration of the liquid phase during squeeze flow.

CHAPTER 2

NORMAL STRESS DISTRIBUTION IN SQUEEZE FLOW OF SUSPENSIONS

2.1. Background

According to Bird et al. (2002), the radial distribution of the normal stress in a Newtonian fluid undergoing squeeze flow in the filled gap between a stationary and a moving disk with no slip at surfaces is given by:

$$\tau_{zz} - p_{atm} = \frac{3\mu V}{8h^3}\left(R^2 - r^2\right) \tag{2.1}$$

where the quantity on the left is the normal stress acting on the plate (p_{atm} is the atmospheric pressure acting on the other side of the plate, and τ_{zz} is the relevant component of the deviatoric stress tensor minus the pressure in the fluid), μ is the viscosity of the fluid, V is the velocity of the moving disk, h is the half of gap between the disks, R is the radius of the disks, and r is the radial position in cylindrical coordinates. This relation clearly shows that for a Newtonian fluid we should expect to see a quadratic normal stress on the surface of the plates that becomes equal to the atmospheric pressure at the edge. Equation 2.1 is derived by assuming lubrication approximation ($h<<R$). The more general form of this equation without this assumption is

$$\tau_{zz} - p_{atm} = \frac{2F}{\pi R^4}\left(R^2 - r^2 + 2z^2\right) \tag{2.2}$$

Equation 2.1 can be integrated to obtain the total force acting on the plate:

$$F = \frac{3\pi\mu V R^4}{8h^3} \tag{2.3}$$

Using Eq. 2.1 the following expression is obtained for the normal stress on the surface of the plate:

$$\tau_{zz} - p_{atm} = \frac{2F}{\pi R^4}\left(R^2 - r^2\right) \tag{2.4}$$

Since Eq. 2.4 was derived assuming a quasi steady state, it applies to squeeze flow with constant velocity, *V*, as well as with constant force, *F*. In the latter case, it is interesting to note that the normal stress distribution on the plate is independent of the viscosity of the fluid, the gap between the plates, and the velocity at which the plates approach one another. Since the weight of the sample undergoing the squeeze test is small compared to the other forces involved, the normal stresses at the top and bottom plate have the same values.

2.2. Experiments

2.2.1. Materials

Suspensions of various concentrations were prepared by mixing glass spheres into a silicone oil. The glass spheres (manufactured by Cataphote Inc., Jackson, MS) were sieved in order to isolate those between 75 and 90 microns (between 200 and 170 mesh). A micrograph of the spheres is shown in Figure 2.1.

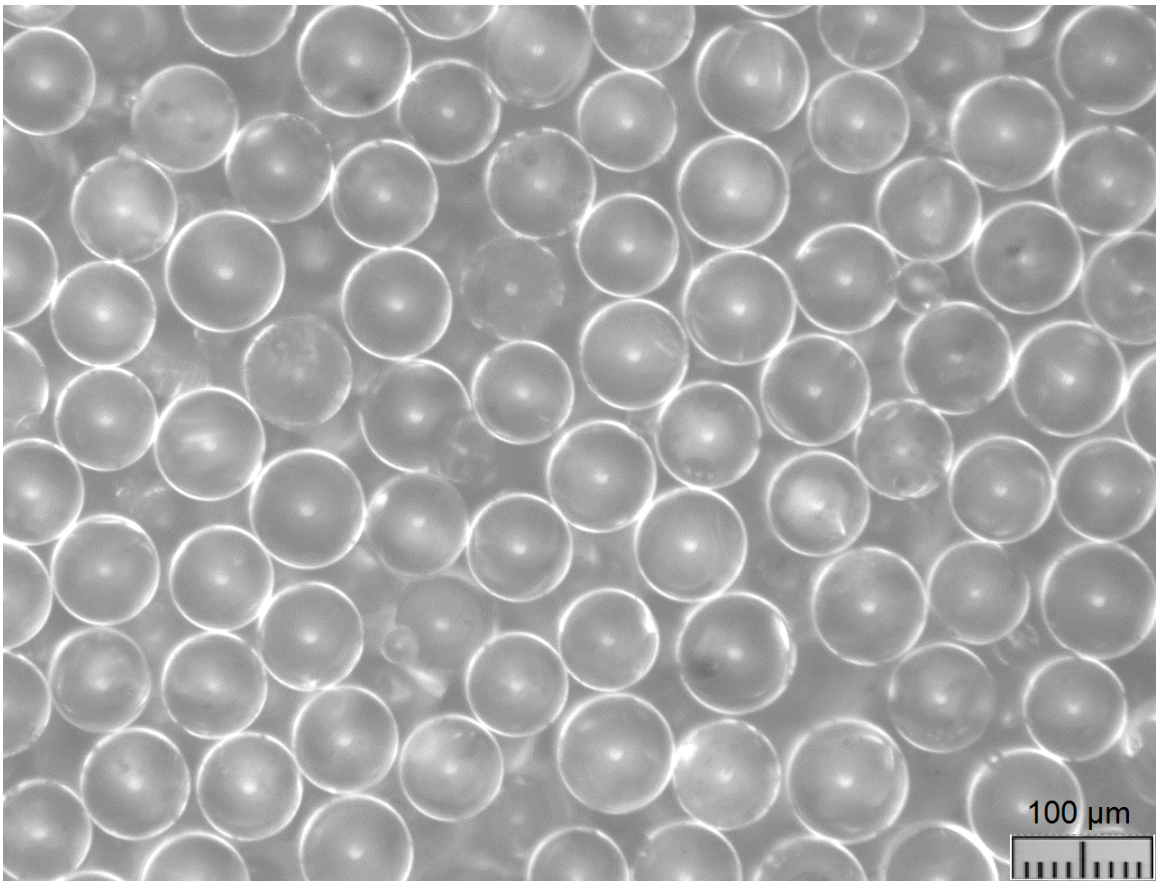

Figure 2.1 Optical micrograph of the glass spheres used in the suspensions

The particle size distribution, shown in Figure 2.2, was obtained with a single-particle optical sizer (Accusizer Model 780, Particle Sizing Systems, Santa Barbara, CA). The number-average diameter of the glass spheres was 74 µm. A considerable number of smaller spheres did not go through the finer sieve and some doublets were able to go through the coarser sieve. The density of the glass spheres was determined to be 2,730 kg/m^3 using a pycnometer and water. The suspending fluid was Dow Corning 200 Fluid 300,000 cSt (Dow Corning Corp., Midland, MI). Its viscosity at 22°C (the temperature near which all experiments were conducted), measured with a Rheometrics Fluid Spectrometer RFS II, was constant at 327.5 Pa·s at all shear rates applied (0.05 s^{-1} to 8.0 s^{-1}). Its density was determined using the pycnometer to be 970 kg/m^3.

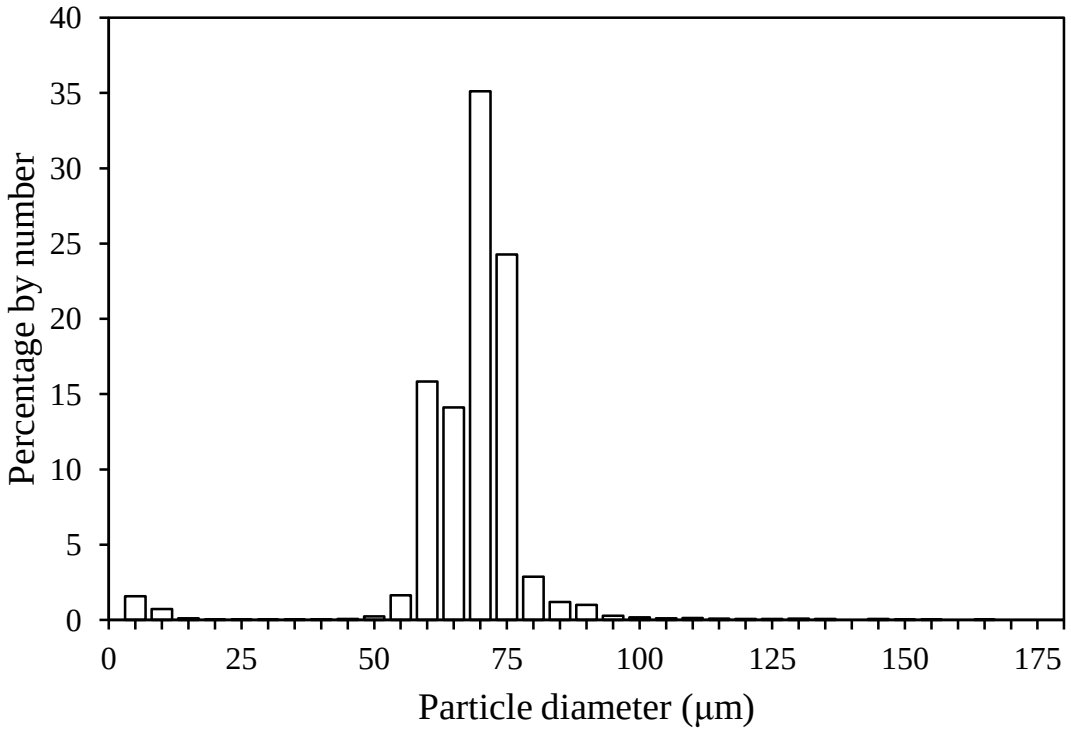

Figure 2.2 Particle size distribution of the glass spheres used in the suspensions

Suspensions were prepared with weight percent of solids of 20%, 60%, 70%, 75%, 77.5%, 79%, and 80%, which correspond to volume fractions of solids of 0.082, 0.348, 0.516, 0.550, 0.572, and 0.586, respectively. The glass spheres were thoroughly mixed into the fluid using a spatula. Most of the air entrained during the mixing process was removed by placing the suspensions in a vacuum chamber for periods up to two hours depending on concentration. Upon removal from the vacuum chamber, the suspensions were lightly stirred to ensure uniformity while trying to avoid the entrainment of any air. Although the particles were much denser than the fluid, the fluid was viscous enough that no settling was apparent for periods of several hours, more than ample time for the completion of a typical squeeze flow experiment. Delhaye et al. (2000) estimates the

sedimentation time of a sphere in a suspension, t_{sed}, that is, the time required for a sphere to fall a distance equivalent to its diameter, as follows

$$t_{sed} = \frac{18\mu}{(\rho_s - \rho_f)gD(1-\varphi)^{6.55}}, \tag{2.5}$$

where μ is the viscosity of the fluid, ρ_s is the density of the spheres, ρ_f is the density of the suspending fluid, g is the acceleration due to gravity, D is the diameter of the sphere, and φ is the volume fraction. For our spheres and fluid, in our most dilute suspension (φ = 0.082), the largest particles present (D = 165 μm), would have a sedimentation time of 3600 s (1.0 h), which is much longer than the duration of the squeeze tests. Therefore, the sedimentation of the particles during the tests was neglected.

2.2.2. Equipment and procedure

The suspensions were squeezed between a circular stainless-steel disk, 3.50 in. (88.9 mm) in diameter, and a large flat steel plate in a 12-ton hydraulic press ordered from Technical Machine Products, Cleveland, OH to our specifications. The circular disk and the plate were covered with stainless steel foil, soft temper, type 304, 0.002-in. (0.051 mm) thick (McMaster-Carr Supply Company, Elmhurst, IL). In all experiments we applied a constant force of 1.5 short tons (13.3 kN) to the suspensions. It is worth noting that the bottom plate, on which the disk rested, approaches the stationary top plate at a relatively high constant velocity until the required force reaches the set point. After that, the force remains constant and the approach velocity changes with time in a way determined by the properties of the sample. We used a closing speed of 50 mm/s (the highest available in our press) to minimize the period of constant velocity relative to the

total duration of the experiment. In a typical experiment, the initial sample height was 18 mm and the force reached its desired value when the sample height had been reduced to about 4 mm. At a closing speed of 50 mm/s, this takes place after about 0.28 s. This period of time is about one hundredth of the total duration of a typical experiment (about 35 s). The disk (resting on the bottom plate) and the top plate were covered with stainless steel foil, and, without a sample between them, were pressed together to flatten the stainless steel foil. The pressure-sensitive films were then placed between the disk and its stainless steel foil. Since the normal stress distribution was radially symmetric, it was enough to measure it on a one-centimeter-wide strip of pressure-sensitive film passing through the axis of the disk. Previously-used pressure-sensitive film of the same thickness was placed on either side of the strip to provide the same thickness throughout. Finally, the sample was placed between the stainless steel foils and squeezed by raising the lower plate of the hydraulic press towards the top plate. The setup is shown in Figure 2.3.

used Pressure-X pressure-sensitive films (Sensor Products Inc., Madison, NJ) to determine the normal stress distribution. These polymer films contain red pigment in micro-capsules which rupture when subjected to pressure. The intensity of the red color that results when the films are pressed increases with the magnitude of the applied pressure. The intensity of the red color of a film already exposed to a moderate pressure increases when the film is exposed to a higher pressure, but it does not decrease when the film is exposed to a lower pressure. The redness of the film thus reflects the highest pressure the film has experienced during a test. In order to convert the intensity of the red color to a pressure, we calibrated the films by applying a known force to a specific area

of the film. We then obtained a bitmap color image of the film on a scanner and determined the average intensity of the pixels in that area using the Matlab image analysis toolbox (The MathWorks, Inc., Natick, MA). Temperature and humidity as well as the time of exposure influence the color intensity of the pressure-sensitive films. Therefore, to minimize error, we kept the conditions in our experiments close to the conditions at which the films were calibrated. The estimated error in measuring the normal stresses using the pressure-sensitive films is about 10%. Three different pressure-sensitive films: medium 1400-7100 psi (9700-49000 kPa), low 350-1400 psi (2400-9700 kPa), and super low 70-350 psi (480-2400 kPa) were used in our experiments. The procedure of pressure sensitive films calibration and use is explained in detail in appendix A.

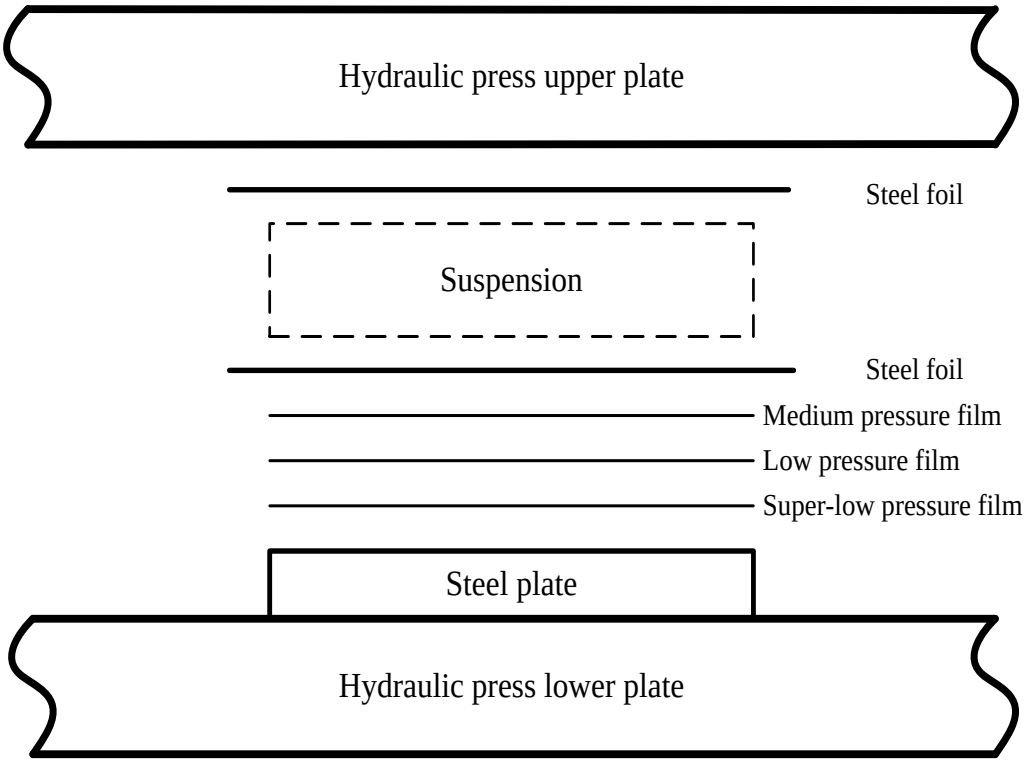

Figure 2.3 Schematic of the squeeze test setup

We Each suspension was squeezed for 35 s and the resulting films were analyzed. Figure 2.4 shows the result of measuring normal stress distribution using this method. As described below, one of the tests on the suspension with a volume fraction of 0.586 (80 wt%), was interrupted at regular intervals in order to replace the pressure-sensitive films to determine how the normal stress profile changed during the squeeze test.

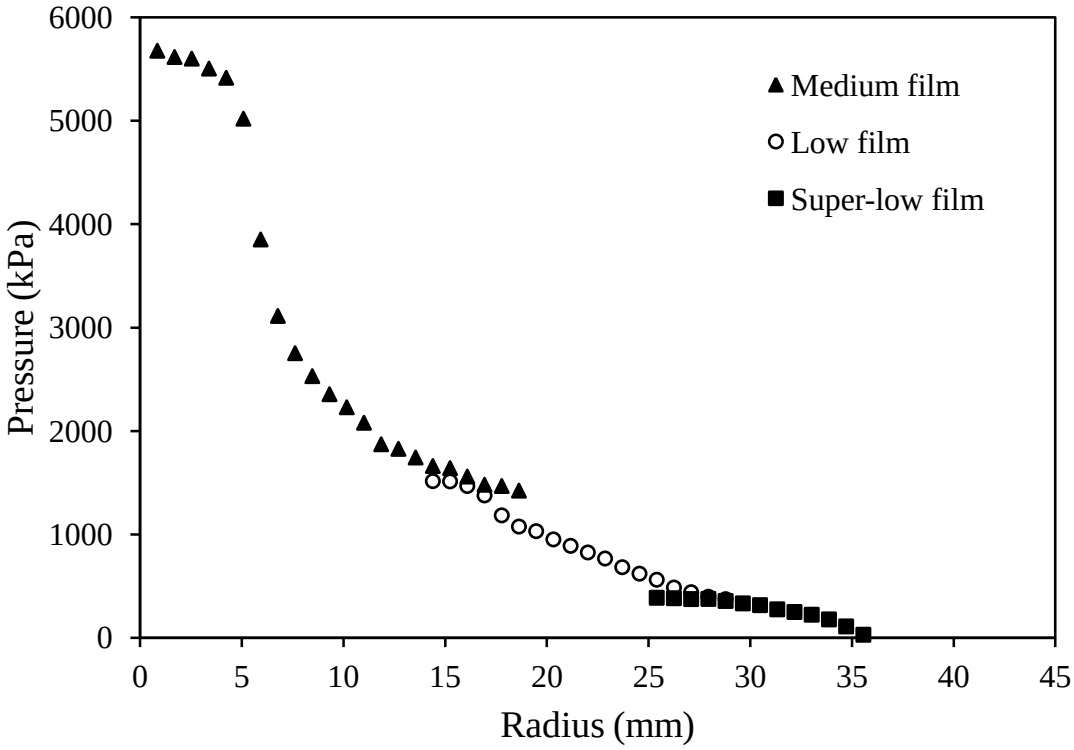

Figure 2.4 Normal stress distribution result from scanning pressure-sensitive films

2.3.Results and Discussions

In order to test the technique for measuring the normal stress distribution with the pressure-sensitive films, the Newtonian Dow Corning fluid was subjected to squeeze flow and the resulting pressure distribution was compared to Eq. 2.4. Figure 2.5 shows

that the results for the Dow Corning fluid, using a force of 13.3 kN, are in close agreement with the predictions.

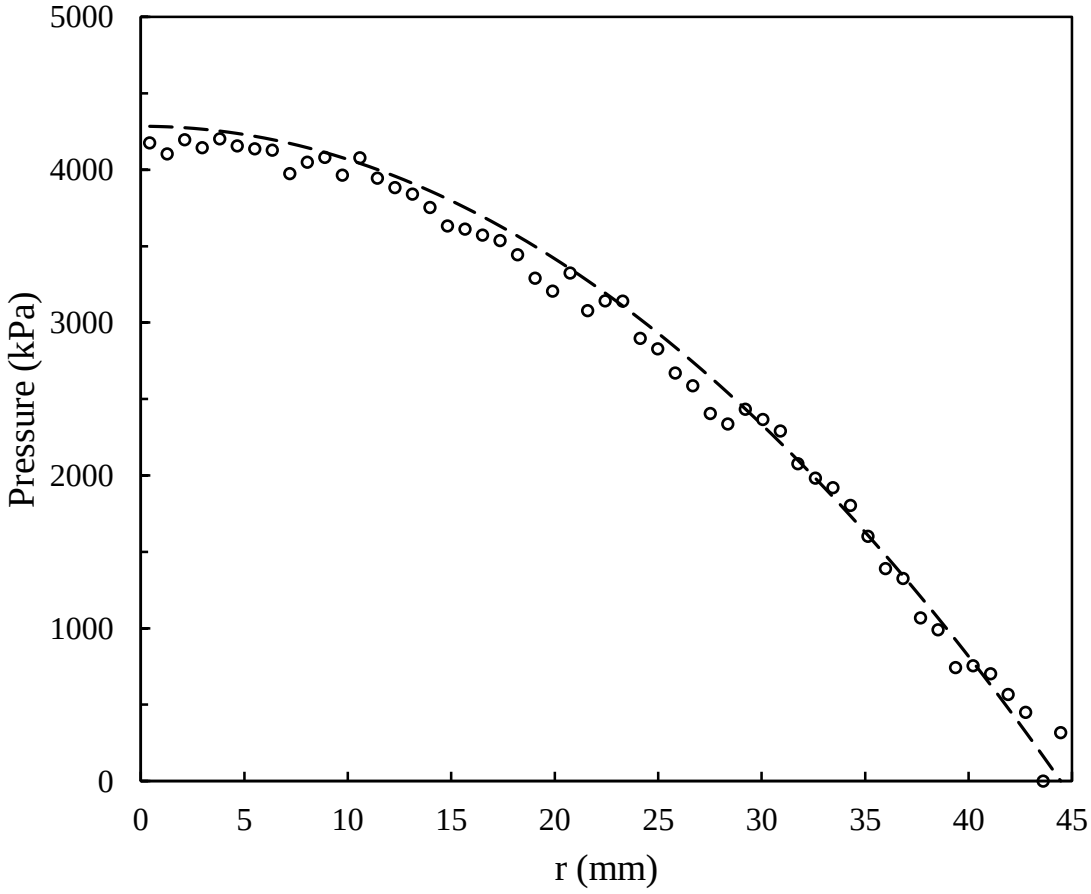

Figure 2.5 Normal stress distribution for Dow Corning 200 Fluid 300,000 cSt squeezed with a constant-force of 13.3 kN for 35 s. The dashed line is the predicted normal stress distribution for a Newtonian fluid

Figure 2.6 shows the appearance of the three different types of pressure-sensitive film after the Dow Corning suspending fluid and the suspensions were subjected to squeeze flow under a constant force of 13.3 kN for 35 s. The impressions on the film are very similar for the pure fluid and for suspensions with volume fractions below 0.55. The impressions on the films for the suspension with volume fraction of 0.550 differ somewhat from those only in the outermost region. The normal stress at the center of disk

for the two suspensions with volume fraction above 0.55 is much higher than for the less concentrated suspensions and reaches the range of the pressure of the medium film. Also, the width of red color on the super-low and low pressure-sensitive films decreases for these two suspensions which means that qualitatively the maximum pressure at the center for the highest volume fraction suspensions increases while the area on which the normal stress is felt decreases.

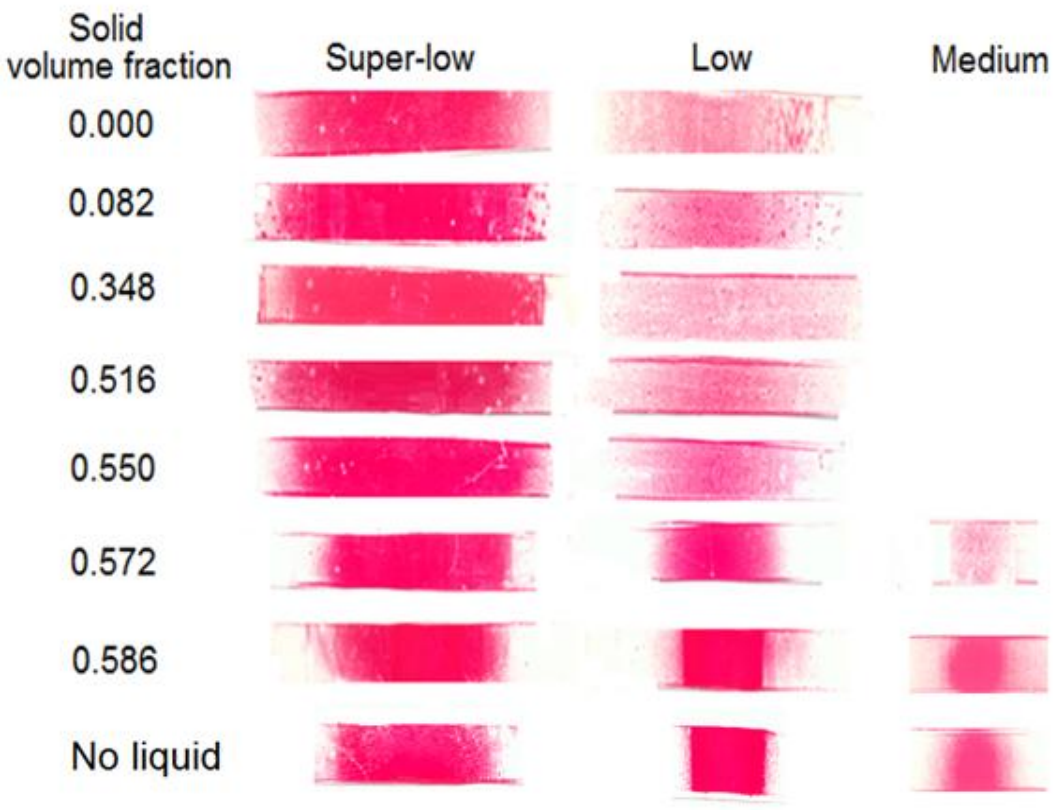

Figure 2.6 Images of the pressure-sensitive films used in the squeeze tests of the suspensions of glass spheres in Dow Corning 200 Fluid 300,000 cSt with volume fractions between zero and 0.586. Also shown are the results of squeezing the glass spheres without fluid. The materials were squeezed between a disk and a flat plate with a constant force of 13.3 kN for 35 s.

Figures 2.7 and 2.8 show the normal stress profiles obtained for suspensions with various volume fractions. The data plotted were taken from the pressure-sensitive films in

the applicable range. Each curve represents a single run, but combines measurements from pressure-sensitive films of various sensitivities; this and the error inherent in the technique contribute to the waviness of some of the curves. In both Figures the prediction for Newtonian fluids is presented for comparison. The suspensions with volume fractions up to 0.55 have normal stress profiles very similar to that for Newtonian fluids. On the other hand, the suspensions with higher volume fraction have normal stress profiles with a prominent region in the middle of the disk in which the normal stress is much higher than that predicted for Newtonian fluids.

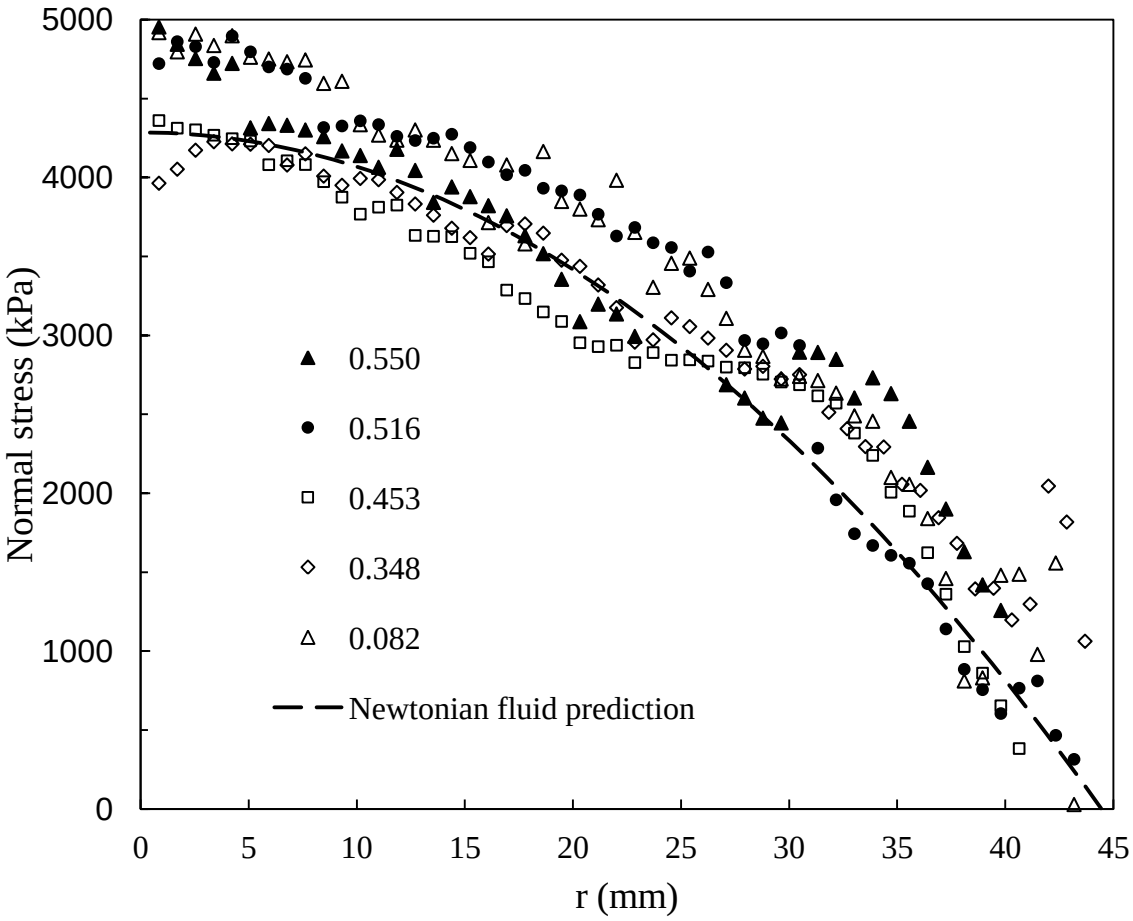

Figure 2.7 Normal stress distributions for suspensions of glass spheres in Dow Corning 200 Fluid 300,000 cSt with volume fractions of 0.55 and below squeezed between a disk and a flat plate with a constant force of 13.3 kN for 35 s. The dashed line is the predicted normal stress distribution for a Newtonian fluid

The normal stress profile for the glass spheres without liquid, also shown in Figure 2.8, is very similar to those for the suspensions with volume fraction above 0.55.

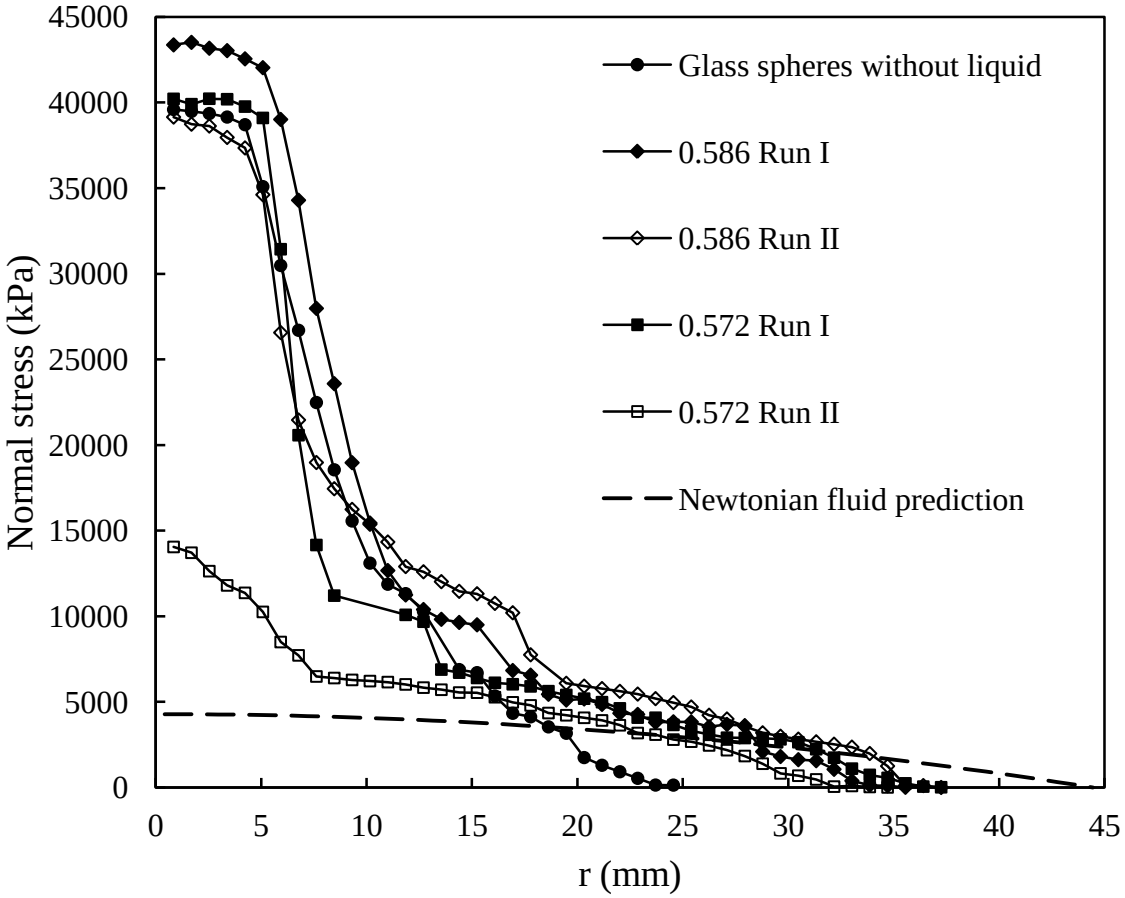

Figure 2.8 Normal stress distributions for suspensions of glass spheres in Dow Corning 200 Fluid 300,000 cSt with volume fractions of 0.572 and 0.586 squeezed between a disk and a flat plate with a constant force of 13.3 kN for 35 s. Also shown is the normal stress distribution for the glass spheres without liquid. The dashed line is the predicted normal stress distribution for a Newtonian fluid

Figure 2.9 plots the total force computed by integrating the pressure profiles of Figures. 2.7 and 2.8 over the area of the disk. For volume fractions less than 0.586, the calculated total force is within 15% of the applied force. On the other hand, for the suspensions with a volume fraction of 0.586 the total calculated force is considerably higher than the applied force. As will be explained below, this discrepancy is due to the

fact that, at this volume fraction, the pressure profile changes during the constant-force squeezing process. Since the pressure-sensitive films do not recover their original color once they have been subjected to pressure, they accumulate the effect of pressure changes during the experiment.

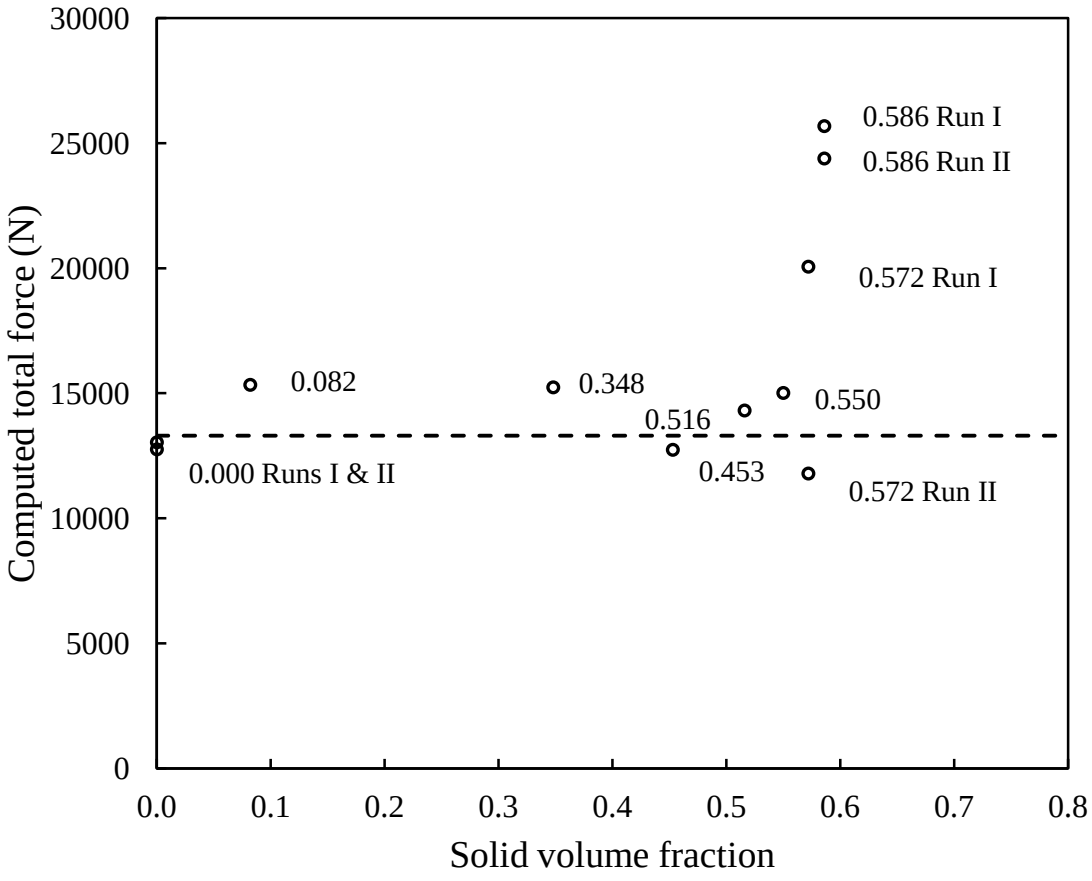

Figure 2.9 The total force on the sample computed by integrating the normal stress distributions of Figures. 2.6 and 2.7 over the area of the disk. The dashed line shows the applied force of 13.3 kN. The label next each data point indicates the volume fraction of the suspension

In order to investigate the "pressure accumulation" effect, we measured the normal stress profile at different times during the squeezing of the suspension with a volume fraction of 0.586. Two sets of pressure-sensitive films were used in this measurement. The first set remained for the entire experiment (0 to 40 s); the second set was replaced at

various intervals, and the squeezing was then resumed. The results are shown in Figure 2.10. In the central region (r < 5 mm), the normal stress increases dramatically after the first three seconds of squeezing, whereas in the middle region (5 mm < r < 15 mm), the normal stress decreases.

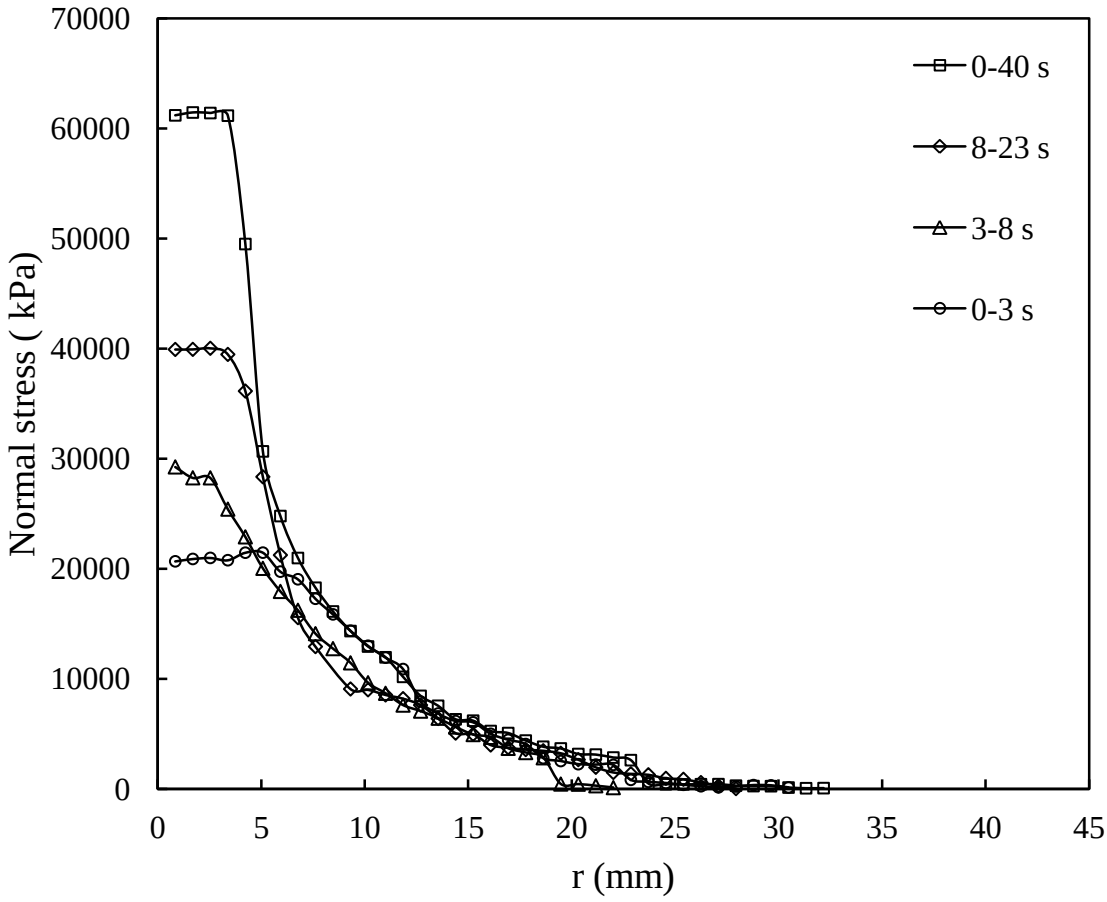

Figure 2.10 Normal stress distributions at various times in a suspension of glass spheres in Dow Corning 200 Fluid 300,000 cSt with a volume fraction of 0.586 squeezed between a parallel disk and a flat plate with a constant force of 13.3 kN

The highest normal stress experienced at each position is close to that of the normal stress distribution measured by the set of pressure-sensitive films that remained for the entire experiment (0 to 40 s). The curve made up from the highest normal stress at each

position is higher than any of the curves for partial squeezing, thus explaining the higher apparent force calculated when the normal stresses are integrated.

In order to determine whether or not there was slip at the wall, we used a transparent Plexiglas disk and plate in one experiment. We drew concentric circles of various radii (after Estellé et al. 2006 and Mascia and Wilson 2007 and 2008) with a felt-tip marker on a suspension with a volume fraction of 0.586 and subjected it to squeeze flow. We interrupted the experiment at various times and photographed the suspension through the transparent plate to measure the change in the radii of the circles. Figure 2.11 shows as data points the radii of the drawn circles at various times, and as curves, their radii if there had been perfect slip at the surface. The results indicate neither perfect slip nor no slip, but an intermediate condition.

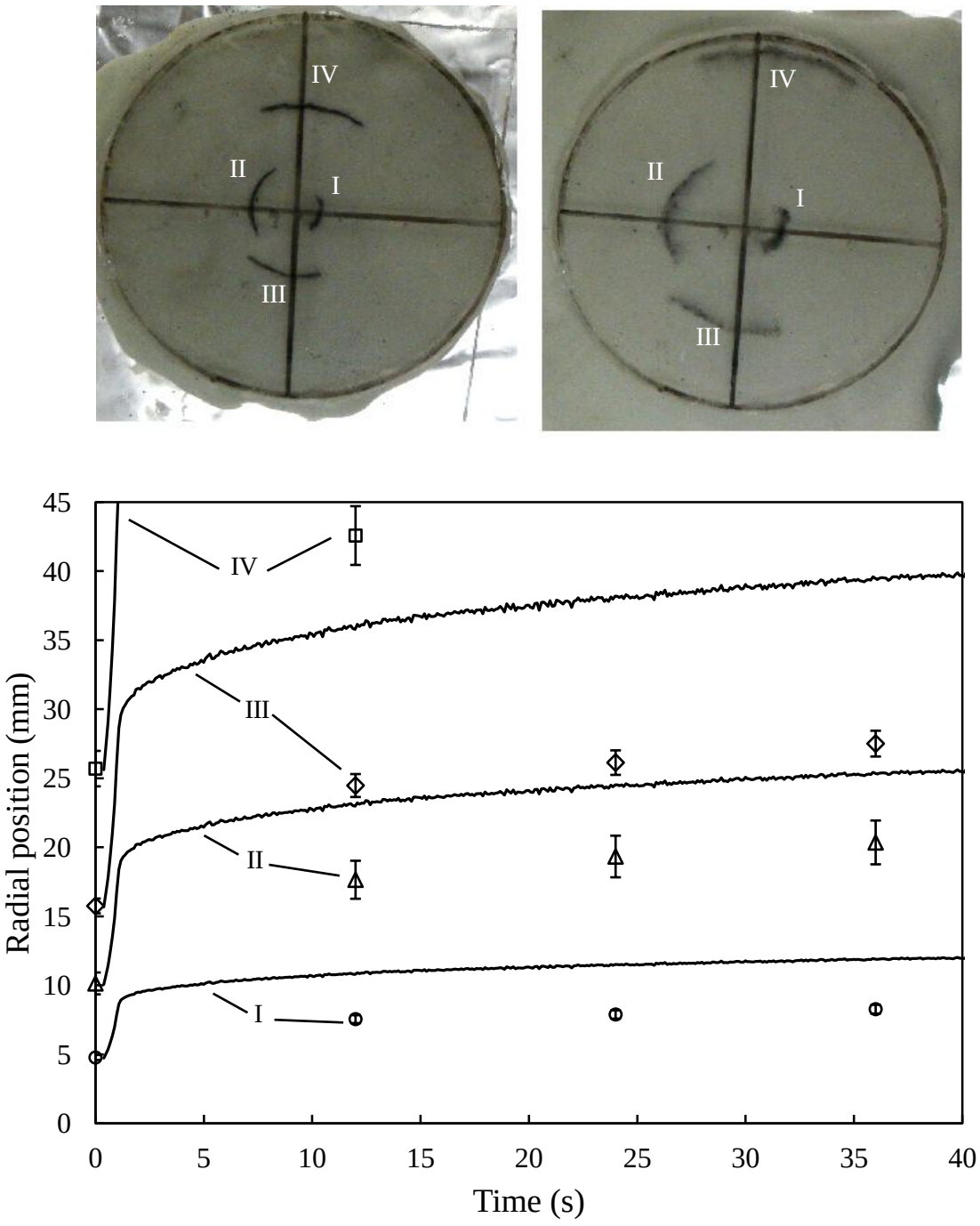

Figure 2.11 Radii of the concentric circles drawn at the plate surface as a function of time during the slip visualization test for a suspension of glass spheres in Dow Corning 200 Fluid 300,000 cSt with a volume fraction of 0.586 squeezed between a parallel disk and a flat plate with a constant force of 13.3 kN. The curves show the radii of the circles predicted assuming perfect slip at the surface

In the suspension with a volume fraction of 0.586, a small region (about 5 mm in diameter) at the center became very dry, as ascertained visually by the change in the appearance of the suspension. The suspension in the central region became whiter and less smooth than before as can be seen in Figure 2.12. This region corresponds to the region of high normal stresses in Figure 2.8. The fact that squeezing the spheres without fluid results in a similar normal stress distribution suggests that at concentrations above 0.55, the liquid phase migrates out of the central region and jamming takes place.

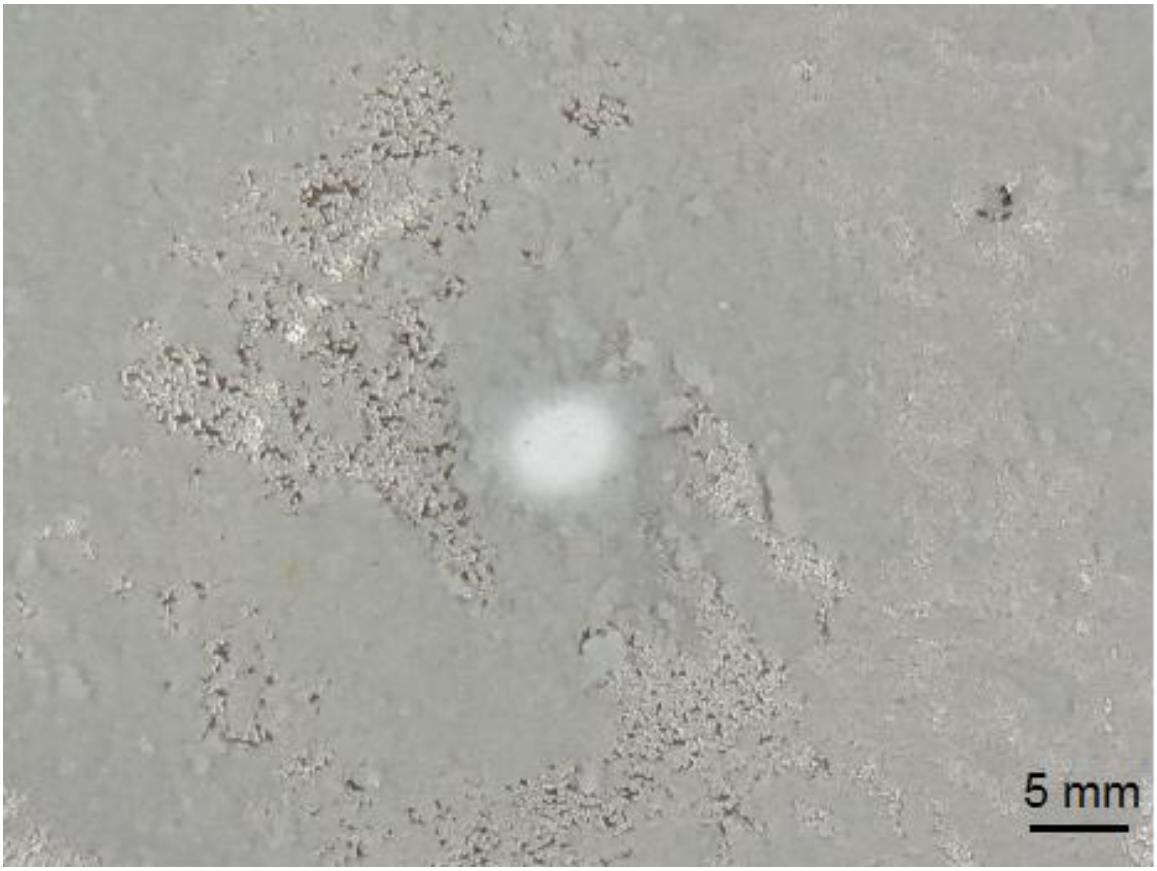

Figure 2.12 Image of the squeezed suspension of glass spheres in Dow Corning 200 Fluid 300,000 cSt with volume fraction of 0.586 showing a whiter and dryer spot at the center.

In squeeze flow, liquid-phase migration becomes important in suspensions when the approach velocity between the surfaces is lower than a critical approach velocity, $V_{critical}$.

For squeeze flow between parallel disks with perfect slip at both surfaces, Mascia and Wilson (2007) obtained an expression for the critical approach velocity by comparing two of the time scales involved. The first relates to the deformation of the suspension as a whole, and the second to the filtration of the liquid phase through the particle network. Their result is equivalent to

$$V_{critical} = \frac{2k\Delta P h}{R^2 \mu} \tag{2.6}$$

where k is the absolute permeability of the solids matrix, ΔP is the pressure difference between the center ($r = 0$) and the edge ($r = R$) of the disks, h is the gap between the disks, R is the radius of the disks, and μ is the viscosity of the liquid phase.

This expression can be easily obtained by finding the approach velocity, V, at which $v_{r,susp}$, the radial velocity at which the suspension as a whole flows when there is perfect slip on both plates,

$$v_{r,susp} = \frac{Vr}{2h} \tag{2.7}$$

is equal to $v_{r,liq}$, the velocity at which the liquid phase filters through the particulate network according to Darcy's law,

$$v_{r,liq} = -\frac{k}{\mu}\frac{\partial P}{\partial r} \approx -\frac{k}{\mu}\frac{\Delta P}{R} \tag{2.8}$$

For our calculations, we estimated the absolute permeability using Happel's (1986) correlation,

$$k = \frac{D^2}{36}\left(\frac{6 - 9\varepsilon^{1/3} + 9\varepsilon^{5/3} - 6\varepsilon^2}{\varepsilon\left(3 + 2\varepsilon^{5/3}\right)}\right), \tag{2.9}$$

where D is the particle diameter and ε is the porosity of the suspension (1 - φ). The absolute permeability for our suspension of 74 μm-diameter spheres with a volume fraction of 0.586 was thus estimated to be 3.54×10^{-11} m^2.

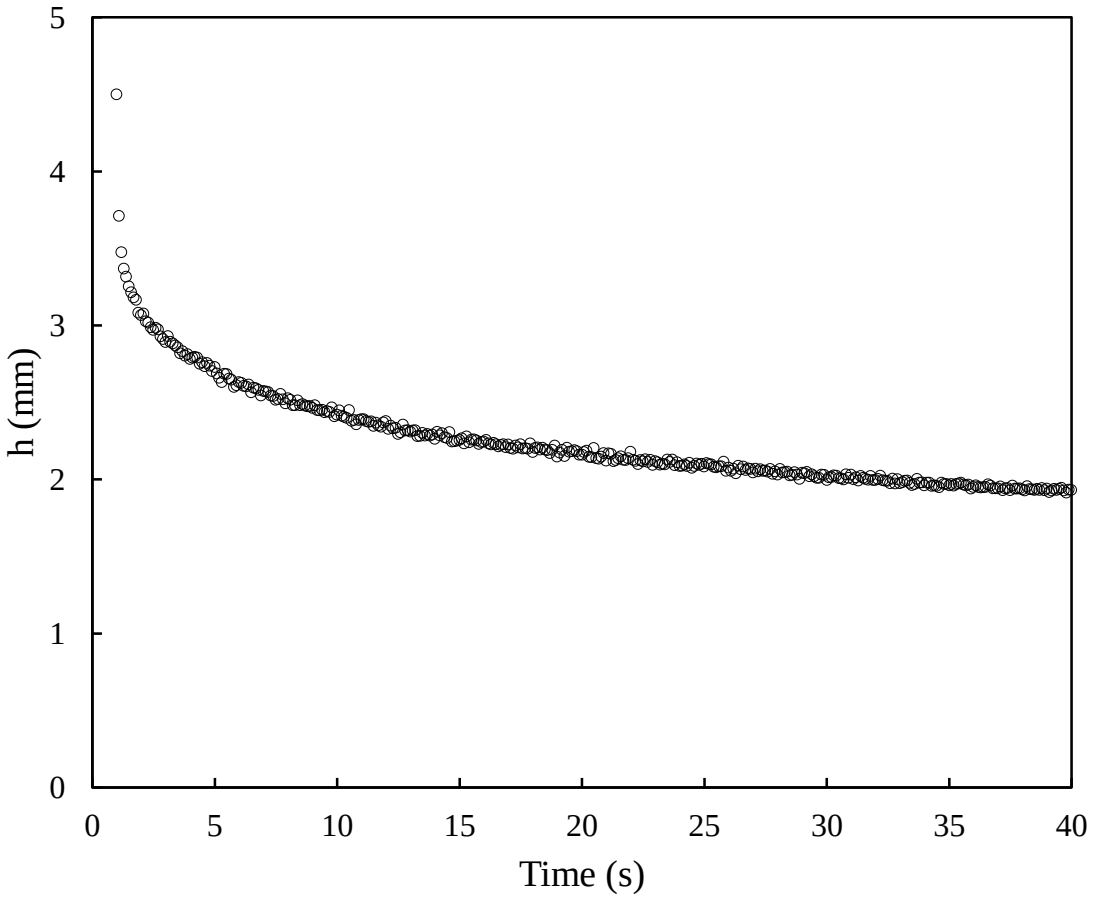

Figure 2.13 Plate separation as a function of time for a suspension of glass spheres in Dow Corning 200 Fluid 300,000 cSt with a volume fraction of 0.586 squeezed between a parallel disk and a flat plate with a constant force of 13.3 kN

Figure 2.13 shows the gap between the disk and the plate as a function of time for this suspension when squeezed with a force of 13.3 kN using the 3.5-in. diameter disk.

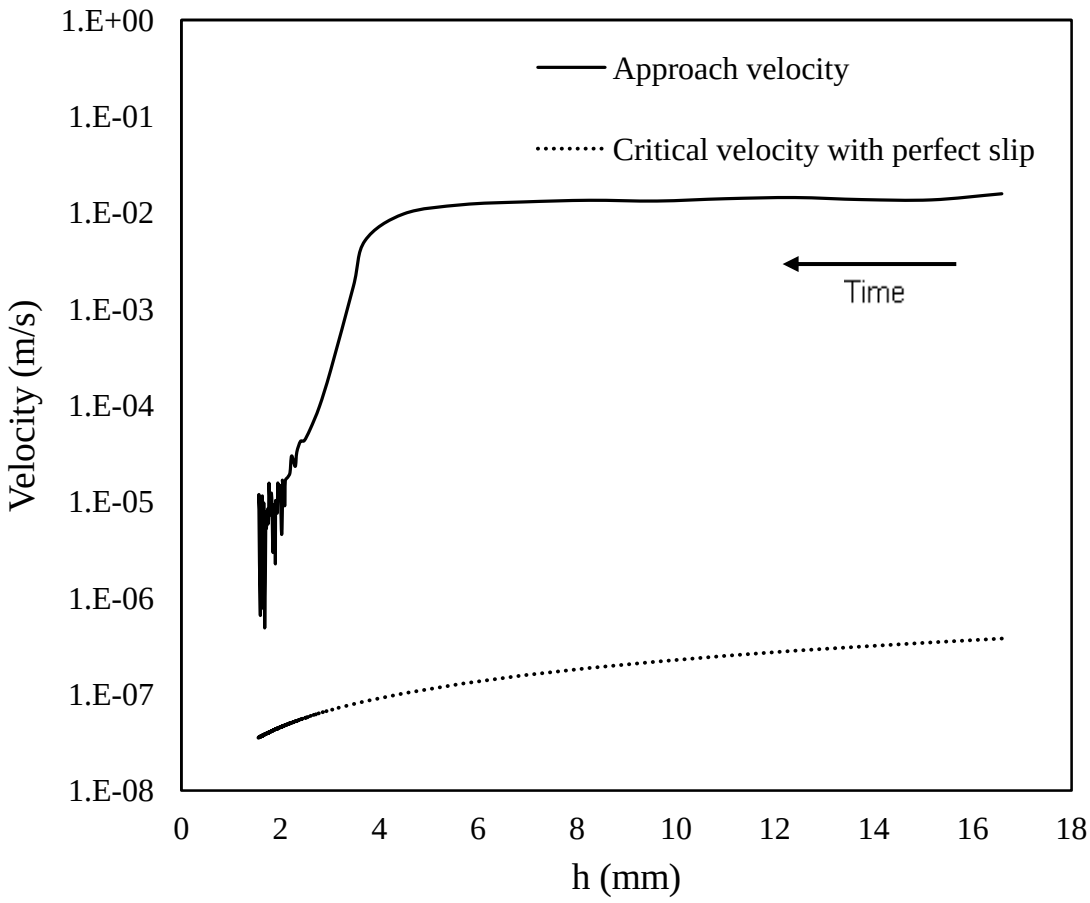

Figure 2.14 Comparison of the approach velocity estimated from the data in Figure 2.12 to the critical approach velocity predicted by Eq. (3) for the case of perfect slip on both plates.

The approach velocity as a function of time was calculated by numerical differentiation of these data and is presented in Figure 2.14. Also plotted are the estimates for the critical approach velocity obtained using Eq. 2.6. These estimates are two orders of magnitude smaller than the actual approach velocity, thus predicting no liquid phase migration in this suspension. That the prediction is contrary to our observations is not surprising in view of the evidence, clear from Figure 2.11, that the assumption of perfect slip does not apply in this case.

If there is no slip or partial slip at the surface, the rheological characteristics of the suspension play a large role in determining whether or not liquid-phase migration takes place. If our suspensions could be modeled approximately as a Bingham plastic, the work of Smyrnaios and Tsamopoulos (2001) would predict an unyielded region near the center of plates. In the unyielded region, where the radial velocity of the suspension as a whole is zero, the pressure gradient would cause the liquid phase to filter out. Eventually, the volume fraction of solids in the central region would be so high that the particles would jam. As squeezing continued the jammed structure would be disturbed and the particles would jam again at a lower plate separation.

2.4. Conclusions

The normal stress distribution for suspensions of glass spheres in a Newtonian fluid near their maximum packing fraction undergoing squeeze flow with a constant-force between a parallel circular disk and a large flat surface is qualitatively different from that for Newtonian fluids. The central region of high normal stresses may be due to migration of the liquid from the central region to the outer regions causing the formation of a highly viscous material with a yield stress in the central region.

It is well documented that the viscosity of suspensions is very sensitive to volume fraction and increases sharply near the maximum packing fraction. The normal stress distribution changes drastically in our suspensions with volume fractions beyond 0.55. At high concentrations, suspensions have a yield stress. It is possible that the yield stress causes the material near the middle of the top surface and of the bottom surface to remain unyielded during a squeeze test. At first these unyielded regions are separated by material

that deforms. As the squeeze test proceeds, the unyielded region on the top surface touches the unyielded region on the bottom surface and the particles jam. Particles of the suspension near the central region jam and the continued squeezing causes the liquid to migrate out of that region.

At lower concentrations the unyielded region does not form in the center of the plates because these suspensions have a small or no yield stress. On the other hand, at high concentrations, a small increase in the solid content in the central region as a consequence of liquid filtration can cause particle jamming in that region. This in turn causes a very large pressure gradient between the center and the outer region forcing the remaining suspending liquid out of that region, which results in an almost dry spot in the center of the disk.

The concentration gradient that results from accumulation of particles in the middle of the disk during the squeeze flow requires that the analysis take into account the time and position dependence of the rheological properties of the material. In these cases, assuming that the material is characterized by a rheological model with constant parameters is not sufficient.

CHAPTER 3

LIQUID PHASE MIGRATION IN SQUEEZE FLOW OF SUSPENSIONS

3.1.Theory of liquid phase migration

The dynamics of a suspension can be characterized by the momentum transport equation for the suspension as a whole and the continuity and transport equations for the solid phase. Darcy's law can be used to determine the particle flux and the relative velocity between the solid particles and the liquid. When inertial effects are negligible, the relative velocity, u_r, defined as the difference between the velocity of the solid, and the velocity of the liquid

$$u_r = u_f - u_s . \tag{3.1}$$

The relative velocity can be determined by Darcy's law,

$$u_r = -\frac{k}{\mu}\frac{\partial P}{\partial r} , \tag{3.2}$$

where k is the absolute permeability of the solids matrix, μ is the viscosity of the liquid, P is the isotropic fluid pressure (pore pressure), and φ is the solid volume fraction. Darcy's law is an expression of conservation of momentum and describes linearity between flow rate and applied pressure. Darcy's law is developed experimentally by Darcy; however, Darcy's law can also be derived from a spatial average of Stoke's equation (Whitaker 1986).

The absolute permeability of the solids matrix can be estimated, for example, from the Carman-Kozeny correlation (Li and Logan 2001),

$$k = \frac{D^2(1-\phi)^3}{180\,\phi^2} \tag{3.3}$$

The hydraulic conductivity of a solid matrix is denoted the permeability and it is typically used to provide an indication of the capacity of the solid matrix for allowing fluid to penetrate; a high permeability means a high throughput. The permeability typically ranges from 10^{-7} m^2 in very permeable materials, such as clean gravel, to 10^{-20} m^2 in materials, which are almost impermeable, such as concrete. The relative velocity is directly proportional to the permeability and the pressure gradient and inversely proportional to the liquid viscosity. The pressure profile for a Newtonian fluid in squeeze fluid is given by (Bird et al. 2002)

$$P(r) = \frac{2F}{\pi R^4}\left(R^2 - r^2\right). \tag{3.4}$$

where F is the applied force and R is the radius of the plate. Consequently the pressure gradient becomes:

$$\frac{\partial P}{\partial r} = -\frac{4F}{\pi R^3}. \tag{3.5}$$

Therefore, the pressure gradient is directly proportional to the combination F/R^3, which is constant in constant-force squeeze flow.

The relation between the applied force and the sample thickness for a Newtonian fluid is given by (Bird et al. 2002):

$$F = \frac{3\pi\mu V R^4}{2h^3}. \tag{3.6}$$

In our experimental set-up, the constant-force squeeze test can be divided into two steps: in the first step, the approach velocity is constant and the force increases until it reaches the desired value, F_1; in the second step, the force remains constant at the desired value and the velocity decreases. It is clear from Equation 3.6 that in the constant-velocity step the product Fh^3 is constant, so that

$$F_0 H_0^3 = F_1 H_1^3 \tag{3.7}$$

and

$$H_1 = H_0 \sqrt[3]{\frac{F_0}{F_1}} . \tag{3.8}$$

The thickness, H_1, at the time the force reaches the desired value is

$$H_1 = H_0 \sqrt[3]{\frac{3\pi\mu V_0 R^4}{2H_0^3 F_1}} , \tag{3.9}$$

and the time that takes to reach desire force becomes

$$t_1 = \frac{H_0 - H_1}{V_0} = \frac{H_0\left(1 - \sqrt[3]{\frac{3\pi\mu V_0 R^4}{2H_0^3 F_1}}\right)}{V_0} . \tag{3.10}$$

In Eq. 3.6, the velocity, V=-dh/dt, can be expressed in terms of thickness and then integrated from H_1 to the final thickness H_2 to find the time it takes to reach the final thickness,

$$t_2 = \frac{3\pi\mu R^4}{4F_1}\left(\frac{1}{H_2^2 - H_1^2}\right) . \tag{3.11}$$

Finally, the total squeeze time becomes

$$t = t_1 + t_2 = \frac{H_0\left(1-\sqrt[3]{\frac{3\pi\mu V_0 R^4}{2H_0^3 F_1}}\right)}{V_0} + \frac{3\pi\mu R^4}{4F_1}\left(\frac{1}{H_2^2 - H_1^2}\right). \tag{3.12}$$

3.2. Dimensional analysis

If we assume that for a suspension of spheres undergoing constant-force squeeze flow the fractional change in volume fraction at the center of the sample, $\Delta\varphi/\varphi_{\text{initial}}$, due to liquid-phase migration is a function of the initial solid volume fraction, φ, the applied force, F, the radius of the disk, R, the particle diameter, D, the viscosity of the suspending fluid, μ, the average squeeze velocity (found by dividing the difference between initial and final thickness of the sample by the squeezing time), V, yield stress, τ_0, and permeability, k, that is,

$$\frac{\Delta\varphi}{\varphi_{initial}} = g(\varphi, F, R, D, \mu, V_{ave}, \tau_0, k) \tag{3.13}$$

then, according to Buckingham's Pi theorem, these nine variables involving six dimensions can be related by three dimensionless groups, which we can choose as

$$\frac{\Delta\varphi}{\varphi_{initial}},\ \varphi,\ \frac{R}{D},\ \frac{k}{D^2},\ \frac{F}{\tau_0 D^2},\ f = \frac{\tau_0 D}{\mu V_{ave}}; \tag{3.14}$$

in what follows we will refer to f as the filterability number.

3.3. Experimental

3.3.1. Materials

Suspensions of various concentrations were prepared by mixing either glass or PMMA spheres in various Newtonian fluids (suspensions A through I in Table 3.1).

Table 3.1 Suspensions used

Suspension	$\varphi_{initial}$	μ (Pa·s)	D (μm)	Spherical particles	k (Eq. 3.3)* (m^2)
A	0.544	1.00	275	PMMA	1.35×10^{-10}
B	0.624	1.00	275	PMMA	5.74×10^{-11}
C	0.546	1.00	74	Glass	9.55×10^{-12}
D	0.618	1.00	74	Glass	5.12×10^{-12}
E	0.602	61.5	74	Glass	5.29×10^{-12}
F	0.482	327	74	Glass	1.82×10^{-11}
G	0.527	327	74	Glass	1.16×10^{-11}
H	0.563	327	74	Glass	8.01×10^{-12}
I	0.586	327	74	Glass	1.26×10^{-10}

* Obtained from Eq. 3.2

The average diameter of the glass spheres was 74-μm (determined with an Accusizer Model 780, Particle Sizing Systems, Santa Barbara, CA) and the diameter of the PMMA spheres varied between 250 and 300 μm as specified by the manufacturer (we use the middle value of 275 μm to describe these particles). The densities of the glass and PMMA spheres are 2,730 and 1,390 kg/m^3, respectively, determined using a pycnometer and water. The suspending fluids were Dow Corning 200 Fluids 300,000 and 60,000 cSt with viscosities of 327.5 Pa·s and 61.5 Pa·s, respectively, and silicone oil DC 200 (Fluka) with a viscosity of 1.0 Pa·s. Liquid viscosities were measured at 22°C in a Rheometrics Fluid Spectrometer RFS II. Figure 3.1 shows the viscosity of the suspensions with various solid volume fractions. The suspensions with volume fractions above 0.35 exhibited shear thinning.

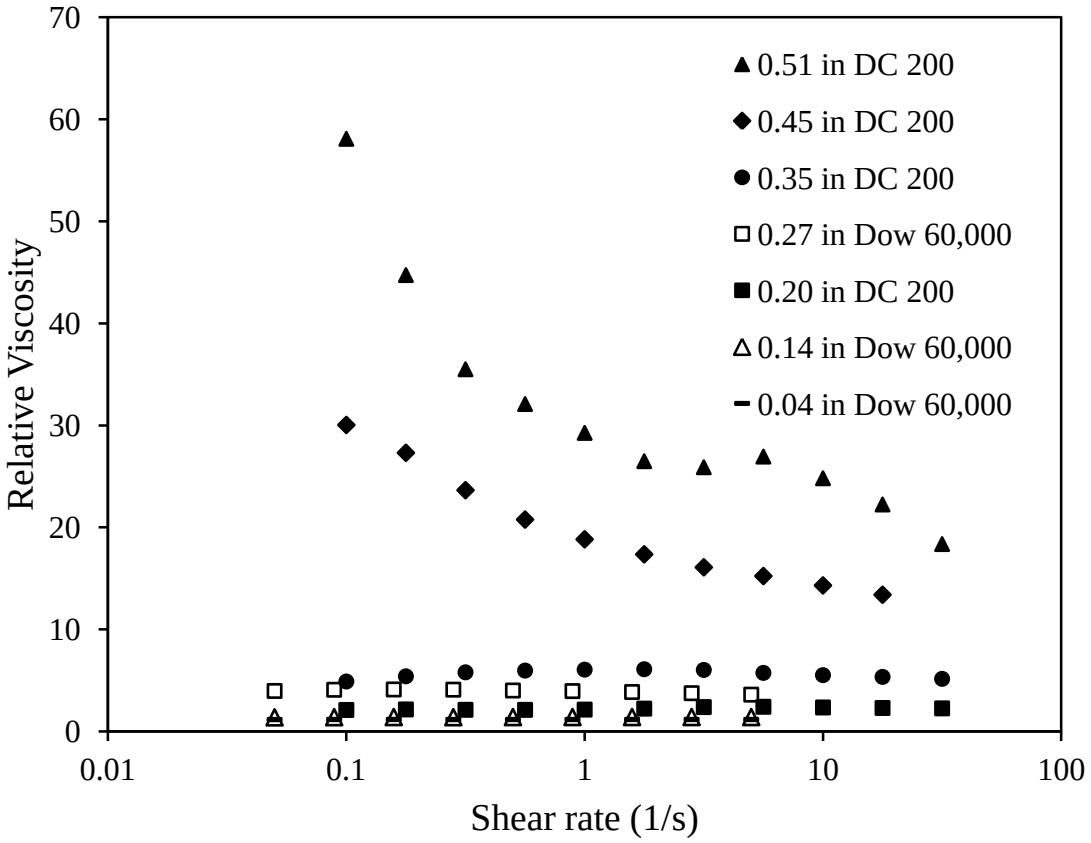

Figure 3.1 Measured relative viscosity of suspensions of 74-μm glass spheres in Dow Corning 200 Fluid 300,000 cSt with various different solid volume fraction

3.3.2. Equipment and procedure

The suspensions were squeezed between a circular Plexiglas disk, 3.5 in. (88.9 mm) in diameter, and a large Plexiglas plate in a hydraulic press (Technical Machine Products (TMP) Inc., Cleveland, OH). The Plexiglas disk and plate were covered with stainless steel foil, soft temper, type 304, 0.002 in. (0.051 mm) thick (McMaster-Carr Supply Company, Elmhurst, IL). The stainless steel foil kept the suspension separate from the pressure sensitive films in the experiments that mentioned in chapter 2 and it was used here to reproduce the same boundary conditions and make it easier to remove the surfaces

from the squeezed suspensions in order to obtain the samples needed to measure the volume fractions at various positions. The setup is shown in Figure 3.2.

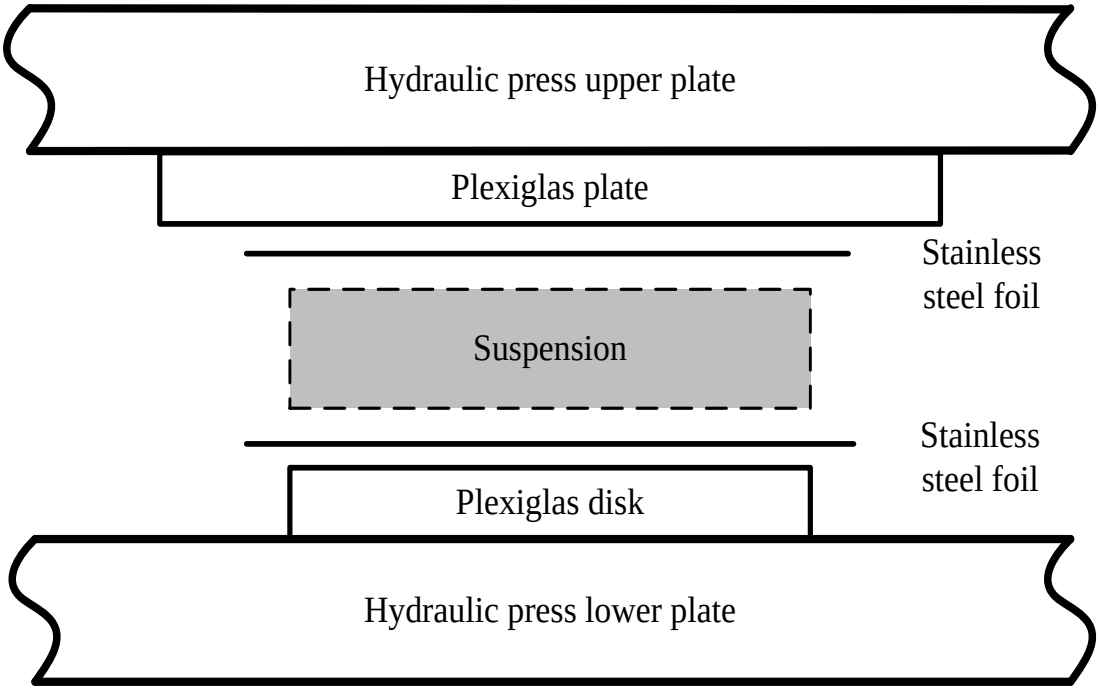

Figure 3.2 Schematic of the squeeze test setup

The top plate of the press was stationary and the bottom plate, on which the disk rested, moved up. In all experiments we applied a constant force of 4.45 kN to the suspensions except in one set of experiments in which we applied a force of 13.3 kN in order to match the conditions used to measure the normal stress distribution. It is worth noting that the bottom plate approaches the top plate at a constant velocity of 5 mm/s until the required force reaches the set point. After that, the force remains constant and the approach velocity changes with time in a way determined by the properties of the sample.

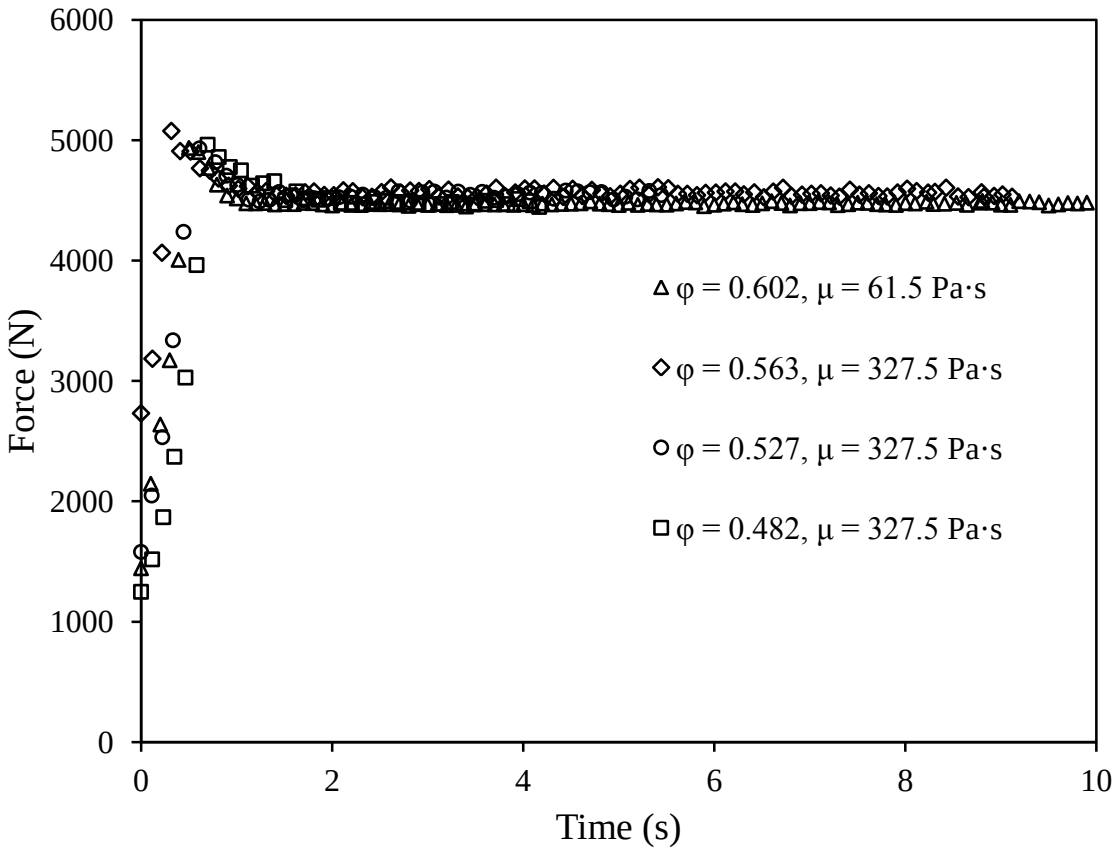

Figure 3.3 Measured force as a function of time for suspensions with different initial solid volume fractions of 74-μm glass spheres squeezed with a constant force of 4.45 kN

Figure 3.3 shows the force applied by the hydraulic press as a function of time for four suspensions of 74-μm glass spheres with different initial volume fractions squeezed to a desired constant force of 4.45 kN. In all cases, the desired constant force is reached in slightly more than 1 s. All samples filled the gap between the two plates at the start of the experiment. The initial thickness of the samples was 8 mm, and the tests stopped before the plate separation reached 1.5 mm.

Samples of the squeezed suspension were removed from three different radial positions by using a spatula and weighed. Then, the samples were washed five times with hexane in order to remove all of the suspending liquid. Finally, the washed particles were

dried in a vacuum chamber and weighed. The mass of the dry particles and the mass of the original suspension, together with the densities of the particles and of the fluid were used to calculate the volume fraction of solids in the suspensions. Except for the value at the center of the sample, the values reported for the volume fractions are the average of measurements on samples from three different locations at the same radial position; Figure 3.4 shows the positions from which the samples were taken.

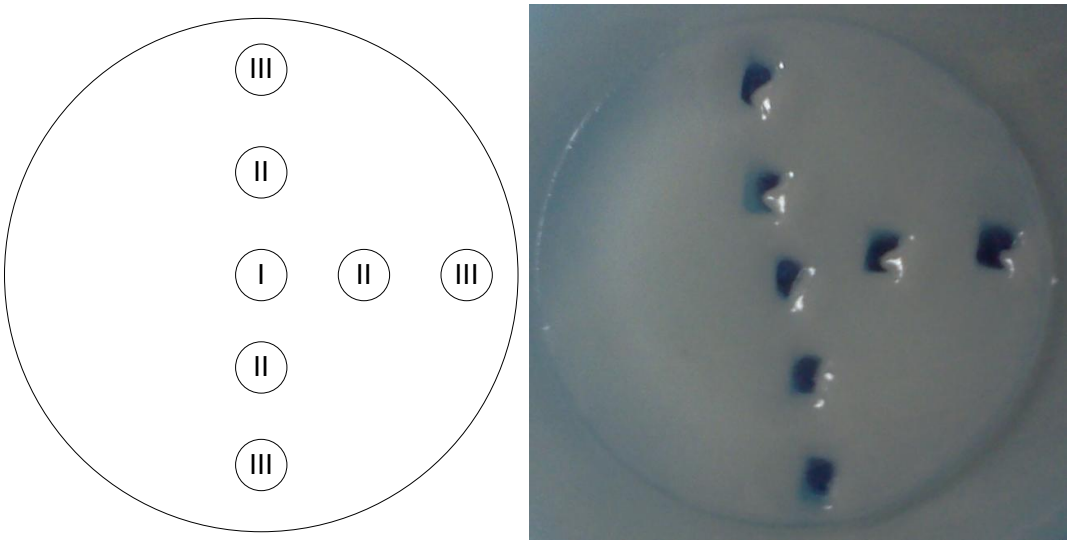

Figure 3.4 Diagram and photograph of a suspension after squeezing showing the positions at which samples were taken to measure the solid volume fraction

We determined the yield stress, τ_0, of our suspensions by measuring their final thickness, *h*, after squeezing them with a constant force using the following relation (Covey and Stanmore 1981), which is valid when there is no slip at the surfaces.

$$\tau_0 = \frac{3Fh}{2\pi R^3} \tag{3.15}$$

In order to measure the yield stress of the suspensions, they were placed between a circular disk on top and a larger disk below, and weights were placed on the top disk. Sand paper was glued to the surfaces of both disks to prevent slip. In order to prevent

liquid-phase migration when measuring the yield stress, the maximum squeeze force used to measure the yield stress was 30 N which is much smaller than the force in the squeeze flow tests used to determine the effect of liquid phase migration (4.45 kN). The lower squeeze force reduces the pressure gradient that causes liquid-phase migration. Also, the initial thickness in the yield stress measurements was less that 4 mm, which was about half the initial thickness of the suspensions used in the squeeze tests. Liquid-phase migration is less important when the plate separation is small because the final plate separation can be reached faster.

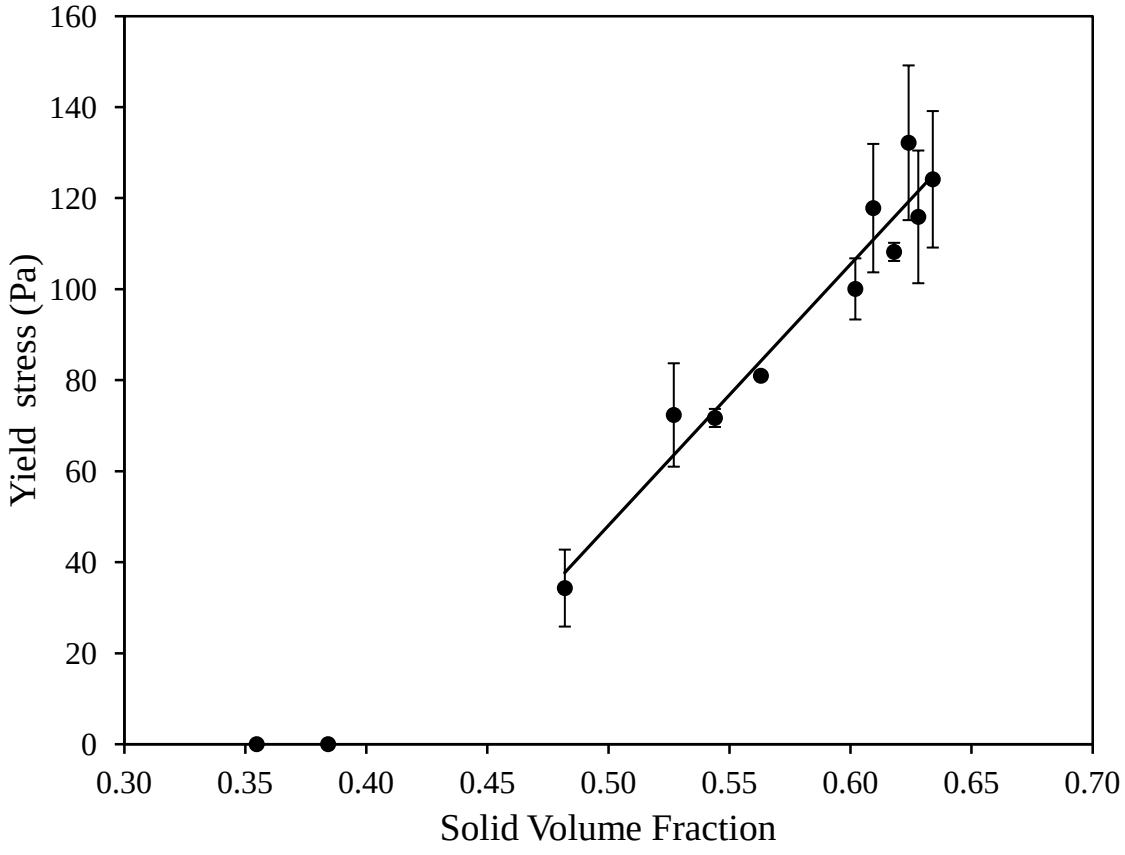

Figure 3.5 Yield stress of suspensions of 74-μm glass spheres in Dow Corning 200 Fluid 300,000 cSt with various solid volume fractions

Figure 3.5 shows the yield stress of our suspensions measured as described above. There was no observable yield stress at low volume fractions, but for volume fractions

between 0.48 and 0.63, the yield stress varied approximately linearly with volume fraction.

3.4. Results and Discussion

We prepared suspensions with different suspending fluid viscosities, particle sizes, and volume fractions in order to observe the effect of these parameters on the concentration profile due to liquid-phase migration during the squeeze flow. The list of suspensions used in our experiments is shown in Table 3.1.

3.4.1. Effect of initial solid volume fraction

In order to study the effect of the initial solid volume fraction on liquid-phase migration during squeeze flow, suspensions with four different initial solid volume fractions in Dow Corning 200 Fluid 300,000 cSt were subjected to squeeze flow (suspensions F through I in Table 3.1). Figure 3.6a presents the solid volume fraction profile after squeezing the suspensions with a force of 4.45 kN. The initial thickness of the suspensions was 8 mm and each test was stopped when the thickness had decreased to 1.5 mm. The volume fraction profiles for the suspensions with φ = 0.482 and 0.527 are almost flat at values close to the initial volume fractions. The volume fraction profile for the suspension with φ = 0.563 shows a slightly larger volume fraction near the center than near the edge, but the volume fractions everywhere are still not very different from the initial volume fraction. On the other hand, for the suspension with φ = 0.586, the volume fraction after squeezing is much larger at the center of the sample than near its edge, and the volume fraction is everywhere significantly higher than the initial volume fraction.

Figure 3.6b shows the normal stress distribution for four similar suspensions with initial solid volume fractions close to the suspensions in Figure 3.6a, squeezed for 35 s with constant force of 13.3 kN. The suspensions with φ = 0.453 and 0.516 have normal stress profiles very similar to that for Newtonian fluids. On the other hand, the suspensions with higher volume fraction have normal stress profiles with a prominent region in the middle of the disk in which the normal stresses are much higher than those predicted for Newtonian fluids. The normal stress distribution of the suspension with φ = 0.586 was very similar to that obtained when squeezing the particles without liquid.

Comparison of Figures. 3.6a and 3.6b leads to conclude that an increase in the volume fraction due to liquid-phase migration was the cause of the observed deviation of the normal stress profile from that for Newtonian liquids, and that at high volume fractions the loss of fluid led to jamming of the particles in the central region. The data obtained in the present work validate those conclusions.

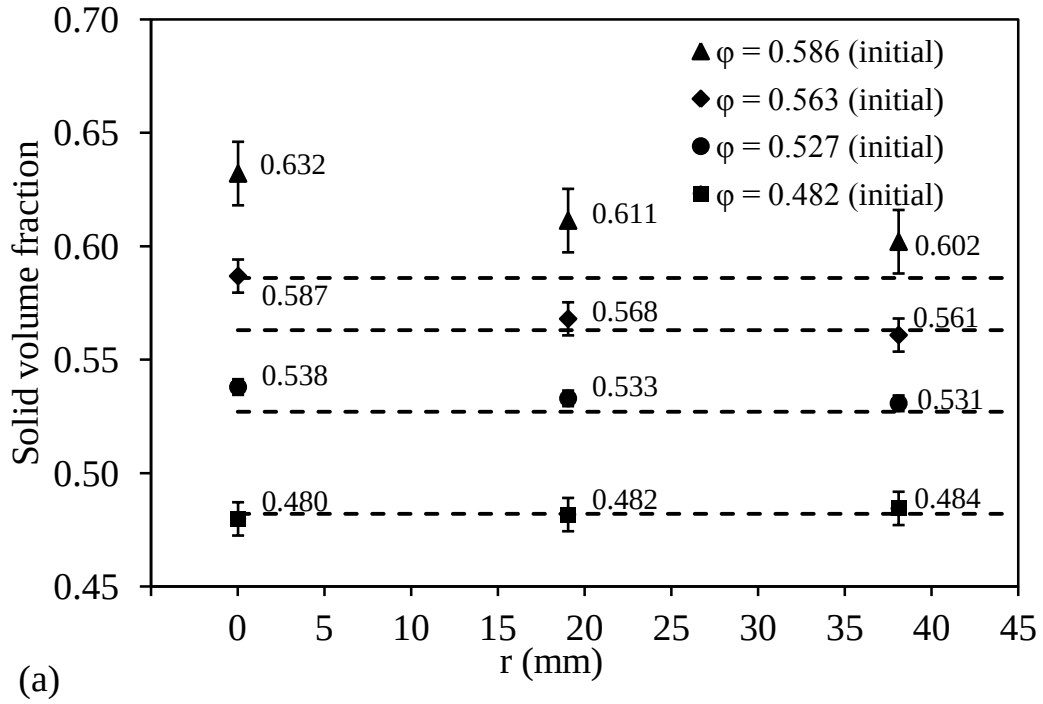

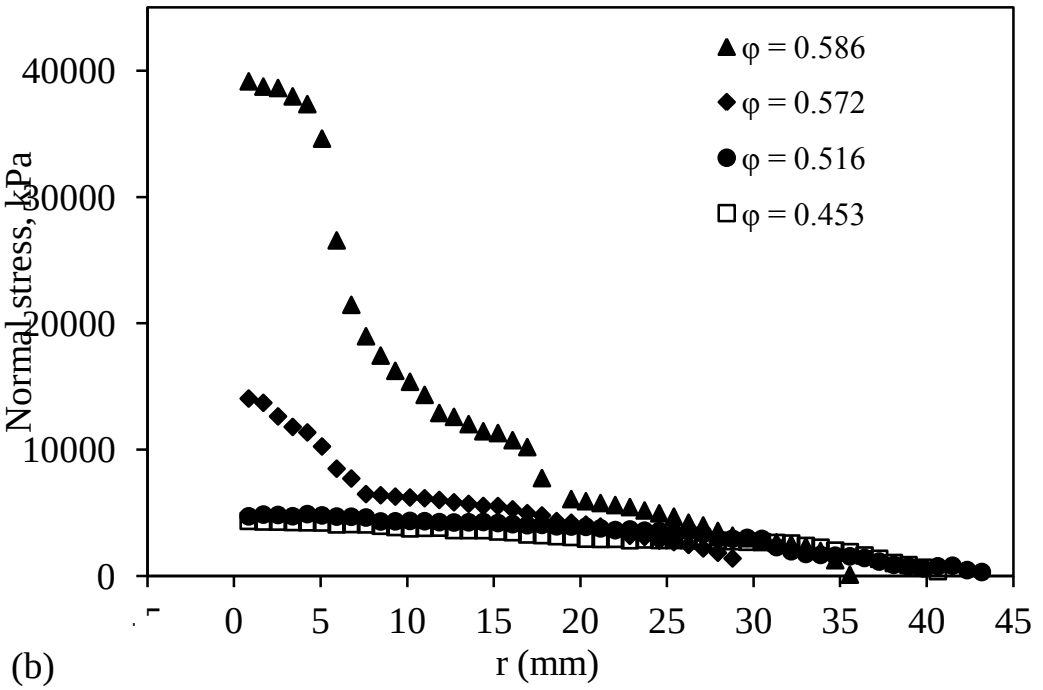

Figure 3.6 (a) Solid volume fraction distributions of suspensions with different initial solid volume fractions of 74-μm glass spheres in Dow Corning 200 Fluid 300,000 cSt squeezed with a constant-force of 4.45 kN from a thickness of 8 mm to a thickness of 1.5 mm (b) Normal stress distributions of suspensions squeezed with a constant force of 13.3 kN for 35 s

Figure 3.7 shows, for the suspensions used to obtain the data in Figure 3.6a, the plate separation as a function of time. The time required for the sample to be squeezed to a final plate separation of 1.5 mm is indicated by a circle at the end of each plot and varied from 4.1 s for the suspension with φ = 0.482 to 34.6 s for the suspension with φ = 0.586.

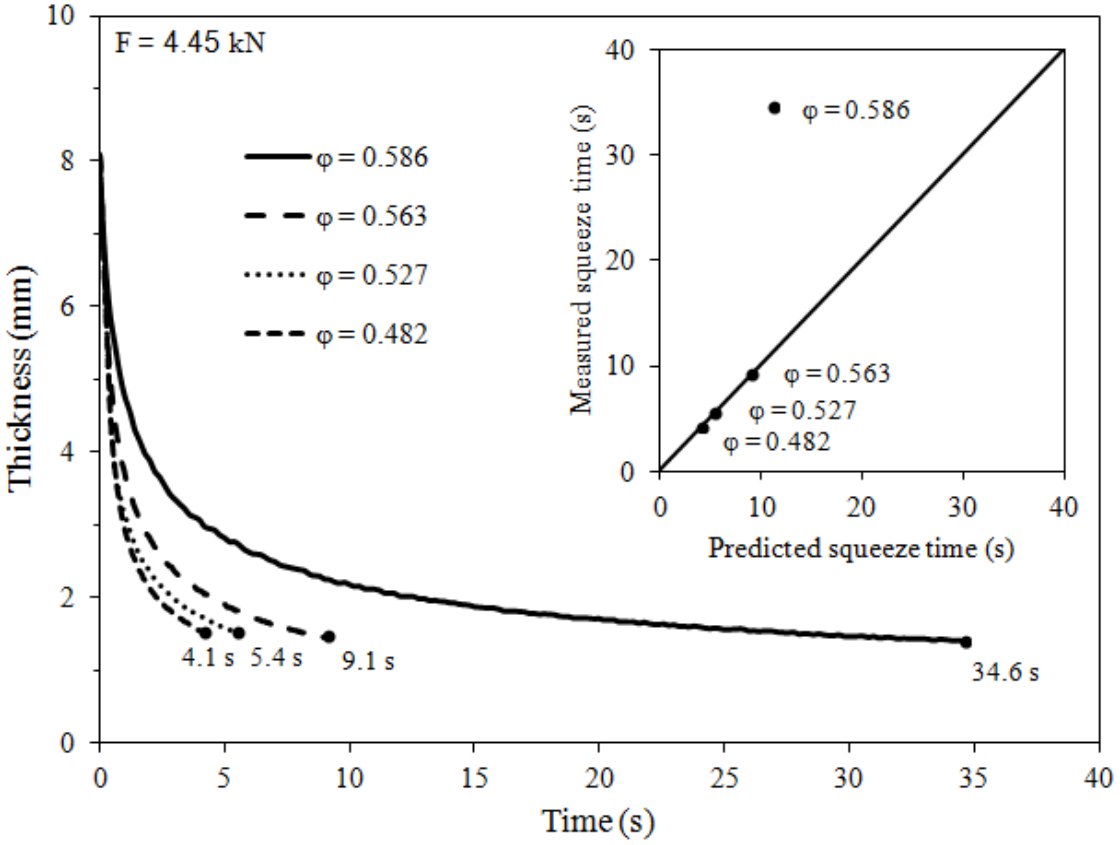

Figure 3.7 Plate separation as a function of time and estimated squeeze time (Eq. 15) for suspensions with different initial solid volume fractions of 74-μm glass spheres in Dow Corning 200 Fluid 300,000 cSt squeezed with a constant-force of 4.45 kN

Figure 3.7 also compares the squeeze time required for the samples to reach the final plate separation of 1.5 mm to the squeeze time predicted using Eq. 3.12, which applies to Newtonian fluids. The estimated time is close to the experimental time for suspensions with initial volume fractions of 0.563 or lower. For the suspension with φ = 0.586, the experimental time is much longer than the estimated time. This discrepancy may be

partly explained by liquid-phase migration during squeezing. The compaction and perhaps jamming of the particles in the central region would make it harder to squeeze the suspension and would cause a disproportionate increase in the squeeze time. The discrepancy between the measured and estimated squeeze times for the suspension with φ = 0.586 may also be due to the deviation of the rheological behavior of this suspension from that for Newtonian fluids. For the suspension with φ = 0.586, the plate separation was still above 1 mm after 600 s of squeezing, although Eq. 3.15 would have predicted a minimum plate separation of 0.4 mm if there had not been no liquid-phase migration and the boundary conditions had been those used to measure the yield stress.

The jamming of the particles in the central region due to the liquid-phase migration hinders the movement of the squeezing surfaces towards one another and may limit the minimum thickness that can be achieved by squeezing the suspension. This has implications for the minimum thickness that can be achieved in compression molded parts.

The enhancement of liquid-phase migration as the initial solid volume fraction increases may be attributed to an increase in the yield stress. Suspensions with larger yield stresses exhibit larger unyielded regions at the center of the disks when the suspensions undergo squeeze flow, and liquid is expelled from these regions under the influence of the pressure gradient between the central region and the edge.

3.4.2. Effect of squeeze force and squeeze time

In one experiment with the suspension of glass spheres in Dow Corning 200 Fluid 300,000 cSt (μ = 327.5 Pa·s) with a solid volume fraction of 0.586, we measured the

solid volume fraction distribution for various squeeze times under constant force. The results of this experiment (Figures. 3.8a and 3.9 for the applied forces of 13.3 kN and 4.45 kN, respectively) indicate that, as the squeezing proceeds, the solid volume fraction increases especially toward the center of the disk. Each curve represents a separate experiment. The difference between the solid volume fraction at the center of the disk and that at the edge increases with squeeze time. Figure 3.8b showed that under conditions similar to those used to generate the data of Figure 3.8a, as the squeeze test proceeds, the normal stress increases in the central region of the suspension while it decreases near its edge. The normal stresses in the central region deviate dramatically from the predicted stress distribution in Newtonian fluids, even after the first three seconds of squeezing, and continue to change as the squeezing proceeds.

The changes in the normal stress distribution occur in the same time frame as the changes in solid volume fraction, suggesting a correlation between liquid-phase migration and the changes in the normal stress profile. The normal stress distribution at very high concentrations is very close to the normal stress distribution of solid particles without fluid; therefore it seems that, due to liquid filtration, the solid volume fraction at the center of the disk reaches a critical concentration at which the particles jam. After jamming, the pressure at the center increases dramatically, setting up a huge pressure gradient between the central and outer regions, which would further boost the migration of the liquid phase away from the center.

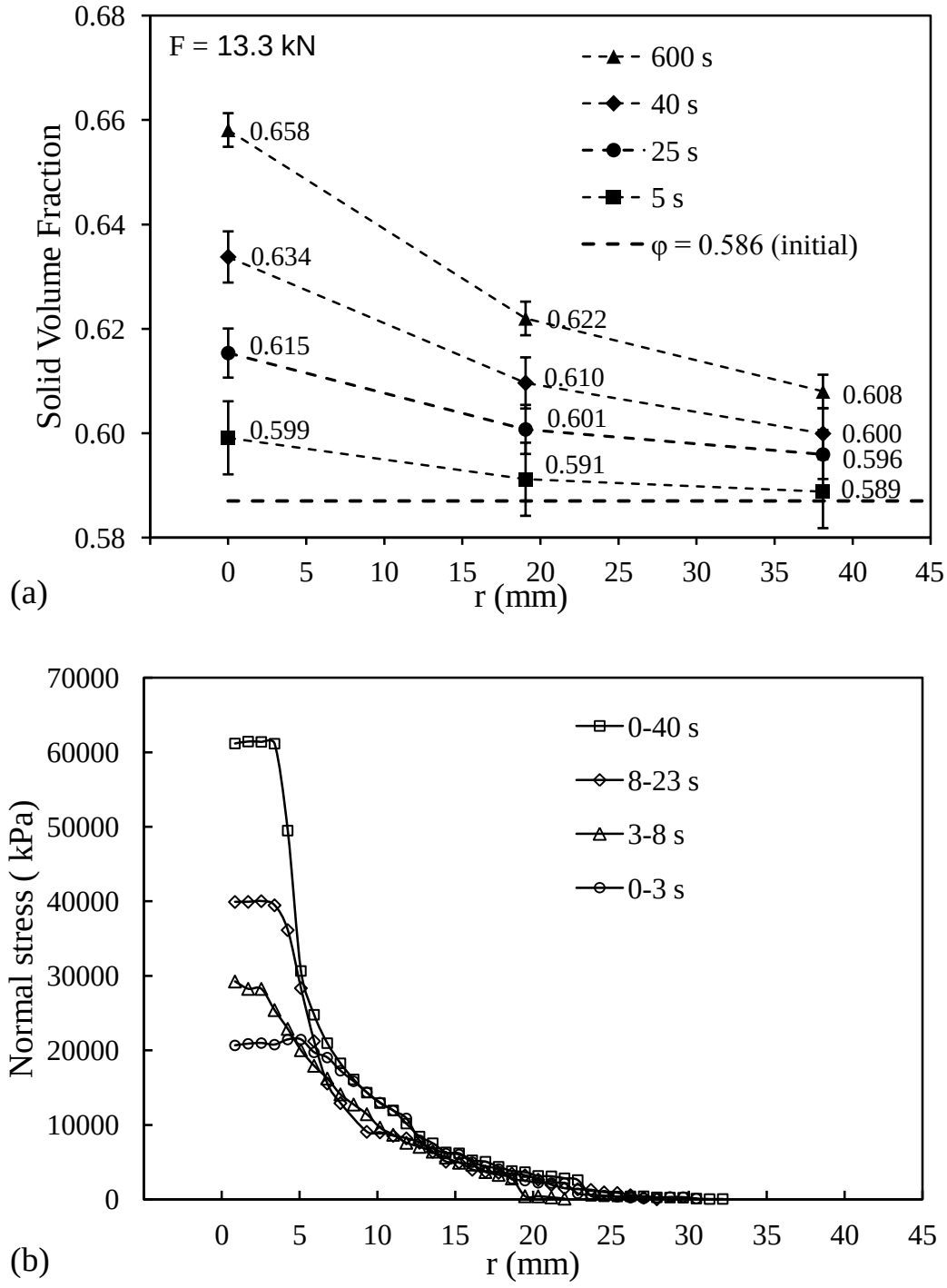

Figure 3.8 (a) Solid volume fraction distributions after various squeezing times for a suspension of 74-μm glass spheres in Dow Corning 200 Fluid 300,000 cSt with an initial volume fraction of 0.586 squeezed with a constant force of 13.3 kN. (b) Normal stress distributions at various times for the same suspension

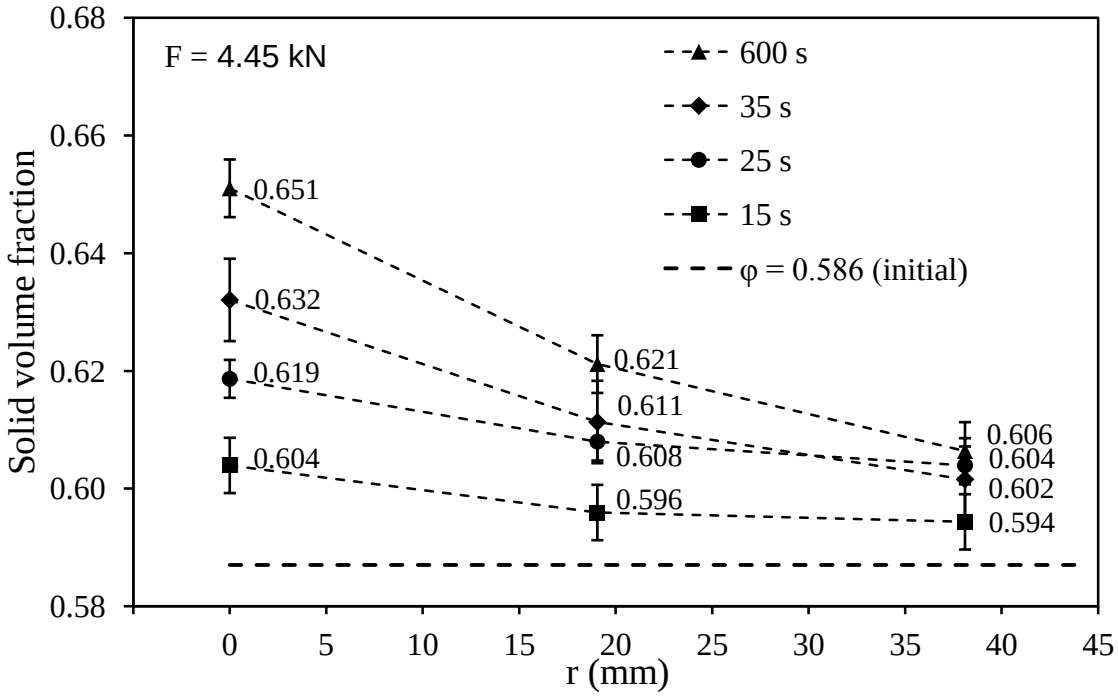

Figure 3.9 Solid volume fraction distributions after various squeezing times for a suspension of 74-μm glass spheres in Dow Corning 200 Fluid 300,000 cSt with an initial volume fraction of 0.586 squeezed with a constant force of 4.45 kN

The volume fractions measured using the two different forces, shown in Figures. 3.8a and 3.9, are quite similar, implying that, in this range, the applied force has little effect on the changes in volume fraction. This point is reinforced in Figure 3.10, which presents the solid volume fraction data of Figures. 3.8a and 3.9 as a function of squeeze time. There is very little difference between the data for the two applied forces. This can be explained in terms of the two competing effects on liquid-phase migration: a larger force creates a larger pressure gradient which boosts liquid-phase migration; on the other hand, the larger force also increases the approach velocity, allowing less time for the liquid to filtrate.

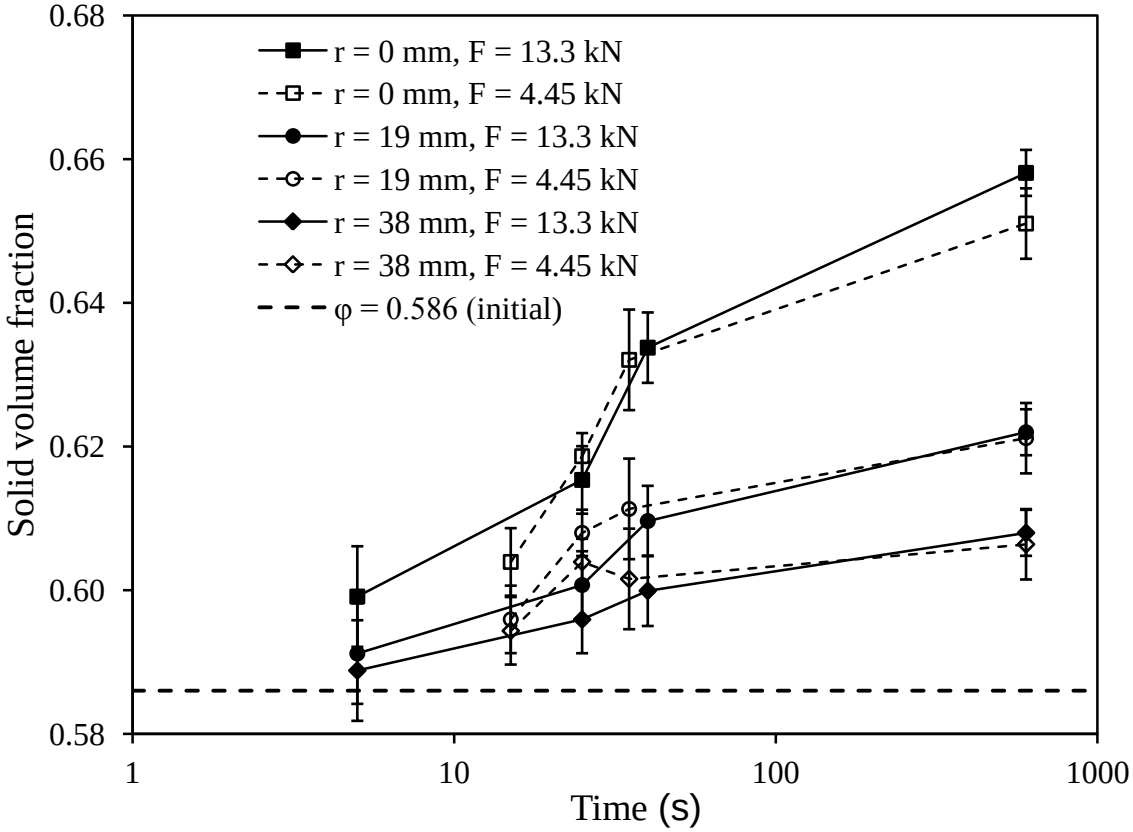

Figure 3.10 The data in Figures. 3.8a and 3.9 plotted as the solid volume fraction as a function of squeeze time at various radial positions. The suspensions consist of 74-μm glass spheres in Dow Corning 200 Fluid 300,000 cSt with a volume fraction of 0.586 squeezed with a constant force of either 4,450 or 13.3 kN

3.4.3. Visual observations

Figure 3.11 presents images of the suspensions with $\varphi = 0.563$ and $\varphi = 0.586$ squeezed for different periods of time with a constant force of 4.45 kN. These experiments were performed without the stainless steel foils, and the images taken through the top Plexiglas plate (refer to Figure 3.2). There was no significant change in the appearance of the suspension with $\varphi = 0.563$ after being squeezed up to 45 s. When this suspension was squeezed for longer periods of time there was so little suspension remaining between the plates that further observations were not pursued. For the suspension with $\varphi = 0.586$ the

increase in the volume fraction at the center was visually apparent after 35 s of squeezing and the central region was noticeably whiter and dryer after 600 s of squeezing. The Figure presents under each image a plot of the relative gray level as a function of position along a five pixel-wide horizontal strip going through the center of the sample. Each point on the plot is the average of the grey level of the five pixels at that horizontal position divided by the average gray level in the whole strip. In these images the diameter of the samples is about 800 pixels long. The relative gray level intensity is fairly constant for the suspension with $\varphi = 0.563$, but shows a peak at the center for the suspension with $\varphi = 0.586$ starting at a squeeze time of 35 s; this peak becomes more prominent as the squeeze time increases.

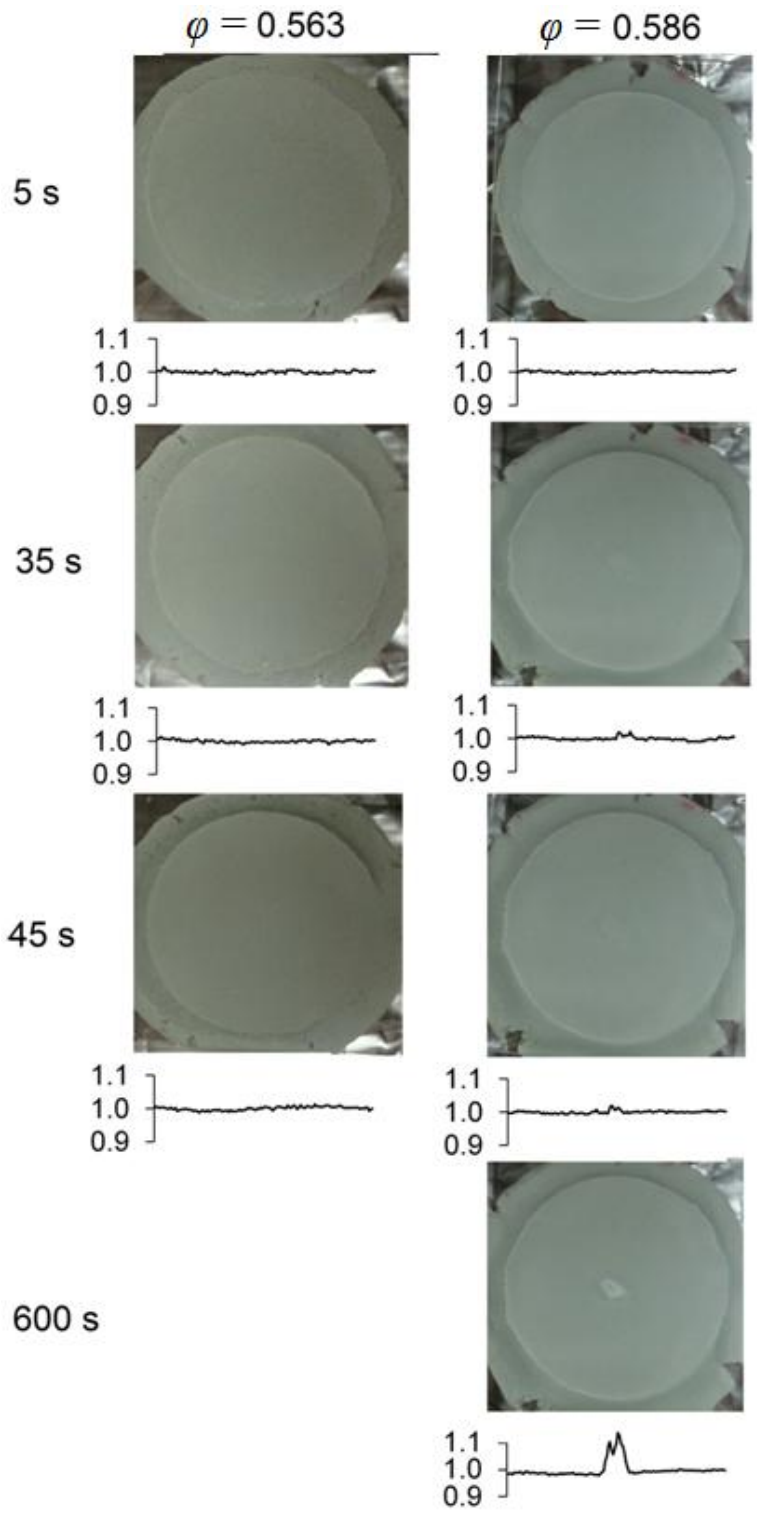

Figure 3.11 Images of suspensions of 74-μm glass spheres in Dow Corning 200 Fluid 300,000 cSt with volume fractions of 0.563 and 0.586 squeezed with a constant-force of 4.45 kN for different periods of time. Also shown are plots of

the relative gray level along a horizontal strip passing through the center of the samples

3.4.4. Effect of particle size

The measured concentration profiles after squeeze flow for suspensions with different particle sizes are shown in Figure 3.12. Suspensions of the 74-μm glass spheres and of the 275-μm PMMA spheres with volume fractions near 0.54 and 0.62 were used in these experiments. It is possible that the surface roughness of the two types of spheres was slightly different; if this affects the behavior, then these results will reflect that in addition to the effect of particle size.

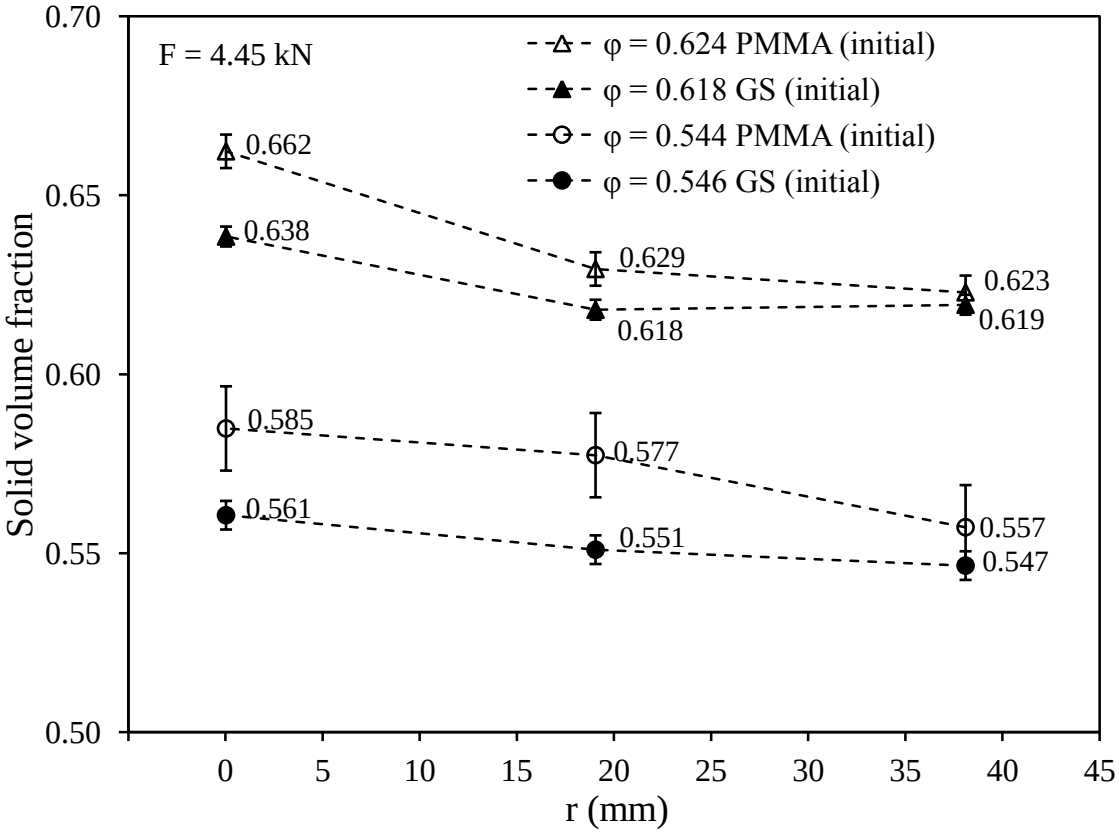

Figure 3.12 Solid volume fraction distributions of suspensions of 74-μm glass spheres and 275-μm PMMA spheres in silicone oil, μ = 1.00 Pa·s, squeezed with a constant-force of 4.45 kN from a thickness of 8 mm to a thickness of 2 mm

In these experiments, the squeezing force was 4.45 kN, the initial thickness of the suspensions was close to 8 mm, and the squeezing was stopped when the thickness reached 1.5 mm. In the suspensions with an initial volume fraction near 0.54, the volume fraction of the suspension of 74-μm glass spheres remained close to the initial value everywhere after squeezing. In contrast, the volume fraction of the suspension of 275-μm PMMA spheres was larger everywhere after squeezing, reaching 0.585 at the center. In the suspensions with an initial volume fraction near 0.62, the final volume fraction was larger than the initial volume fraction mostly near the center of the sample. The final volume fraction near the edge was very close to the initial volume fraction. At this volume fraction also, the effect is more pronounced in the suspension of 275-μm PMMA spheres than in the suspension of 74-μm glass spheres.

The effect of particle size on liquid-phase migration can be understood from Eq. 3.3; larger particles have larger permeability allowing the fluid to filter more easily through the network of the larger particles.

3.4.5. Effect of suspending fluid viscosity

Figure 3.13 shows the volume fraction profile after squeeze flow for suspensions with suspending fluids of different viscosities. The suspensions were made with the 74-μm glass spheres with an initial volume fraction close to 0.595. A constant force of 4.45 kN was applied to all suspensions. The initial thickness of the samples was 8 mm and squeezing was stopped when the thickness reached 2 mm. The suspending fluids were Newtonian silicone oils with viscosities of 1.0, 61.5 and 327.5 Pa·s. The increase in the volume fraction in the central region was highest for the suspension with the lowest

suspending fluid viscosity. This result is consistent with the theory because the flow rate of a fluid through porous media is inversely proportional to its viscosity according to Darcy's law (Eq. 3.2). Although the range of suspending fluid viscosities was large, the effect of fluid viscosity on liquid-phase migration was not as large as the effect of particle size or initial volume fraction. This is mainly because the time required to squeeze the suspension from a thickness of 8 mm to a thickness of 2 mm is shorter for the suspension with lower liquid viscosity; therefore, although liquid-phase migration is facilitated by the lower viscosity, the time during which it is allowed to take place is shorter because the sample reaches the final thickness faster.

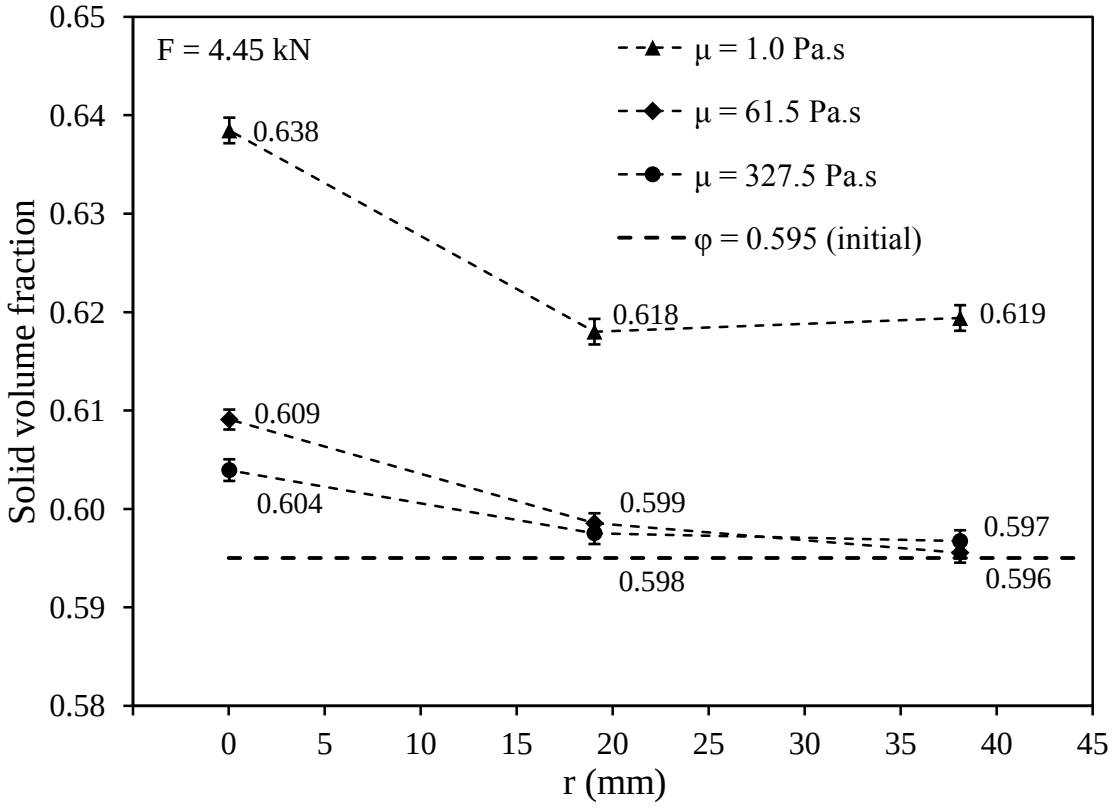

Figure 3.13 Solid volume fraction distributions of suspensions of 74-μm glass spheres with an initial volume fraction of 0.595 in three fluids of different viscosities squeezed with a constant-force of 4.45 kN from a thickness of 8 mm to a thickness of 2 mm

Figure 3.14 shows the fractional change in solid volume fraction at the center of the sample, $\Delta\varphi/\varphi_{initial}$, during squeeze flow as a function of the filterability number, f, (Eq. 3.14).

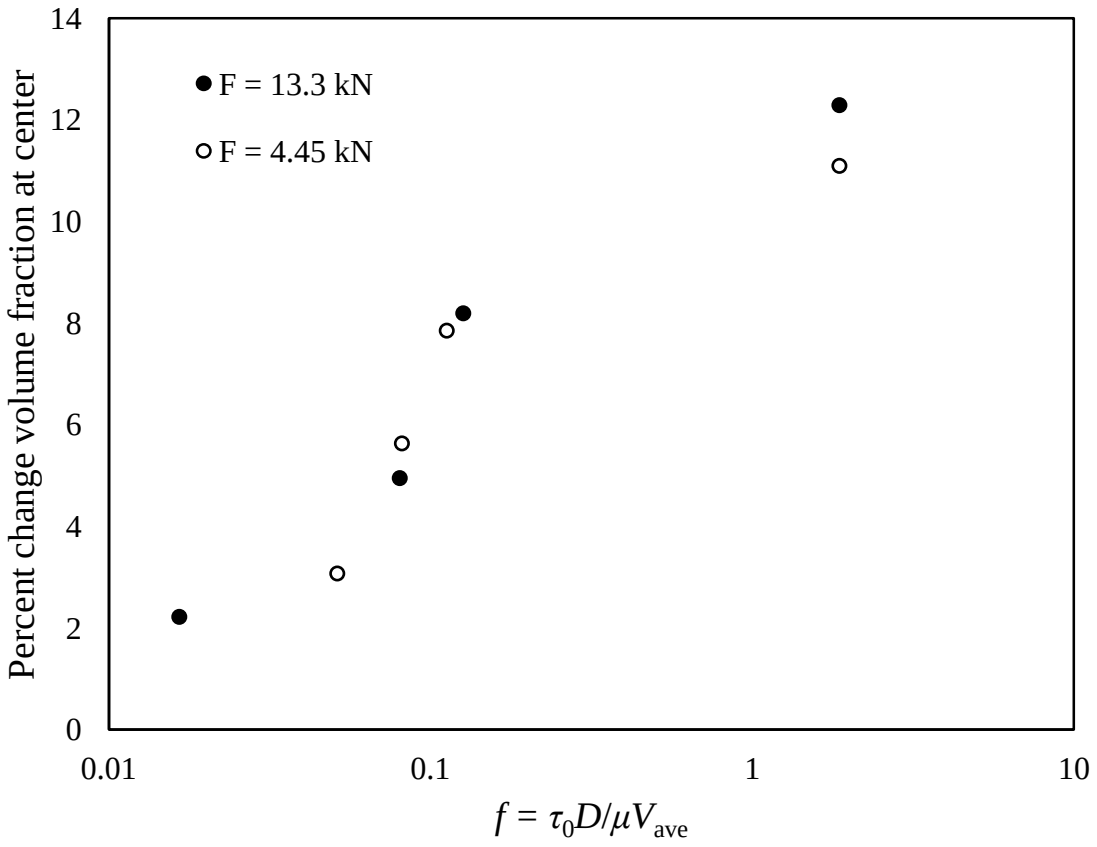

Figure 3.14 Fractional change in the solid volume fraction at the center of the sample after squeeze flow for suspensions with φ = 0.586 and different filterability numbers. The parameters for each data point are given in Table 3.2.

For all data points in this Figure the R/D, k/D^2, and $F/\tau_0 D^2$ ratios are constant. The parameters for each data point are given in Table 3.2. The data for the suspension with φ = 0.586 was obtained using the same suspending fluid viscosity; the changes in filterability number for this suspension are due to the use of different squeeze forces and different initial and final thicknesses, which affect the average squeeze velocity. Although there are some scatter in the data, for the suspensions with φ = 0.586 the

fractional increase in the solid volume fraction at the center increases with filterability number along a fairly well defined curve.

Table 3.2 Parameters for the data points in Figure 3.14

Suspension	$\varphi_{initial}$	h_{final} (mm)	t (s)	F (kN)	$F/\tau_0 D^2$	f*
I	0.586	1.7	5	13.3	2.63×10^{10}	0.0165
I	0.586	1.5	25	13.3	2.63×10^{10}	0.0801
I	0.586	1.4	40	13.3	2.63×10^{10}	0.1263
I	0.586	1.3	600	13.3	2.63×10^{10}	1.8656
I	0.586	1.9	15	4.45	8.81×10^{10}	0.0512
I	0.586	1.6	25	4.45	8.81×10^{10}	0.0814
I	0.586	1.5	35	4.45	8.81×10^{10}	0.1122
I	0.586	1.3	600	4.45	8.81×10^{10}	1.8656

* Obtained from Eq. 3.14

CHAPTER 4

NUMERICAL MODELING OF RADIAL FILTRATION

4.1. Theory

We model the dynamics of the suspension by solving the momentum transport equation for the whole suspension and the conservation of mass equation for the solid phase volume fraction. Constitutive equation for computing particle concentration and velocity fields consists of two parts: a non-Newtonian part in which the viscosity depends on the local particle volume fraction and a filtration equation that accounts for solid particle migration.

In the diffusion model we assumed that the liquid and solid phases are not in mechanical equilibrium, so their velocities can differ from each other and from the velocity of the suspension. In this model, the relative velocity, u_r, between the solid and liquid phases, is defined as,

$$u_r = u_f - u_s, \tag{4.1}$$

where u_f and u_s are, respectively, the velocities of the solid and the fluid and phases. u_r is assumed to obey Darcy's law,

$$u_r = -\frac{k}{\mu}\frac{\partial P}{\partial r} \tag{4.2}$$

where μ is the liquid phase viscosity, P is the pore pressure, and k is the absolute permeability of the solids matrix. The absolute permeability is estimated by using Carman-Kozeny correlation (Li and Logan 2001),

$$k = \frac{D^2(1-\varphi)^3}{180\varphi^2} \tag{4.3}$$

where φ is the solid volume fraction and D is the particle diameter. For an axisymmetric deformation of the suspension, when gravity is neglected, the equations for the conservation of momentum reduce to (Engmann et al. 2005)

$$\rho\left(\frac{\partial v_z}{\partial t} + v_r\frac{\partial v_z}{\partial r} + v_z\frac{\partial v_z}{\partial z}\right) = -\frac{\partial p}{\partial z} + \frac{1}{r}\frac{\partial(r\tau_{rz})}{\partial r} + \frac{\partial \tau_{zz}}{\partial r} \tag{4.4}$$

$$\rho\left(\frac{\partial v_r}{\partial t} + v_r\frac{\partial v_r}{\partial r} + v_z\frac{\partial v_r}{\partial z}\right) = -\frac{\partial p}{\partial r} + \frac{1}{r}\frac{\partial(r\tau_{rr})}{\partial r} + \frac{\partial \tau_{zz}}{\partial z} - \frac{\tau_{\theta\theta}}{r} \tag{4.5}$$

where the ρ is the density of the suspension, defined as

$$\rho = \varphi\rho_s + (1-\varphi)\rho_f \tag{4.6}$$

where ρ_s and ρ_f are, respectively, the densities of solid and fluid phases.

The conservation equation for the solid volume fraction can be expressed as

$$\frac{\partial \varphi}{\partial t} + \vec{v}\cdot\nabla\varphi = -\nabla\cdot N_s, \tag{4.7}$$

where the solid phase flux, N_s, can expressed as a function of relative velocity and the solid mass fraction, m_s,

$$N_s = u_r\varphi(1-m_s) \tag{4.8}$$

The viscosity of concentrated suspension was approximated by the Krieger (1972) correlation,

$$\mu_K = \mu_f \left(1 - \frac{\varphi}{\varphi_{\max}}\right)^{-2.5\varphi_{\max}} \tag{4.9}$$

where μ_K and μ_f are the viscosity of suspension and fluid respectively. φ_{max} is the maximum packing fraction and determined by fitting with the viscosity data, obtained experimentally. Figure 4.1 shows the dependence of the relative viscosity of the glass spheres suspensions on volume fraction and the fit to the Krieger correlation, using φ_{max} = 0.68.

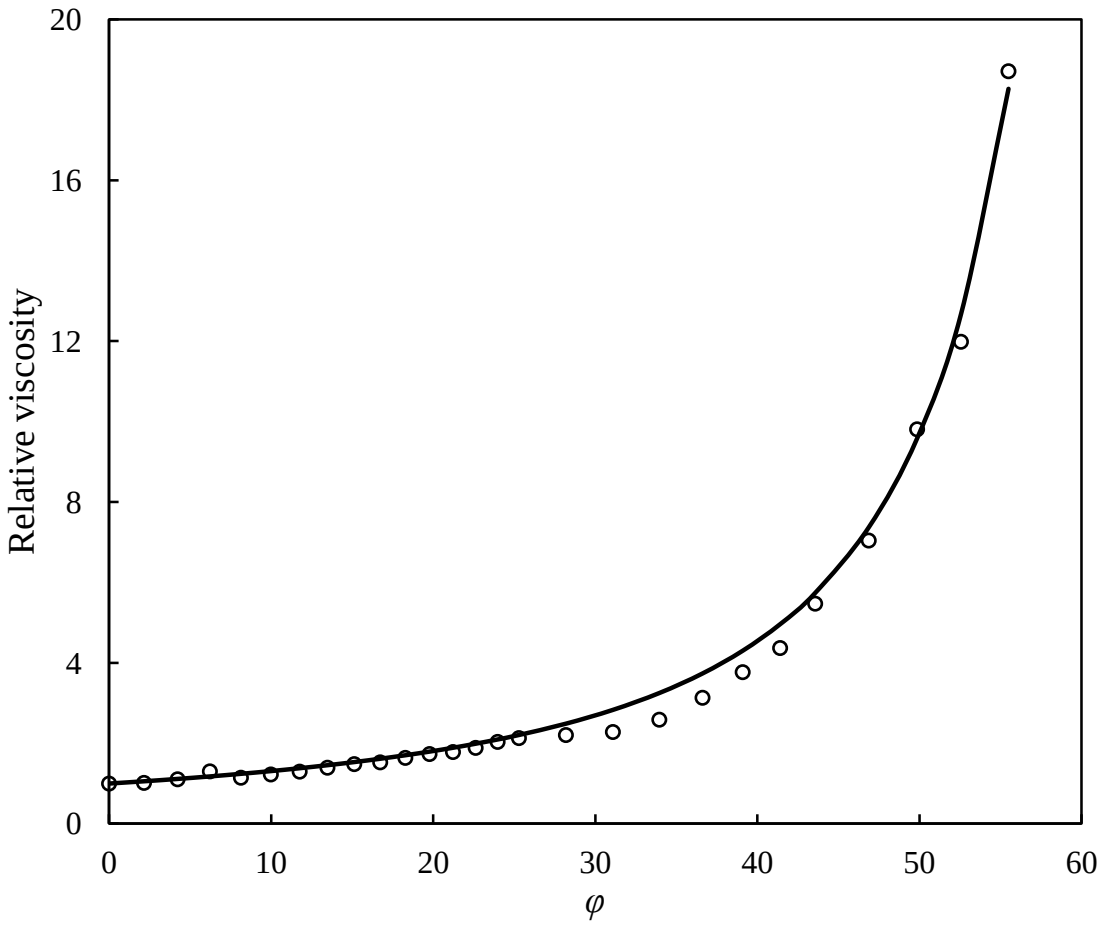

Figure 4.1 Measured relative viscosity of suspensions with different solid volume fractions

At volume fractions above 0.5, suspensions exhibit a yield stress (Mueller et al. 2010). This yield stress can change the velocity profile and cause the formation of an unyielded

region during squeeze flow (O'Donovan and Tanner 1984). In order to consider yield stress, τ_0, and have continuous conservation equations, we use the following exponential function for suspension viscosity, μ_s (Papanastasiou 1987).

$$\mu_{susp} = \mu_f \left(1 - \frac{\varphi}{\varphi_{\max}}\right)^{-2.5\varphi_{\max}} + \frac{\tau_0}{\dot{\gamma}}\left(1 - e^{-n\dot{\gamma}}\right) \tag{4.10}$$

where n is a constant. With a relatively large exponent, n, a quick stress growth (large viscosity) can be achieved at relatively very low strain rates, which is consistent with the behavior of the Bingham material in its practically unyielded state. Typically, a value of 100 for n is large enough to approximate the yield stress behavior (Ellwood et al. 1990). We used the value of n = 1000 in our model. The yield stress values in our model are extracted from experimental results (Figure 3.5).

To control the slip at surface we defined the slip parameter, δ, as follows (after Laun et al. 1999)

$$\delta = \frac{h v_{slip}}{(-V) r} \tag{4.11}$$

Here v_r is the radial slip velocity at the plate which increases linearly with radius and V is the approaching velocity. The value of δ varies from 0 for no slip to 0.5 for perfect slip at surfaces. The value of slip parameter can be determined either by the slip test or by fitting the force versus time result from squeeze test.

The numerical solutions were obtained with COMSOL Multiphysics version 4.1 (COMSOL, Inc., Burlington, MA), using as the primary variables the two velocity components, v_r and v_z, the solid-phase volume fraction, φ, and the pressure, p. Due to symmetry, just half of the cross section is modeled. The mesh was triangular with 2,420 elements as shown in Figure 4.2, with a finer mesh used close to the boundaries. The

largest elements were 0.70 mm long (at the upper and lower surfaces) and the smallest elements were 0.32 mm long (at the axis and at the edge). It is worth noting that the meshing deformed as the upper boundary moved down while the lower boundary remained stationary.

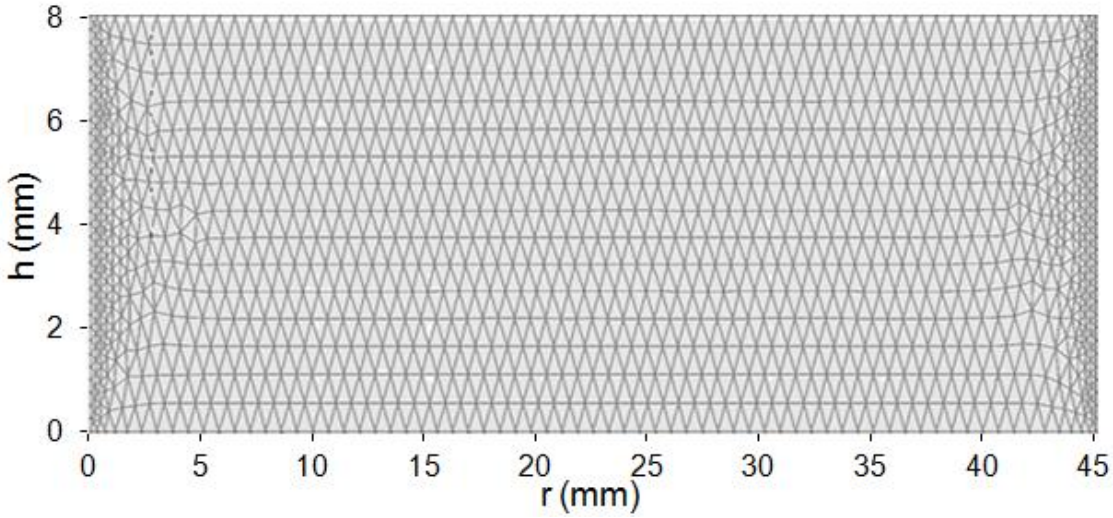

Figure 4.2 Finite-element mesh used to model the squeeze flow

The direct (MUMPS) linear system solver of COMSOL Multiphysics was chosen because it was faster and more stable that the other solvers available.

4.2. Boundary conditions

The boundary conditions for the system shown in Figure 4.3 are:

(1) Symmetry along axis AB: $v_r = 0$, $\partial P/\partial r = 0$

(2) Slip along the stationary bottom wall BC: $v_r = v_{slip}$, $v_z = 0$

(3) Atmospheric pressure along edge CD where suspension exits: $P = 0$

(4) Slip along the moving top wall DA: $v_r = v_{slip}$, $v_z = -V$

The approach velocity, *V*, is constant during the constant velocity stage, before the force reaches the set value. Subsequently, in the constant force stage, the approach velocity is determined in such a way that the following constrain along DA is maintained:

$$F = \int_0^R 2\pi\tau_{zz} r dr \tag{4.12}$$

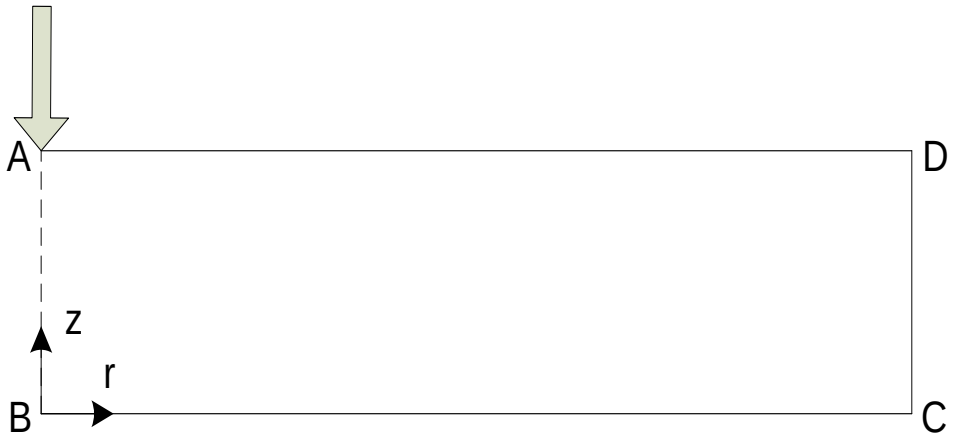

Figure 4.3 Nomenclature for the coordinates and boundaries

4.3.Experimental

Suspensions of various concentrations and with two different particle sizes were prepared by mixing glass spheres and PMMA in silicone oils with different viscosities. The suspending fluids were Dow Corning 200 Fluid 300,000 and 60,000 cSt with viscosities of 327.5 Pa·s and 61.5 Pa.s, respectively, and silicone oil with a viscosity of 1.0 Pa·s. Fluids viscosity was measured at 22°C (the temperature near which all experiments were conducted) with a Rheometrics Fluid Spectrometer RFS II and suspensions viscosity was measured with a NDJ-8S digital viscometer at constant shear rate of 10 s^{-1}. The suspensions were squeezed between a circular Plexiglas disk, 3.5 in.

(88.9 mm) in diameter, and a large Plexiglas plate in the hydraulic press (Technical Machine Products, Cleveland, OH) with a constant force of 4,450 N. All samples filled the gap between two plates at the start of the experiments. The initial thickness of the samples was 8 mm, and the tests were stopped before the thickness reached to 1 mm. The particle average diameter of the glass beads used was 74 μm and their density was determined to be 2,730 kg/m^3. PMMA microspheres with the diameters between 250 and 300 microns were used in some suspensions.

It is worth noting the bottom plate approaches the top plate at a constant velocity until the required force reaches the set point. After that, the force remains constant and the approach velocity changes with time in a way determined by the properties of the sample.

Samples from three different radial positions of the squeezed suspension were weighted. Then, the samples were washed with hexane to dissolve the silicone oil. The washing was repeated 5 times in order to remove all of the silicone oil. Finally, the particles were dried in a vacuum chamber and weighted again. To get the average concentration throughout the squeezed suspension, we took the samples from three different points with the same radius and averaged the concentrations.

4.4. Results and Discussion

In order to validate the model we used it to analyze the constant-force squeeze flow of a Newtonian fluid between two parallel disks and compared the thickness and pressure profile predicted by our model to those of the analytical solution by Laun et al. (1999).

Figure 4.4 shows the thickness as a function of time predicted by our numerical model for constant-force squeeze flow of a Newtonian fluid with a viscosity of 1000 Pa·s, squeezed for 1 s with a constant force of 50 N between two parallel disks with a radius of 44.45 mm (1.75 in.) which initially are 20 mm apart. Results for three degrees of slip (as defined by eq. 4.11) are presented: no-slip (δ = 0), intermediate slip (δ = 1/4), and perfect slip (δ = 1/2).

Also presented in the Figure are the predictions of the analytical solution by Laun et al. (1999):

$$F = -\frac{3}{2}\frac{V\pi\mu R^4}{h^3}\left[(1-2\delta)+\frac{h^2}{R^2}(1+2\delta)\right], \tag{4.13a}$$

where

$$V = -\frac{dh}{dt}, \tag{4.13b}$$

is the approach velocity. This expression includes, as special cases, the previously reported solutions for no-slip and perfect slip, and does not require the ratio h/R to be small (lubrication approximation).

The analytical solution is an ordinary differential equation for h, for which there is no explicit solution. Therefore, it was solved numerically using Euler's method.

The predictions of our numerical model are in close agreement with those of the analytical solution.

Figure 4.5 presents the predictions of our numerical model for the same fluid in the same set up, but only for the case of no slip at the plates. Also presented are the predictions of the analytical solution by (Laun et al. 1999);

$$P = -\frac{3V\mu R^2}{h^3}\left[(1-2\delta)\left(1-\frac{r^2}{R^2}\right)+\frac{h^2}{2R^2}\left(1+\frac{2}{3}\delta\right)\right] \tag{4.14}$$

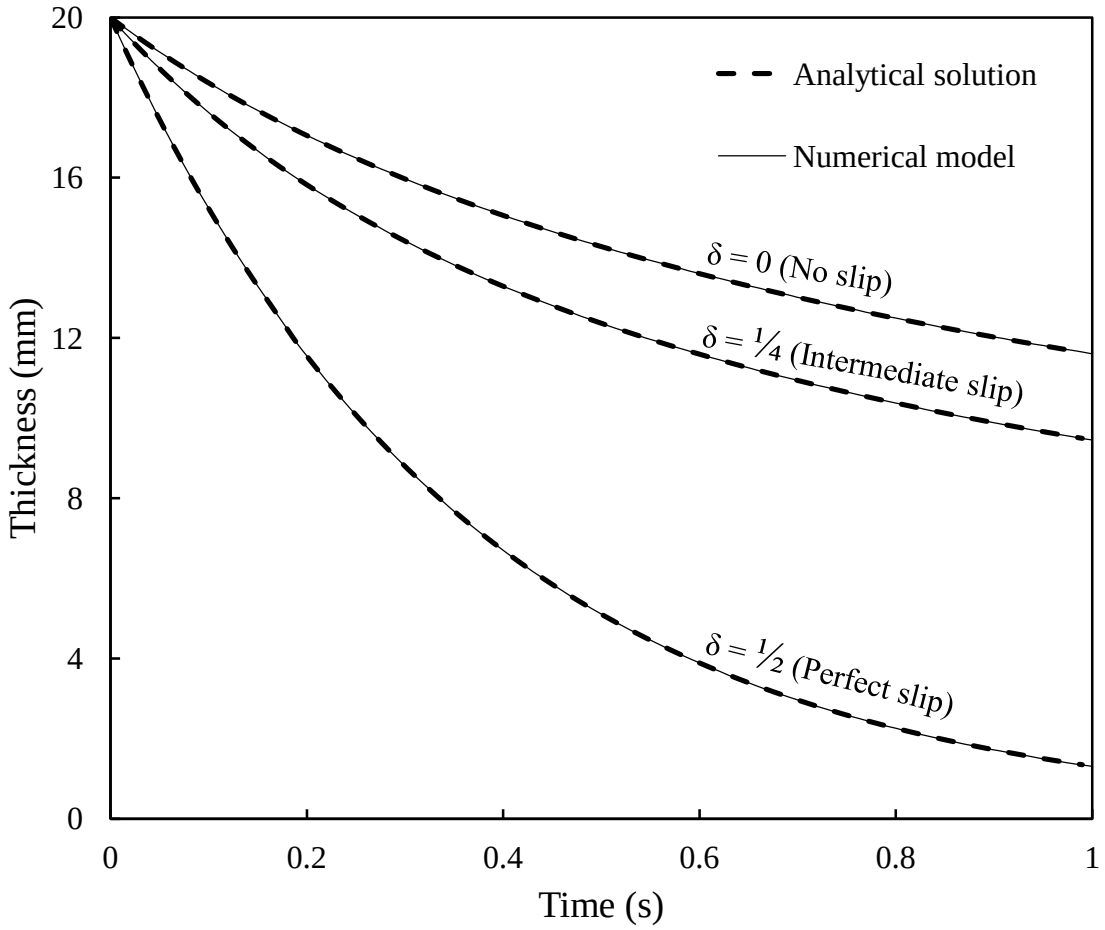

Figure 4.4 Comparison of the thickness of the sample as a function of time predicted by our numerical model to the analytical solution by Laun et al. (1999) of a Newtonian fluid with a viscosity of 1000 Pa·s, squeezed for 1 s with a constant force of 50 N between two parallel disks with a radius of 44.45 mm

Note that when h/R is very small, and there is no slip (δ = 0), we obtain the well known result (see for example Bird, et al. 2002)

$$P = -\frac{3V\mu}{h^3}(R^2 - r^2) \tag{4.15}$$

Again, the predictions of our numerical model are in close agreement with those of the analytical solution.

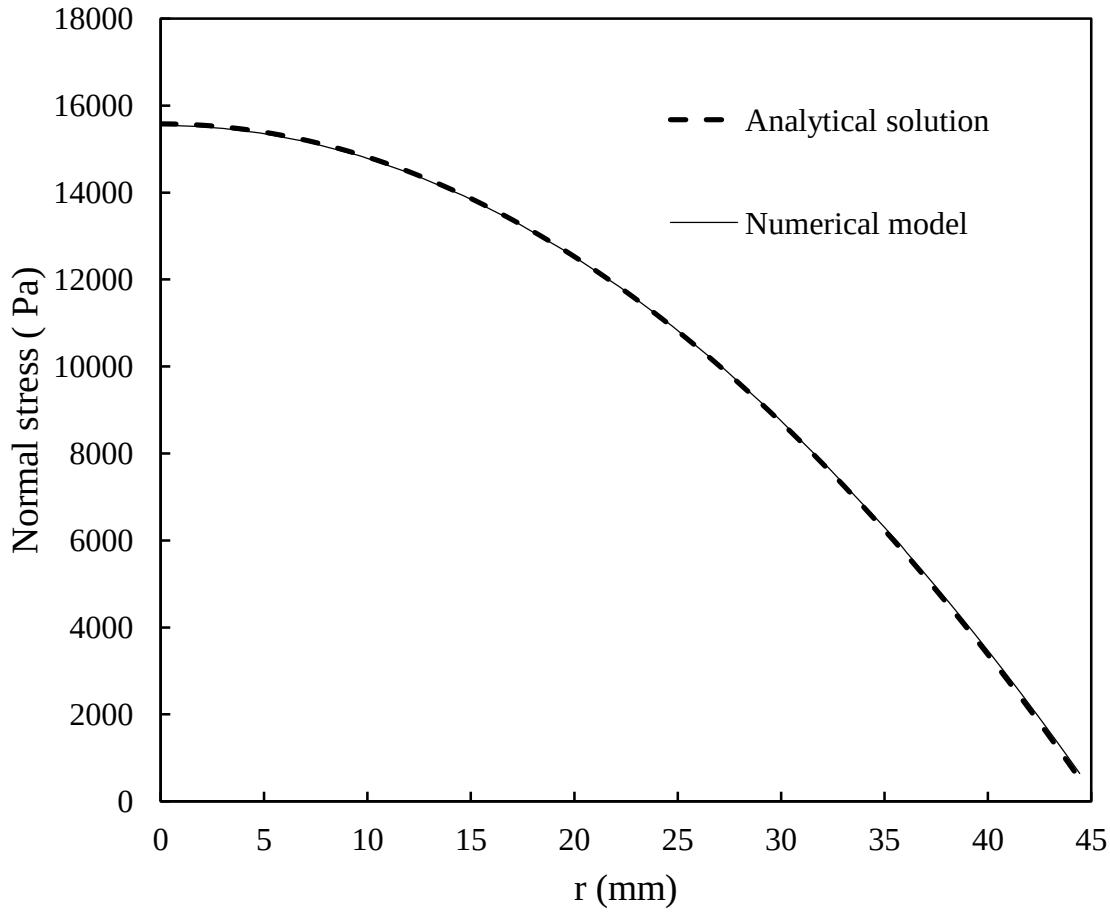

Figure 4.5 Comparison of the pressure profile predicted by our numerical model to the analytical solution by Laun et al. (1999) of a Newtonian fluid with a viscosity of 1000 Pa·s, squeezed for 1 s with a constant force of 50 N

Figure 4.6 shows the force applied by the hydraulic press as a function of time for the squeezing of four suspensions of 74 μm glass spheres with different initial volume fractions when the force is set to 4,450 N. The suspensions were squeezed from a thickness of 8.0 mm to thickness of 1.5 mm. In the first stage of the squeeze test the

lower plate rises at a constant velocity of 5 mm/s and the force increases sharply toward the set point. In all of experiments a small overshoot of the force was observed due to the pressure control system of the press. In the second stage, the press keeps the force constant at the set point and the velocity varies depending on the properties of the sample being squeezed. The model takes into account the two stages of the squeeze flow test in order to imitate the experimental conditions. We calculate the total force by integrating the pressure profile on the top plate using Eq. 4.12. The lines through data points in Figure 4.6 represent the result from our squeeze flow model. The model predictions agree well with the experimental measurements.

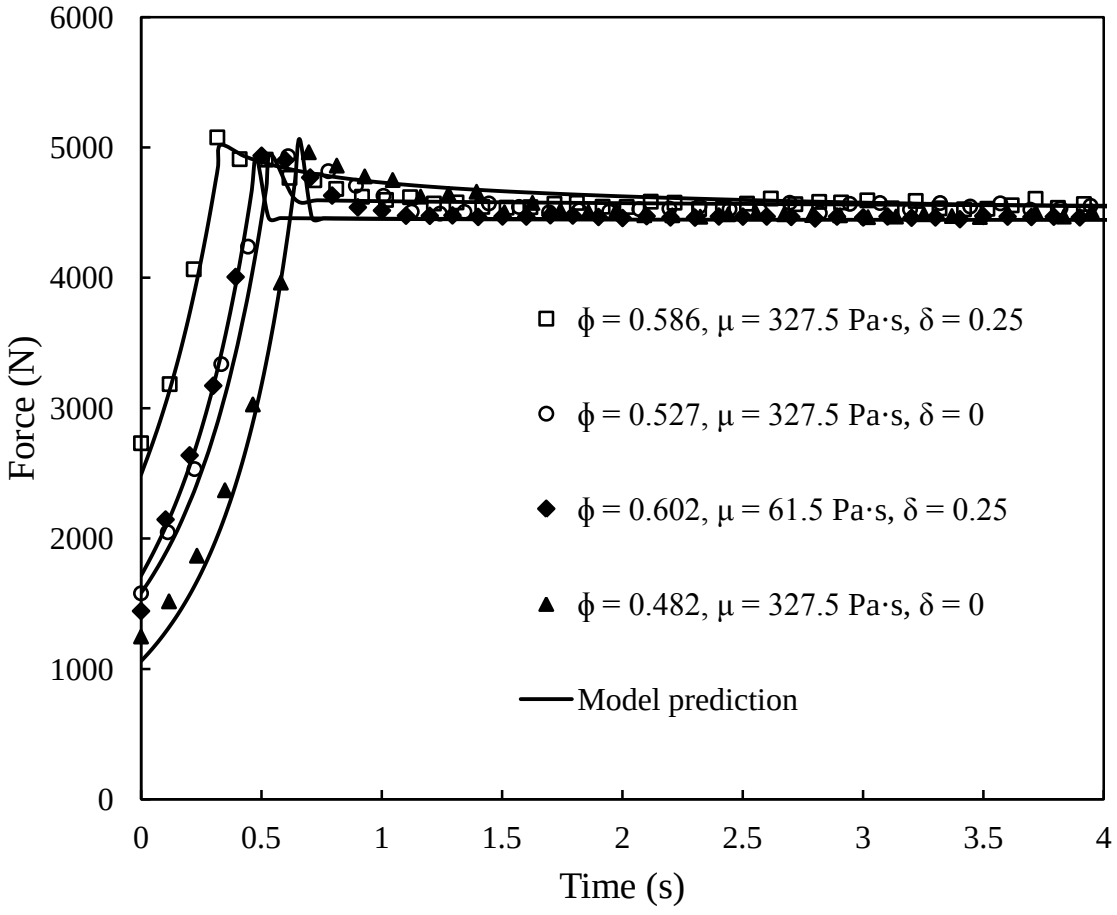

Figure 4.6 Measured force as a function of time and the result of fitting model prediction by changing slip parameter for suspensions with different initial solid

volume fractions of 74-μm glass spheres in Dow Corning 200 Fluid 300,000 cSt squeezed with a constant force of 4,450 N

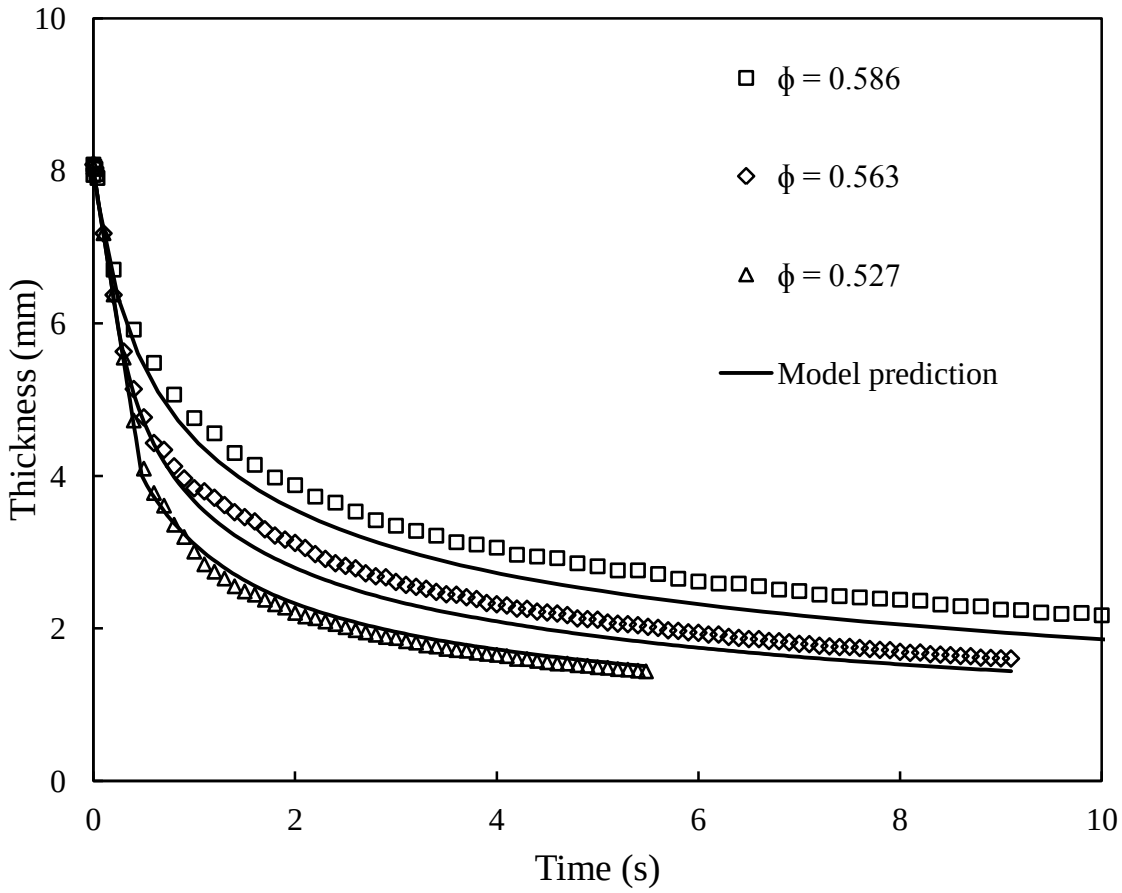

Figure 4.7 Comparison of the measured gap as a function of time with the prediction of model for suspensions with different initial solid volume fractions of 74-μm glass spheres in Dow Corning 200 Fluid 300,000 cSt squeezed with a constant force of 4,450 N

Figure 4.8 compares the result of the solid volume fraction profile predicted by our model to the experimental measurements for four different suspensions with volume fraction between φ = 0.482 and 0.586 squeezed with a constant force of 4,450 N from a thickness of 8.0 mm to a thickness of 1.5 mm. Experimental and modeling results shows that the deviations from the initial solid volume fraction increase with solid volume fraction and that the deviation is greater in the central region. Modeling confirmed that

liquid-phase migration is more prevalent at higher concentrations, that the solid volume fraction increases throughout the sample, and that concentration profile is almost flat except at the central region, where there is a sharp increase in solid volume fraction. The reason of increasing solid volume fraction at the central region is due to formation of unyielded region at this region.

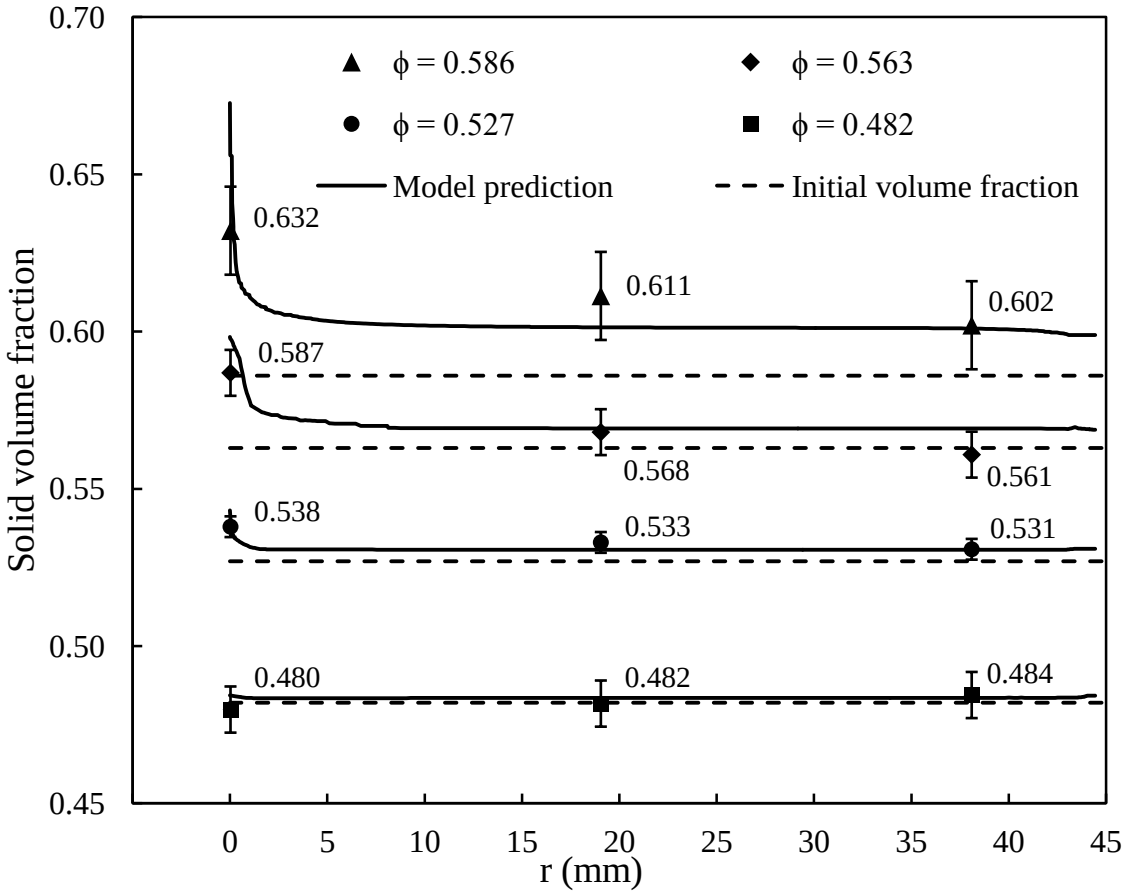

Figure 4.8 Experimental and model prediction of the solid volume fraction distributions of suspensions with different initial solid volume fractions of 74-μm glass spheres in Dow Corning 200 Fluid 300,000 cSt squeezed with a constant force of 4,450 N

Figure 4.9 compares the solid volume fraction distributions predicted by our model after various squeeze times to the experimental measurements for the suspension with φ =

0.586 squeezed with a constant force of 4,450 N. The solid volume fraction throughout the sample increases with squeezing time exhibiting a sharp peak at the center. The volume fraction everywhere in the sample was higher than the initial volume fraction in all cases. The data point at the center is the average volume fraction of a region with a radius of 2.5 mm centered at the axis; the small horizontal lines in the Figure show the predicted average volume fractions for this region. The agreement between the model predictions and the experimental measurements is fair.

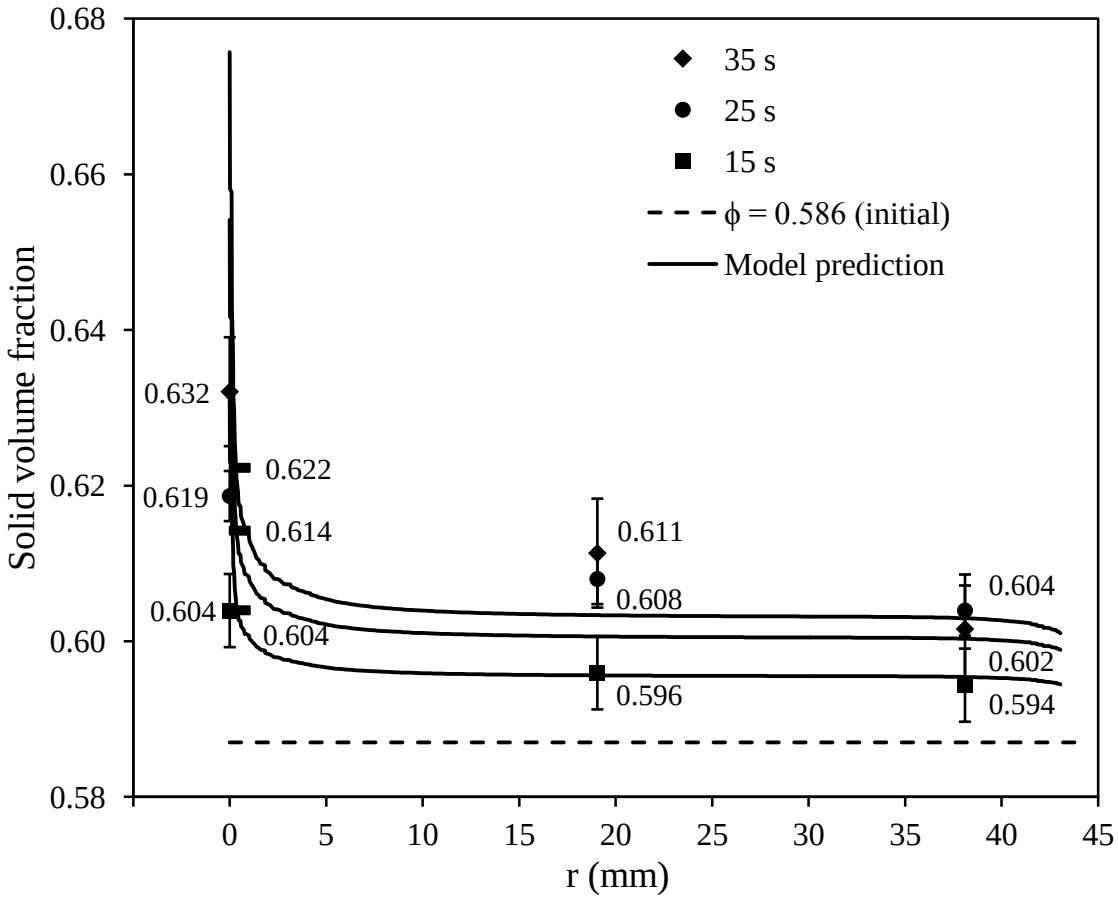

Figure 4.9 Experimental and model prediction of the solid volume fraction distributions after various squeezing times for a suspension of 74-μm glass spheres in Dow Corning 200 Fluid 300,000 cSt with a volume fraction of 0.586 squeezed with a constant force of 4,450 N

The effect of suspending fluid viscosity is shown in Figure 4.10, where we compare the volume fraction distributions predicted by the model to the experimental results for three suspensions with $\varphi = 0.595$ with suspending fluids with viscosities of 1.0, 61.5, and 327.5 Pa·s after they have been squeezed with a constant force of 4,450 N from a thickness of 8 mm to a thickness of 2 mm. The increase in the solid volume fraction is becomes more pronounced as the suspending fluid viscosity decreases, a trend that the model predicts very well.

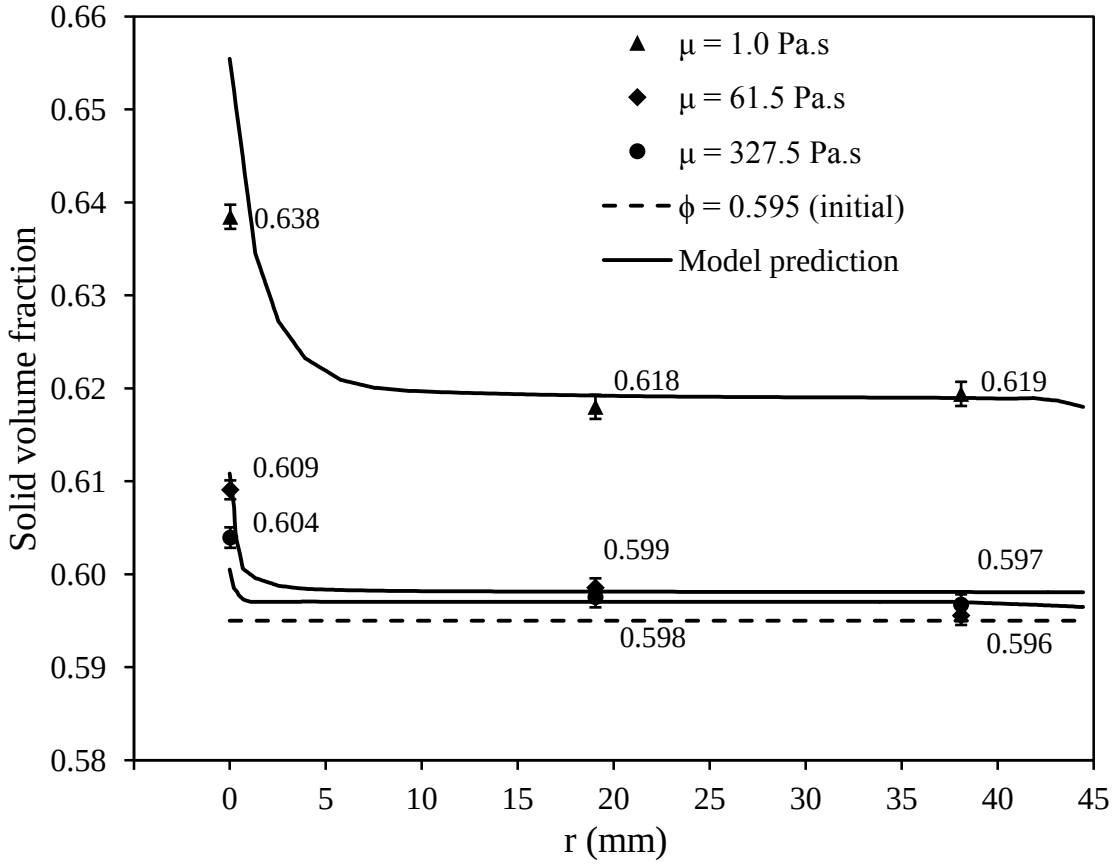

Figure 4.10 Experimental and model prediction of the solid volume fraction distributions of suspensions of 74-μm glass spheres in three different suspending fluids squeezed with a constant-force of 4,450 N from a thickness of 8 mm to a thickness of 2 mm

The effect of yield stress on liquid-phase migration is shown in Figure 4.11. We model the squeeze flow of a suspensions with φ = 0.560 and yield stress of 0, 10, and 100 Pa squeezed with constant force of 4,000 N when the thickness decreases from 8 mm to 1 mm. The suspending liquid viscosity is assumed to be 50 Pa·s. The time required to squeeze the suspensions does not vary significantly in this range of yield stress, varying from 5.15 s for the suspension without yield stress to 5.64 s for the suspension a yield stress of 100 Pa. The solid volume fraction profiles of the squeezed suspensions in the outer region are almost equal but there is a large difference in the solid volume fraction at the central region due to the formation of the unyielded region. For the suspension with a yield stress of 100 Pa, the solid volume fraction has two maxima because the liquid filtrates out of the central region very quickly and decreases the solid volume fraction in the region adjacent to it.

Figure 4.12 shows that radial velocity at h = 0.5 mm and parallel to the plates for the suspensions in Figure 4.11 after 5 s of squeezing. The radial velocity for the suspension with a yield stress of 100 Pa is negligible for r < 3 mm due to the unyielded region so the difference between liquid radial velocity and suspension radial velocity is higher for this suspension.

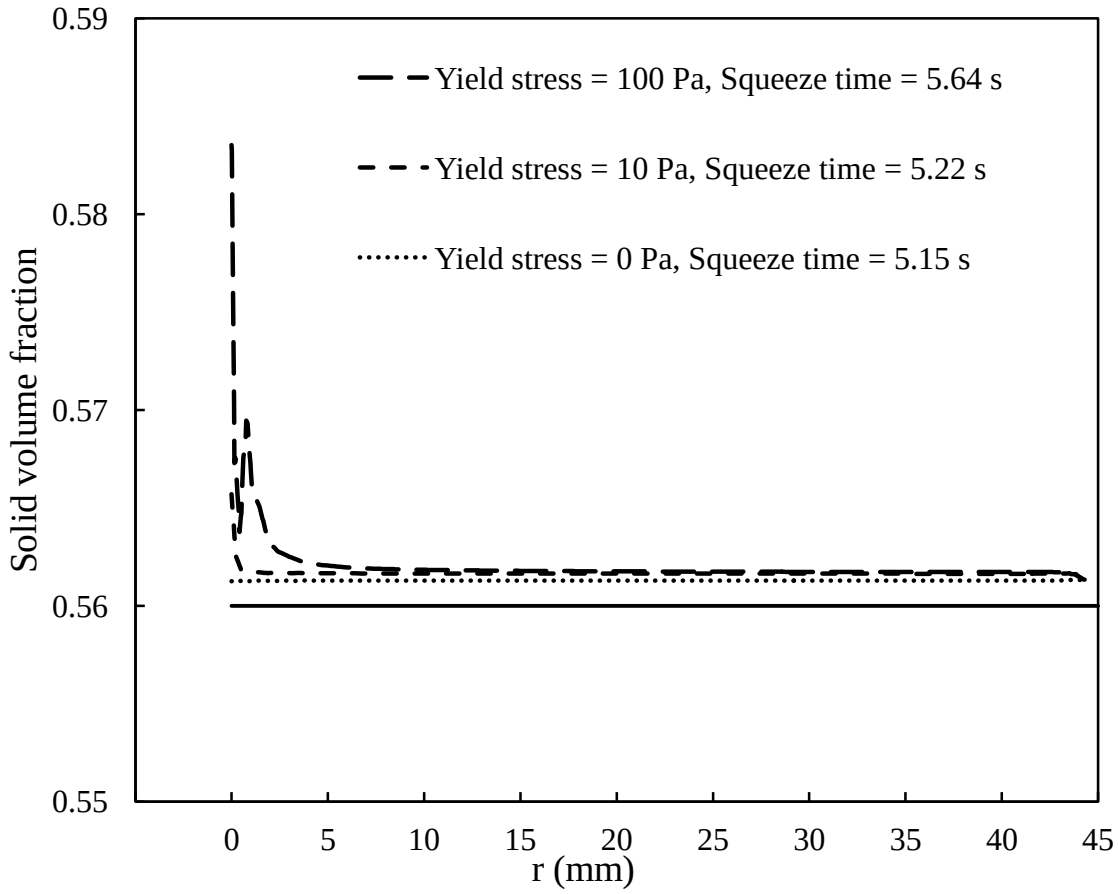

Figure 4.11 Model prediction of the solid volume fraction distributions of suspensions with different yield stress and φ = 0.560 of 74-μm glass spheres in a Newtonian fluid with μ = 50 Pa·s squeezed with a constant force of 4,000 N from thickness of 8 to 1 mm

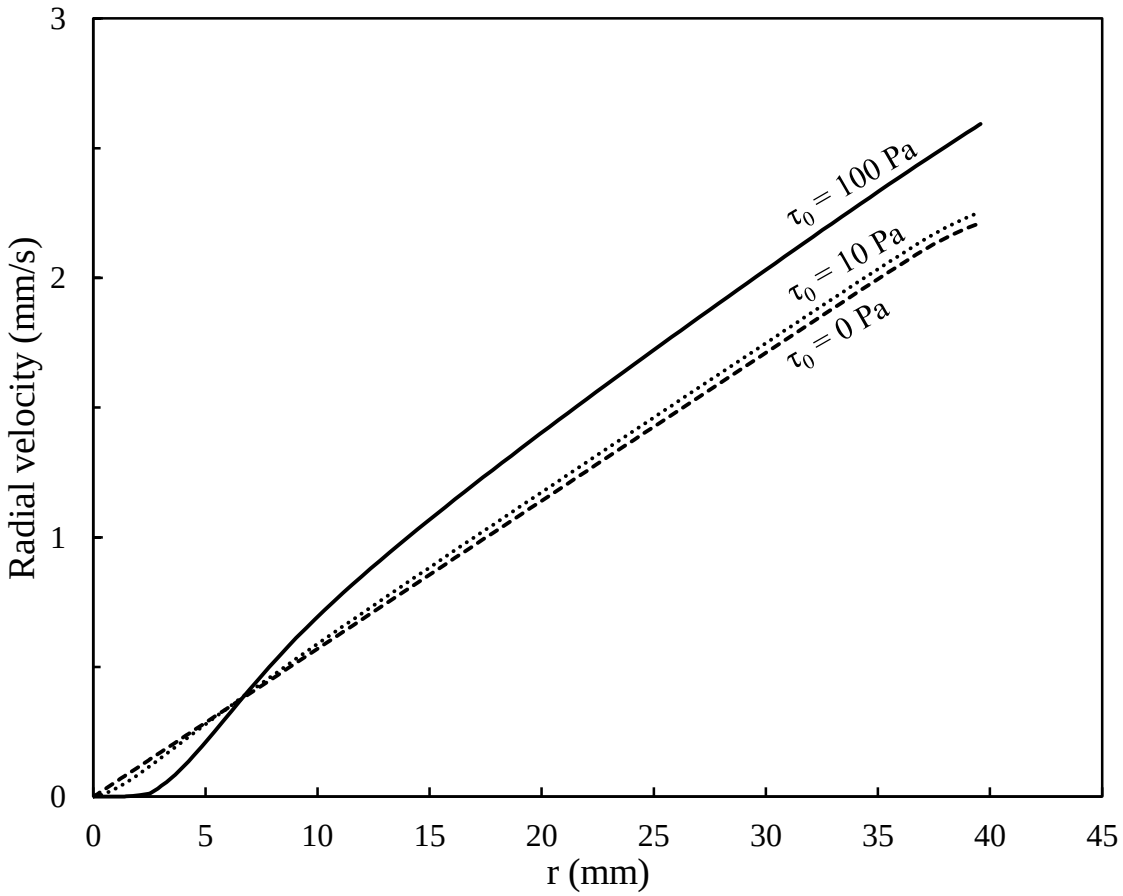

Figure 4.12 Model prediction of the radial velocity profile at h = 0.5 mm of suspensions used in Figure 4.7 after 5 s squeeze time

Figure 4.13 presents the boundary of the unyielded region around the center of lower plate for a suspension with φ = 0.560 and τ_0 = 100 Pa yield stress squeezed with constant velocity of 2 mm/s. The initial thickness of suspension is 20 mm and the boundary is defined were the radial velocity is 1×10^{-5} mm/s. At the constant velocity the unyielded region radius decreases with time.

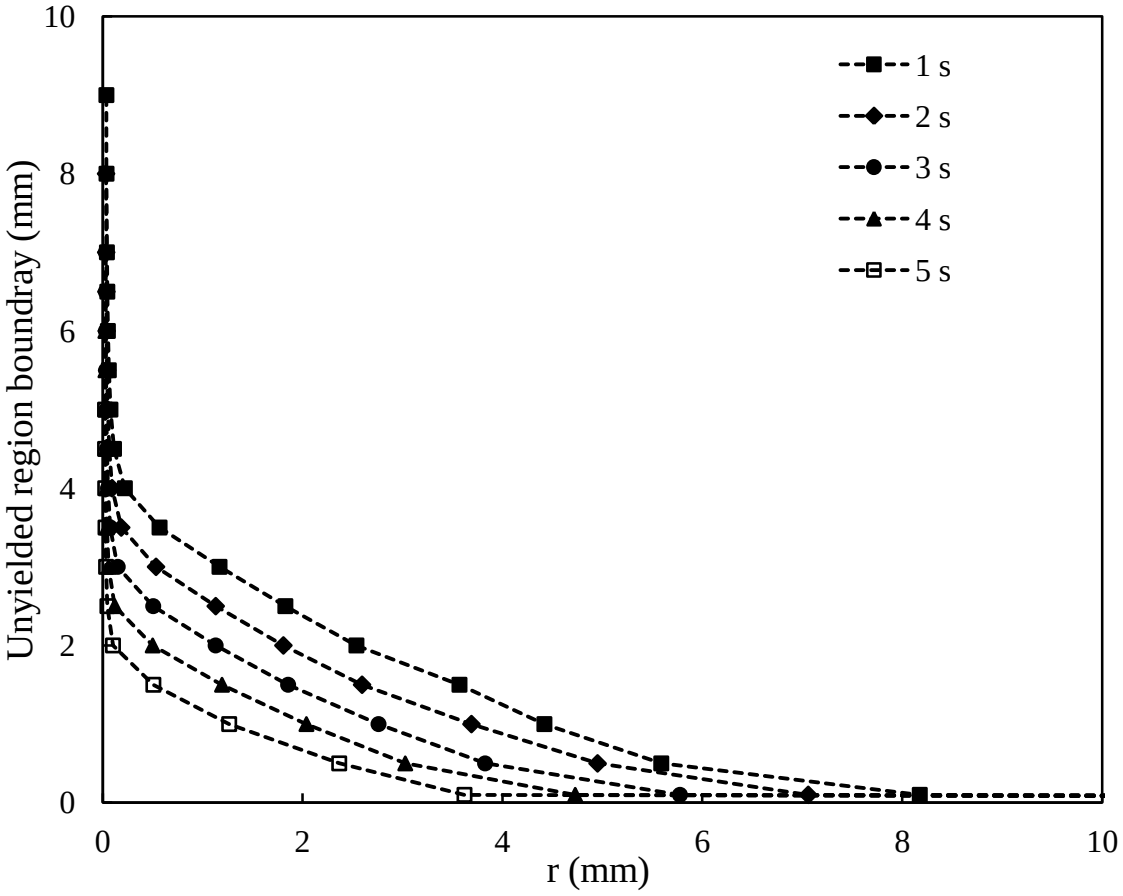

Figure 4.13 Model prediction of changing the boundary of the unyielded region around the center of the lower plate versus time for a suspension with φ = 0.560 and τ_0 = 100 Pa squeezed at constant velocity of 2 mm/s.

In order to investigate the effect of slip at surface on liquid phase migration, the constant-force squeeze flow of the suspension with φ = 0.560 and τ_0 = 100 Pa yield stress was modeled. Figure 4.14 shows the solid volume fraction profile for different value of slip parameter, δ. The solid volume fraction increases at the center when the amount of slip decreases. The reason is that the radial velocity of suspensions between the plates increases by decreasing the slip at surfaces. Also the time required to squeeze the suspension from 8 mm to 1 mm in thickness with constant force increases as slip at

the surface decreases. In our model the time to squeeze the suspension with no slip is 5.39 s and decreases to 2.29 s for perfect slip at surface.

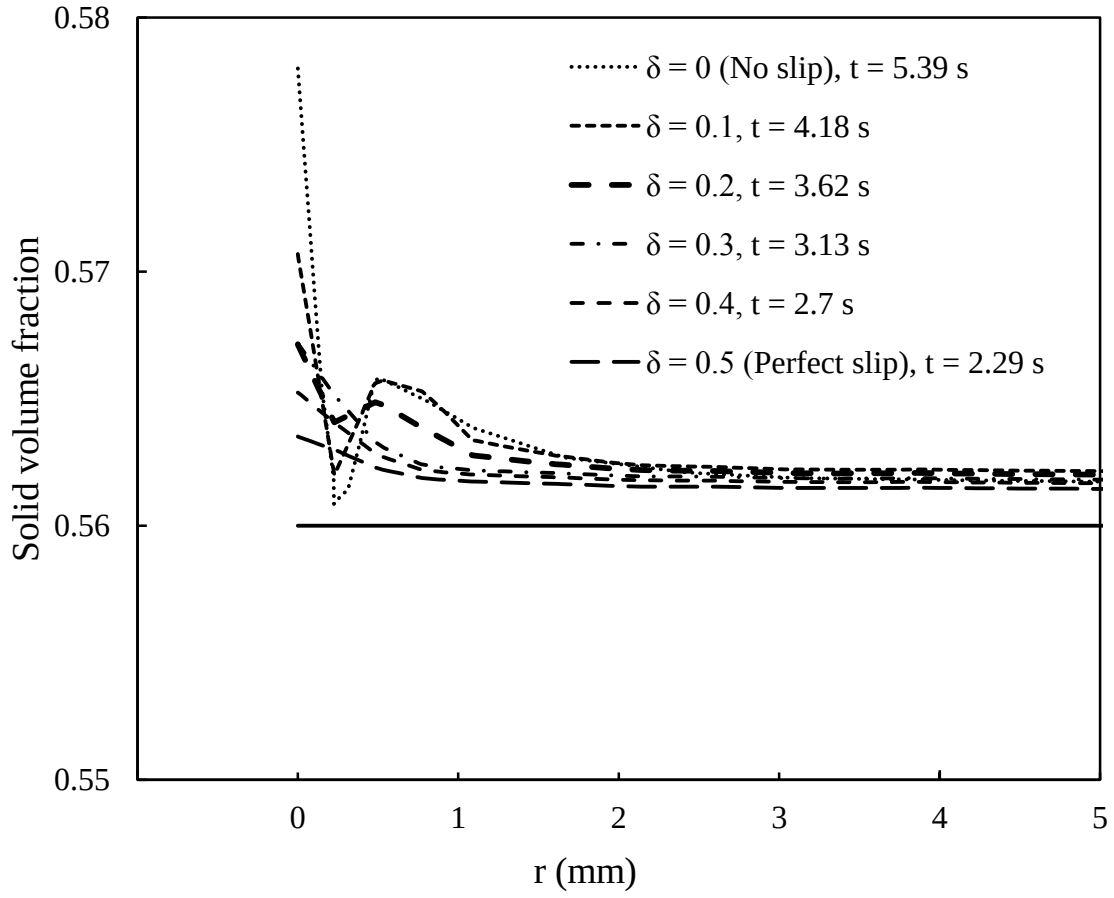

Figure 4.14 Model prediction of solid volume fraction profile for the suspension with φ = 0.560 and τ_0 = 50 Pa squeezed with a constant force of 4,000 N from thickness of 8 to 1 mm of 74-μm glass spheres in a Newtonian fluid with μ = 50 Pa·s

The effect of the magnitude of the applied force on the liquid-phase migration is complicated because increasing the force will increase the pressure gradient, thus increasing the migration rate, but on the other hand increasing the force shortens the squeezing time so the liquid has less time to migrate. Modeling results showed that the former in more important so generally increasing the force can decreases the liquid phase

migration. Figure 4.15 shows the solid volume fraction profile of a suspension with φ = 0.560 after squeeze flow with four different forces ranging from 500 N to 4,000 N. The thickness of sample was decreased from 15 mm to 1 mm. There is a larger increase in the solid volume fraction after the squeeze test for suspensions squeezed with smaller forces, the reason it that the time required for squeeze increases sharply for smaller forces. The squeeze time is 129.6 s for F = 500 N and is 10.6 s for F = 4,000 N.

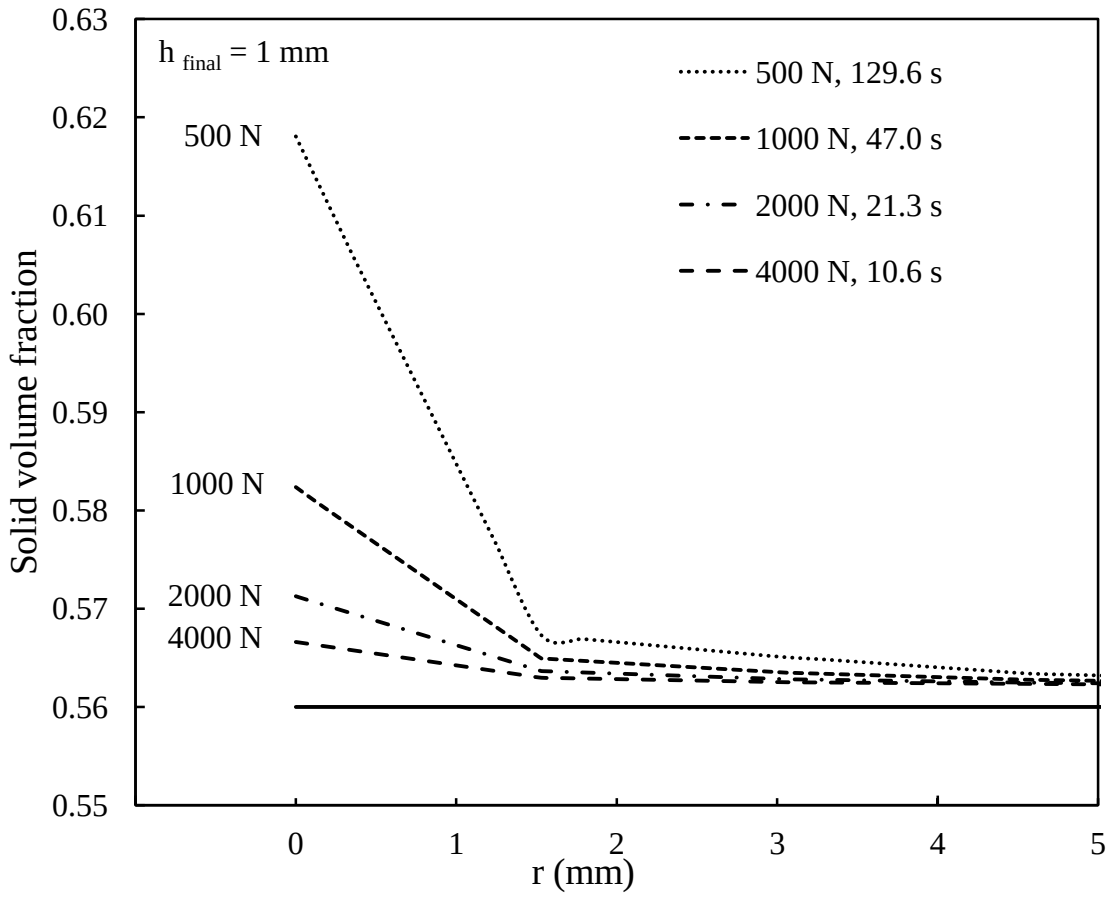

Figure 4.15 Model prediction of solid volume fraction profile for a suspension with φ = 0.560 and 50 Pa yield stress of 74-μm glass spheres in a Newtonian fluid with μ = 50 Pa·s squeezed with different constant force from thickness of 15 to 1 mm

Figure 4.16 represent the solid volume fraction profile of the same suspension in Figure 4.15 after squeeze to the final thickness of 2 mm. The difference between the solid volume fractions in Figure 4.16 is small for different forces.

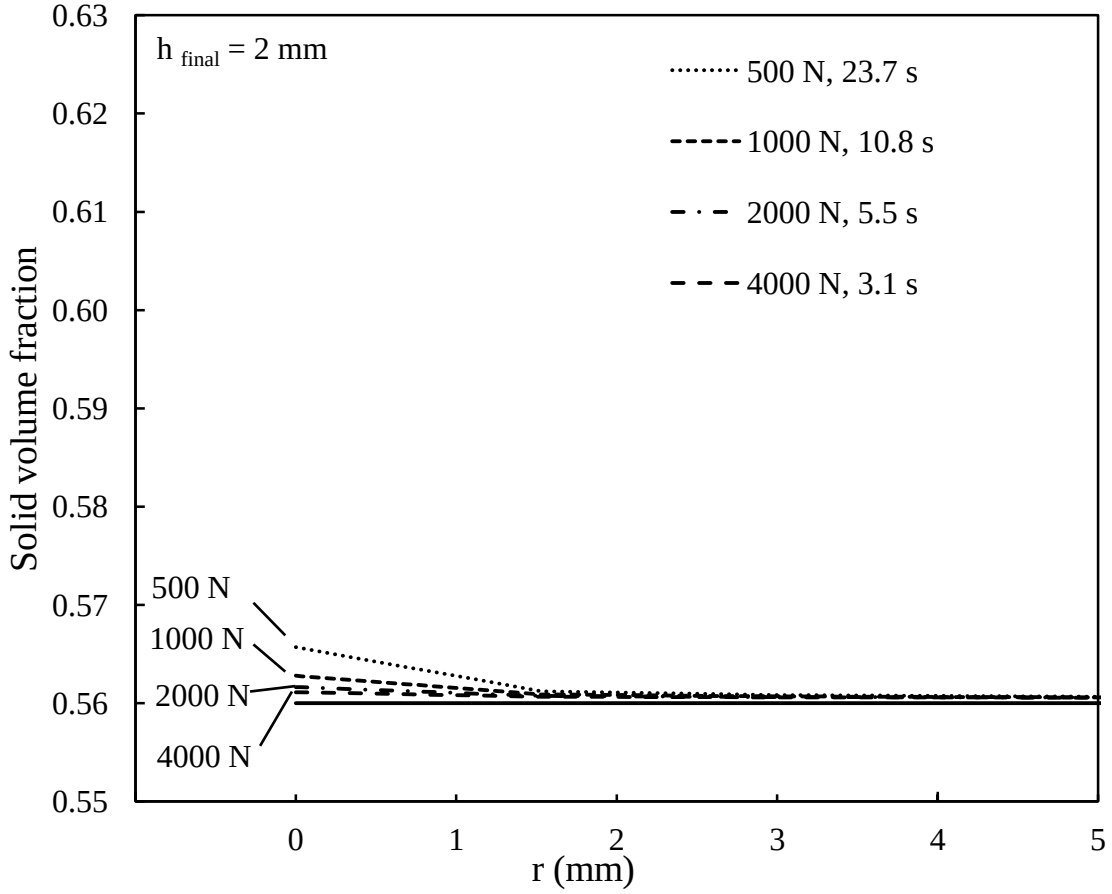

Figure 4.16 Model prediction of solid volume fraction profile for a suspension with φ = 0.560 and 50 Pa yield stress of 74-μm glass spheres in a Newtonian fluid with μ = 50 Pa·s squeezed with different constant force from thickness of 15 to 2 mm

In order to investigate the effect of different parameters on liquid phase migration a series of simulations were performed using the model we developed. The results are shown in Table 4.1. In this table, $\Delta\varphi/\varphi_{initial}$ is the fractional change in the volume fraction at the center (r < 2.5 mm) of the sample due to liquid-phase migration. Squeeze flow of suspensions with φ = 0.480, 0.520, 0.560, and 0.600 with constant forces, F, of 3.0 and

6.0 kN were modeled. Liquid viscosities, μ, of 10 and 50 Pa·s and particle diameters, D, of 50 and 150 μm were considered in this study. In this simulation, the initial thickness was 8 mm and the final thickness was 1 mm. The permeability, k, was calculated from φ and D using the Carman-Kozeny correlation (Eq. 4.3). The yield stress τ_0 was interpolated from the experimental measurements presented in Figure 3.5. The numerical model is used to calculate the squeeze time, t, and $\Delta\varphi/\varphi_{\text{initial}}$. Other factors being the same, the results were very similar for the two forces used. The results indicate, however, that liquid-phase migration increases with increasing initial solid volume fraction, increasing particle size, and decreasing liquid viscosity. These points are illustrated in Figures 17 to 19.

Table 4.1 Parameters and results of the simulations

φ	F (kN)	μ (Pa·s)	D (μm)	k (m^2)	τ_0 (Pa)	t (s)	$\Delta\varphi/\varphi_{initial}$
0.48	3.0	50	50	8.48×10^{-6}	36.5	3.37	0.0402
0.48	6.0	50	50	8.48×10^{-6}	36.5	2.20	0.0403
0.48	3.0	10	50	8.48×10^{-6}	36.5	1.60	0.0404
0.48	6.0	10	50	8.48×10^{-6}	36.5	1.45	0.0406
0.48	3.0	50	150	7.63×10^{-6}	36.5	3.42	0.0645
0.48	6.0	50	150	7.63×10^{-6}	36.5	2.20	0.0670
0.48	3.0	10	150	7.63×10^{-6}	36.5	1.63	0.0839
0.48	6.0	10	150	7.63×10^{-6}	36.5	1.45	0.0962
0.52	3.0	50	50	5.68×10^{-6}	59.5	4.55	0.0424
0.52	6.0	50	50	5.68×10^{-6}	59.5	2.75	0.0411
0.52	3.0	10	50	5.68×10^{-6}	59.5	1.79	0.0416
0.52	6.0	10	50	5.68×10^{-6}	59.5	1.52	0.0449
0.52	3.0	50	150	5.11×10^{-6}	59.5	4.60	0.0765
0.52	6.0	50	150	5.11×10^{-6}	59.5	2.75	0.1008
0.52	3.0	10	150	5.11×10^{-6}	59.5	1.80	0.1026
0.52	6.0	10	150	5.11×10^{-6}	59.5	1.53	0.1127
0.56	3.0	50	50	3.77×10^{-6}	82.5	7.55	0.0536
0.56	6.0	50	50	3.77×10^{-6}	82.5	3.94	0.0540
0.56	3.0	10	50	3.77×10^{-6}	82.5	2.16	0.0561
0.56	6.0	10	50	3.77×10^{-6}	82.5	1.69	0.0561
0.56	3.0	50	150	3.40×10^{-5}	82.5	7.50	0.0762
0.56	6.0	50	150	3.40×10^{-5}	82.5	3.94	0.1129
0.56	3.0	10	150	3.40×10^{-5}	82.5	2.28	0.1204
0.56	6.0	10	150	3.40×10^{-5}	82.5	1.70	0.1328
0.60	3.0	50	50	2.47×10^{-6}	105.4	17.26	0.0630
0.60	6.0	50	50	2.47×10^{-6}	105.4	7.57	0.0570
0.60	3.0	10	50	2.47×10^{-6}	105.4	4.50	0.0847
0.60	6.0	10	50	2.47×10^{-6}	105.4	2.31	0.1019
0.60	3.0	50	150	2.22×10^{-5}	105.4	17.35	0.1520
0.60	6.0	50	150	2.22×10^{-5}	105.4	7.77	0.1471
0.60	3.0	10	150	2.22×10^{-5}	105.4	4.20	0.1650
0.60	6.0	10	150	2.22×10^{-5}	105.4	2.33	0.1678

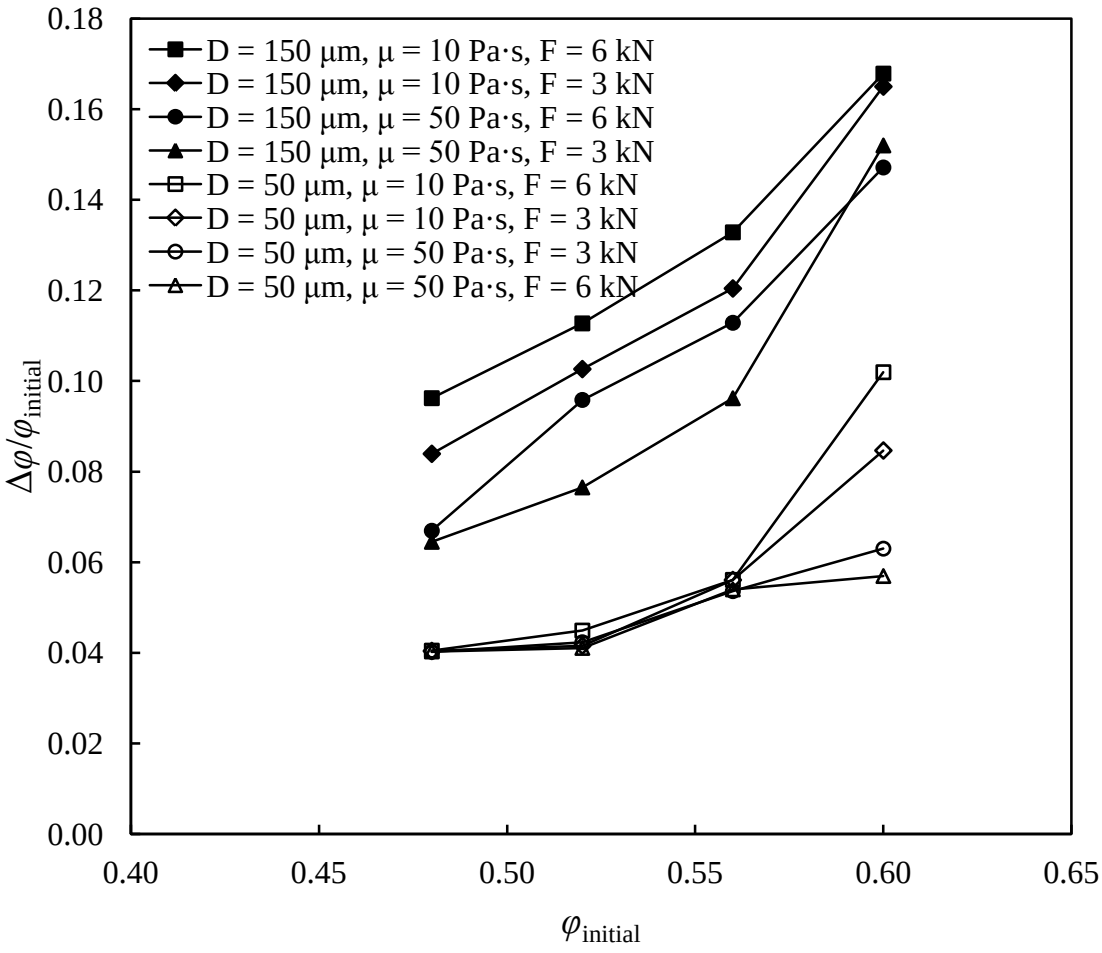

Figure 4.17 Model predictions of the effect of initial solid volume fraction on fractional changes in solid volume fraction

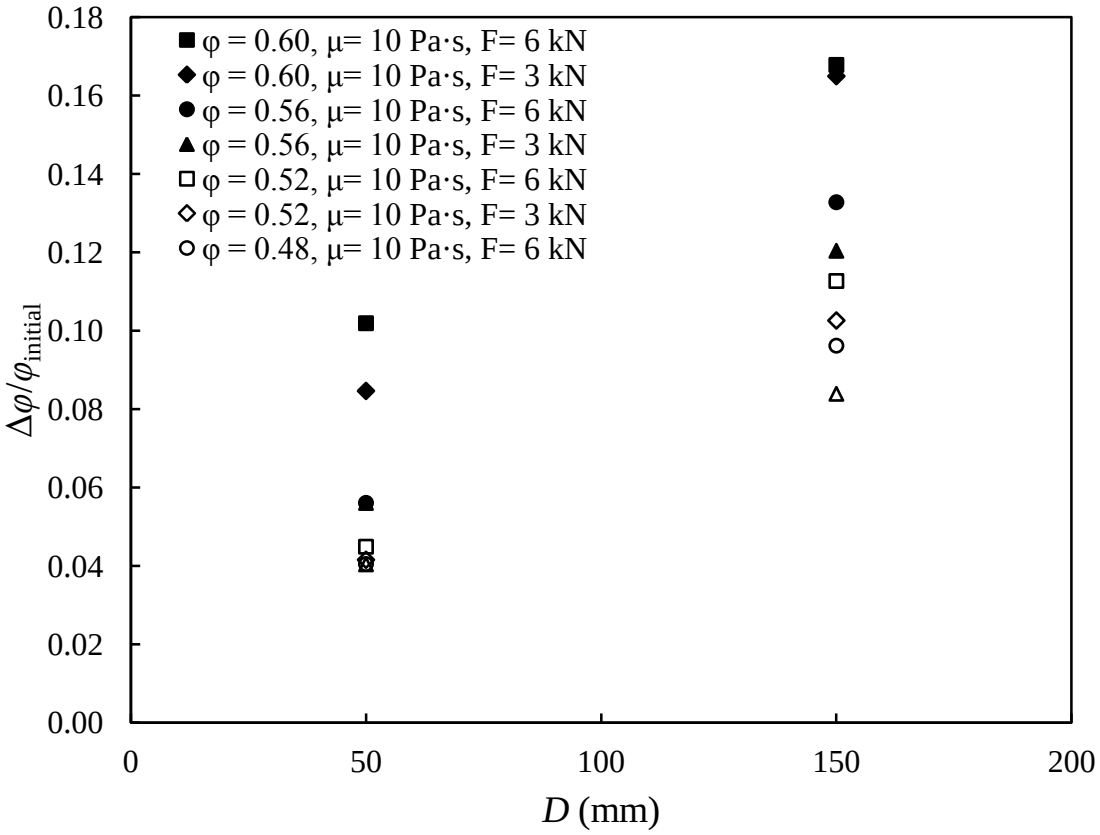

Figure 4.18 Model predictions of the effect of particles diameter on fractional changes in solid volume fraction

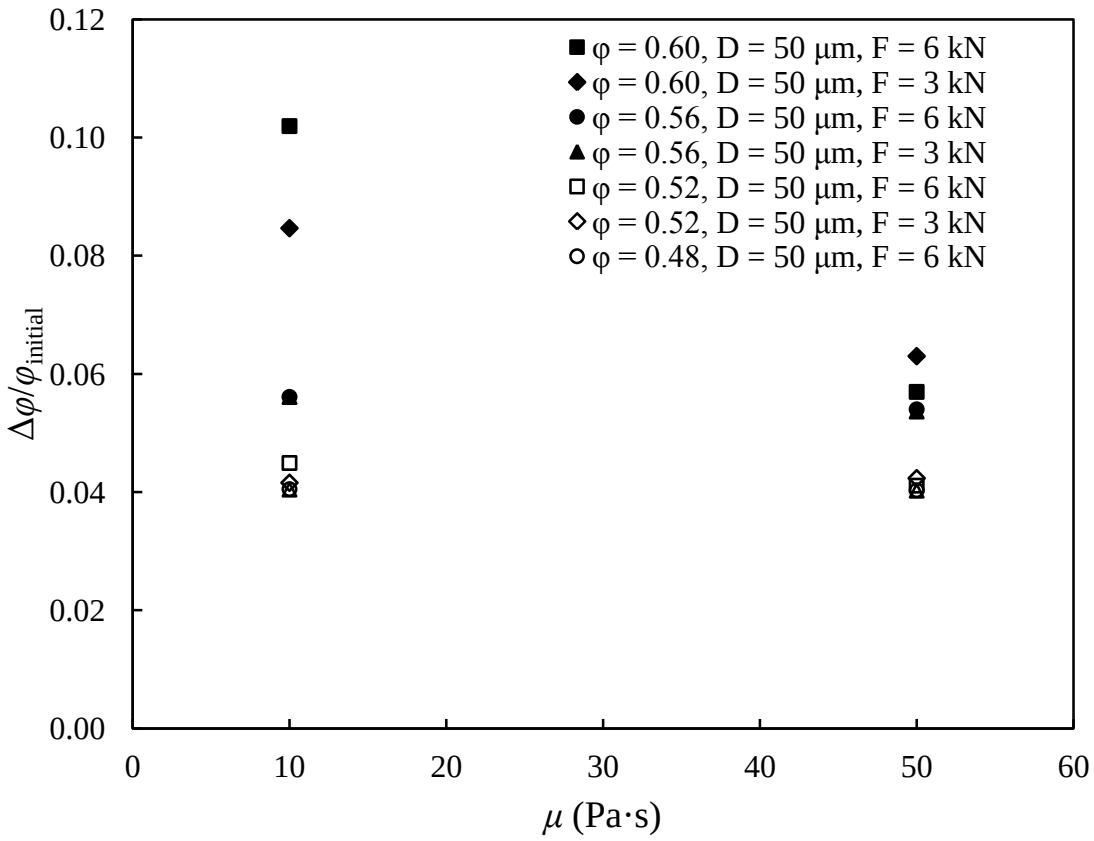

Figure 4.19 Model predictions of the effect of suspending fluid viscosity on fractional changes in solid volume fraction

Figure 4.20 and Table 4.2 compare the model predictions with the measured fractional changes in solid volume fraction for a suspension with φ = 0.586 at different squeeze times. The experimental data are for squeeze times of 5, 25, and 40 s with a squeeze force of 13.3 kN, and for squeeze times of 15, 25, and 35 s with a squeeze force of 4.45 kN. The model predictions are in good agreement with the experimental results.

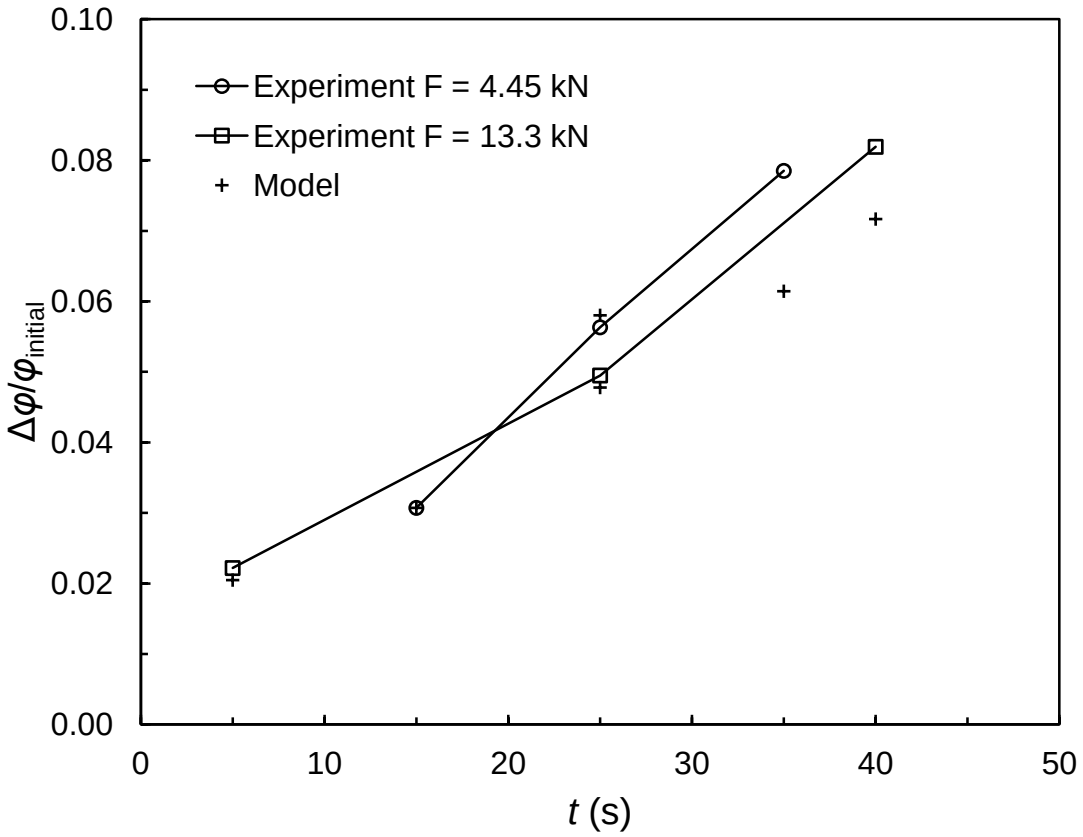

Figure 4.20 Comparison of model predictions to measured fractional changes in solid volume fraction for a suspension with φ = 0.586 for squeeze times of 5, 25, and 40 s with a squeeze force of 13.3 kN, and for squeeze times of 15, 25, and 35 s with a squeeze force of 4.45 kN.

Table 4.2 Parameters and results for data points in Figure 4.20

φ	F (kN)	μ (Pa·s)	D (μm)	t (s)	τ_0 (Pa)	$\Delta\varphi/\varphi_{initial}$ simulation	$\Delta\varphi/\varphi_{initial}$ experiment
0.586	4.45	327.5	74	15	92.2	0.031	0.031
0.586	4.45	327.5	74	25	92.2	0.048	0.056
0.586	4.45	327.5	74	35	92.2	0.061	0.078
0.586	13.3	327.5	74	5	92.2	0.020	0.022
0.586	13.3	327.5	74	25	92.2	0.058	0.050
0.586	13.3	327.5	74	40	92.2	0.072	0.082

CHAPTER 5

CONCLUSION

Properly calibrated pressure-sensitive films were used to measure the normal stress distribution in materials undergoing squeeze flow. The technique was validated by squeezing a highly viscous Newtonian fluid with a constant force between a circular disk and a large parallel flat surface. As predicted, the normal stress distribution was found to be parabolic with a maximum at the center and atmospheric pressure at the edge. The technique was then used for measurements on suspensions of glass spheres in that fluid.

Although suspensions are expected to deviate from Newtonian behavior as their volume fraction of solids increases, the normal stress distribution in our suspensions with volume fractions of solids up to 0.55 was found to be, within experimental error, very similar to that for Newtonian fluids. Thus, up to these volume fractions, the normal stress distribution in squeeze flow seems to provide very little information on the rheological character of these suspensions.

At higher volume fractions, the normal stress distribution was qualitatively different, exhibiting very high normal stresses in the central region and low normal stresses beyond that. Slip tests showed that the boundary condition on the surface of the plates was intermediate between perfect slip and no slip. Since this normal stress distribution was very similar to that obtained when particles without fluid were subjected to squeeze flow, it is apparent that the normal stress distribution at volume fractions above 0.55 reflects

jamming of the solid particles. The normal stress distribution can thus be used as an indicator of the occurrence of jamming in suspensions subjected to squeeze flow, and may serve as a guide to the improvement of compression molded parts.

Replacing, at intervals during the squeeze test, the pressure-sensitive films used to measure the normal stress distribution, showed that the normal stress distribution changes for highly concentrated suspensions as the test proceeds: the normal stress in the central region increases dramatically while the normal stress in the outer regions decreases. Examination of these suspensions after they had been subjected to squeeze flow revealed that fluid had migrated away from the central region, thus contributing to jamming. The concentration gradient that results from this liquid phase migration requires that the analysis of squeeze flow for highly concentrated suspensions take into account the time and position dependence of the rheological properties of the material.

The solid volume fraction profile in highly concentrated suspensions after constant-force squeeze flow clearly demonstrates that the liquid phase filtrates through the solid matrix. This liquid-phase migration can be attributed to the pressure gradient that develops between the center and the edges of the disks during squeeze flow. Considering the normal stress distribution and solid volume fraction profile simultaneously showed that the phase separation and increasing the solid volume content at the center of the disks led to the jamming of the particles at the center region and increasing the normal stress at this region. The jamming of the particles in the central region hinders the squeezing of the suspensions causing the squeeze time required to reach a desired thickness to increase or and even making it impossible to reach the desired thickness.

These experiments suggest that liquid-phase migration can be avoided in principle by increasing the squeeze velocity, increasing the liquid viscosity, or using smaller particles. The effect of these parameters can be seen in the filterability number. Results indicated that in order to limit the percent change in volume fraction at the center, the filterability number has to be small. Suspensions with same initial solid volume fraction exhibited phase separation at larger filterability numbers which may lead to jamming and drastic changes in the normal stress distribution. In these cases, assuming that the material is characterized by a rheological model with constant parameters is not sufficient. A more complete analysis would need by taking into account the time and position dependence of the rheological properties of the material due to the change in the volume fraction of solids. This can be done by pairing the equation of motion with a continuity equation that includes diffusive flux such as Darcy's law for motion of liquid relative to solids.

Coupling the equation of motion for a non-Newtonian material that approximates a Bingham plastic with a continuity equation that includes a diffusive flux based on Darcy's law resulted in a numerical model that accounts well for the pressure-induced liquid-phase migration during squeeze flow of highly concentrated suspensions. The constitutive equation includes a yield stress and a viscosity at high shear rates, both of which were obtained experimentally. The permeability was estimated from the particle diameter and the volume fraction using the Carman-Kozeny correlation. A slip parameter, δ, was introduced in order to account for the degree of slip at the surfaces, and it was assumed to be the same throughout the surface. The slip parameter was determined by fitting the experimentally-measured force as a function of time in the first stage (the constant-velocity stage) of the squeeze flow experiments; it was zero (no slip) for all but

the suspensions with the highest volume fractions. The predictions of the model required no other adjustable parameters.

The volume fraction distributions predicted by the numerical model for suspensions of various volume fractions subjected to squeeze flow agreed well with the experimental measurements. For suspensions with $\varphi < 0.5$ the solid volume fraction remains constant during the squeeze test. At higher volume fractions, the volume fraction everywhere in the squeezed suspension, but more markedly near the center, is higher than the initial volume fraction. The numerical model also predicted fairly well the effect of the squeeze time and the viscosity of the suspending liquid on the volume fraction distribution of suspensions subjected to squeeze flow.

The numerical model was also used to predict the effect of various parameters on the volume fraction distribution of the squeezed suspensions. The yield stress, which causes the formation of an unyielded region close to the central region of the suspension (near $r = 0$), was the key parameter controlling liquid-phase migration. In the central region, when the yield stress increased, the radial velocity of the suspension as a whole decreased sharply, while the fluid velocity, which depends mostly on the pressure gradient remained high. Therefore, the velocity of the liquid relative to that of the suspension increased with yield stress, leading to enhanced liquid-phase migration. The magnitude of the applied force was found critical on boosting the liquid phase migration only when the final thickness was very thin. The model predicted that increasing the slip velocity at the surface reduces the liquid-phase migration and also shortens the squeeze time.

REFERENCES

Ayadi A (2011) Exact analytic solutions of the lubrication equations for squeeze-flow of a biviscous fluid between two parallel disks. J Non-Newtonian Fluid Mech 166:1253-1261

Barnes HA (1995) A review of the slip (wall depletion) of polymer solutions, emulsions and particle suspensions in viscometers: its cause, character, and cure. J Non-Newtonian Fluid Mech 56:221-251

Barnes HA (1999) The yield stress-a review or 'παυτα ρει'-everything flows? J Non-Newtonian Fluid Mech 81:133-178

Bird RB, Stewart WE, Lightfoot EN (2002) Transport Phenomena, 2nd Edition. Wiley, p. 110

Chaari F, Racineux G, Poitou A, Chaouche M (2003) Rheological behavior of sewage sludge and strain-induced dewatering. Rheol Acta 42:273-279

Chan TW, Baird DG (2002) An evaluation of a squeeze flow rheometer for the rheological characterization of a filled polymer with a yield stress. Rheol Acta 41:245-256

Collomb J, Chaari F, Chaouche M (2004) Squeeze flow of concentrated suspensions of spheres in Newtonian and shear-thinning fluids. J Rheol 48:405-416

Covey GH, Stanmore BR (1981) Use of the parallel-plate plastometer for the characterization of viscous fluids with a yield stress. J Non-Newtonian Fluid Mech 8:249-260

Delhaye N, Poitou A, Chaouche M (2000) Squeeze flow of highly concentrated suspensions of spheres. J Non-Newtonian Fluid Mech 94:67-74

Ellwood KRJ, Georgiou GC, Papanastasiou TC, Wilkes JO (1990) Laminar jets of Bingham-plastic liquids. J Rheol 34:787-812

Engmann J, Servais C, Burbidge AS (2005) Squeeze flow theory and applications to rheometry: A review. J Non-Newtonian Fluid Mech 132:1-27

Estellé P, Lanos C, Perrot A, Servais C (2006) Slipping zone location in squeeze flow. Rheol Acta 45:444-448

Gulmus SA, Yilmazar U (2005) effect of volume fraction and particle size on wall slip in flow of polymeric suspensions. Journal of Applied Polymer Science 98:439-448

Happel J, Brenner H (1986) Low Reynolds Number Hydrodynamics, 2nd ed. Martinius Nijhoff Publ, Dordrecht.

Heymann L, Peukert S, Aksel N (2002) On the solid-liquid transition of concentrated suspensions in transient shear flow. Rheol Acta 41:307-315

Kaci A, Ouari N, Racineux G, Chaouche M (2011) Flow and blockage of highly concentrated granular suspensions in non-Newtonian fluid. European Journal of Mechanics B/Fluids 30:129-134

Kolenda F, Retana P, Racineux G, Poitou A (2003) Identification of rheological parameters by the squeezing test. Powder Technology 130:56-62

Krieger IM (1972) Rheology of monodisperse lattices. Adv Colloid Interface Sci 3:111–136

Laun HM, Rady M, Hassager O (1999) Analytical solution for squeeze flow with partial wall slip. J Non-Newtonian Fluid Mech 81:1-15

Leighton D, Acrivos A (1987) The shear-induced migration of particles in concentrated suspensions. J Fluid Mech 181:415-439

Li XY, Logan BE (2001) Permeability of fractal aggregates. Wat Res 35:3373-3380

Lipscomb GG, Denn MM (1984) Flow of Bingham fluids in complex geometries. J Non-Newtonian Fluid Mech 14:337-346

Mascia S, Seiler C, Fitzpatrick S, Wilson DI (2006) Extrusion-spheronisation of microcrystalline cellulose pastes using a non-aqueous liquid binder. International Journal of Pharmaceutics 389:1-9

Mascia S, Wilson DI (2007) Rheology of concentrated granular suspensions undergoing squeeze flow. J Rheol 51:493-515

Mascia S, Wilson DI (2008) Biaxial extensional rheology of granular suspensions: The HBP (Herschel-Bulkley for pastes) model. J Rheol 52:981-998

Meeten GH (2004) Effects of plate roughness in squeeze-flow rheometry. J Non-Newtonian Fluid Mech 124:51-60

Meeten GH (2007) Radial filtration during constant-force squeeze flow of soft solids. Rheol Acta 46:803-813

Meeten (2010) Comparison of squeeze flow and vane rheometry for yield stress and viscous fluids. Rheol Acta 49:45-52

Mueller S, Liewellin EW, Mader HM (2010) The rheology of suspensions of solid particles. Proc. Soc. A 466:1201-1228

Navier CL, Sur MH (1827) Les lois du mouvement des fluides. Mem Acad R Sci Inst Fr 6:389–440

O'Donovan EJ, Tanner RI (1984) Numerical study of the Bingham squeeze film problem. J Non-Newtonian Fluid Mech 15:75-83

Patel MJ, Blackburn S, Wilson DI (2007) Modeling of paste flow subject to liquid phase migration. Int J Numer Meth Engng 72:1157-1180

Papanastasiou TC (1987) Flows of materials with yield. J Rheol 31:385-404

Phillips RJ, Armstrong RC, Brown RA (1992) A constitutive equation for concentrated suspensions that accounts for shear-induced particle migration. Phys. Fluids A 4:30-40

Poitou A, Racineux G (2001) A squeezing experiment showing binder migration in concentrated suspensions. J Rheol 45:609-625

Ramachandran A, Leighton DT (2010) Particle migration in concentrated suspensions undergoing squeeze flow. J Rheol 54:563-589

Rabideau BD, Lanos C, Coussot P (2009) An investigation of squeeze flow as a viable technique for determining the yield stress. Rheol Acta 48:517-526

Ritz JB, Bertrand F, Thibault F, Tanguy PA (2000) Shear-induced particle migration in a short-dwell coater. Chemical Engineering Science 55:4857-4867

Roussel N, Lanos C (2004) Particle fluid separation in shear flow of dense suspensions: experimental measurement on squeezed clay paste. J Rheol 51:493-515

Sherwood JD, Durban D (1996) Squeeze flow of a power-law viscoplastic solid. J Non-Newtonian Fluid Mech 62:35-54

Sherwood JD, Durban D (1998) Squeeze flow of a Herschel-Bulkley fluid. J Non-Newtonian Fluid Mech 77:115-121

Sherwood JD (2002) Liquid-solid relative motion during squeeze flow of pastes. J Non-Newtonian Fluid Mech 104:1-32

Smyrnaios DN, Tsamopoulos JA (2001) Squeeze flow of Bingham plastics. J Non-Newtonian Fluid Mech 100:165-190

Toutou Z, Roussel N, Lanos C (2005) The squeezing test: a tool to identify firm cement-based material's rheological behavior and evaluate their extrusion ability. Cement and Concrete Research 35:1891-1899

Whitaker S (1986) Flow in porous media I: A theoretical derivation of Darcy's law. Transport in porous media 1:3-35

Yang SP, Zhu KQ (2006) Analytical solutions for squeeze flow of Bingham fluid with Navier slip condition. J Non-Newtonian Fluid Mech 138:173-180

Yates NM, Barigou M, Fryer PJ, Moore SR (2001) Squeeze flow of food pastes. 6th World Congress of Chemical Engineering Melbourne, Australia

APPENDIX A: PRESSURE SENSITIVE FILMS CALIBRATION

Pressure-x pressure-sensitive films are used as to measure pressure in a variety of applications including the aerospace, electronics, automotive, and medical industries. A film can be placed between two surfaces that exert a pressure and will turn red according to the amount of the applied pressure. A darker red film indicates a higher applied pressure. The films come in 7 sensitivities to accommodate a wide range of pressures but we used 3 varieties, Super Low 70-350 psi (480-2,400 kPa), Low 350-1,400 psi (2,400-9,700 kPa), and Medium 1,400-7,100 psi (9,700-49,000 kPa).

Though pressure-x films are a good indication of pressure distribution over an area, they are not, as sold, meant to accurately measure pressure. Pressure-x Inc. includes in their manual some curves to measure pressure by comparing the intensity of the pressed film visually. These curves provide an insufficient amount of information to effectively be used as pressure readings, and the act of comparing the used film to a scale is far too subjective. To effectively use pressure-x films to quantitatively measure pressure distribution, an independent calibration of these films is necessary. According to Pressure-x, the darkening of the film is a function of pressure, humidity, temperature, and time. Pressure of course, plays the largest role, but the latter three conditions significantly affect the reddening of the film. Theoretically, the film becomes darker with time until it reaches a limit for that pressure for which it will not become darker no matter how long it is subjected to that pressure. At a higher temperature or humidity, the film will become

darker under the same pressure than at a lower temperature or humidity. Because of these variations, it is necessary to generate a large number of calibration curves for the pressure film.

In order to effectively measure pressure distribution, a calibration must be performed on the pressure-x pressure film. Calibrations were to be carried out for the Super Low, Low, Medium, and High pressure films. A number of pressures ranging from the lower to the upper limit of pressure for each film are to be used. One range of pressures constitutes a run, and can be used to make a calibration curve. Each of these runs was to be done for a time of 5, 15, and 35, seconds and at temperatures of 20ºC, 35ºC, and 45ºC. Humidity was to be measured for each run but not manipulated. Calibration curves had developed using a known area of post-it sticky notes to cover a known area of pressure film. The sticky portions left on and used to keep the film aligned with the paper for the pressing. Approximately ten sheets of sticky notes placed on top of the film which was placed on top of a circular metal disk. The disk, film, and paper were pressed for a known amount of time and at varying pressures. The films then scanned and the image saved as a bitmap file. Matlab Image toolbox was used to convert the image into a matrix of grayscale intensity values which were averaged in Microsoft Excel to obtain an average intensity value for a film. A series of films could be analyzed in this way and plotted to yield a calibration curve.

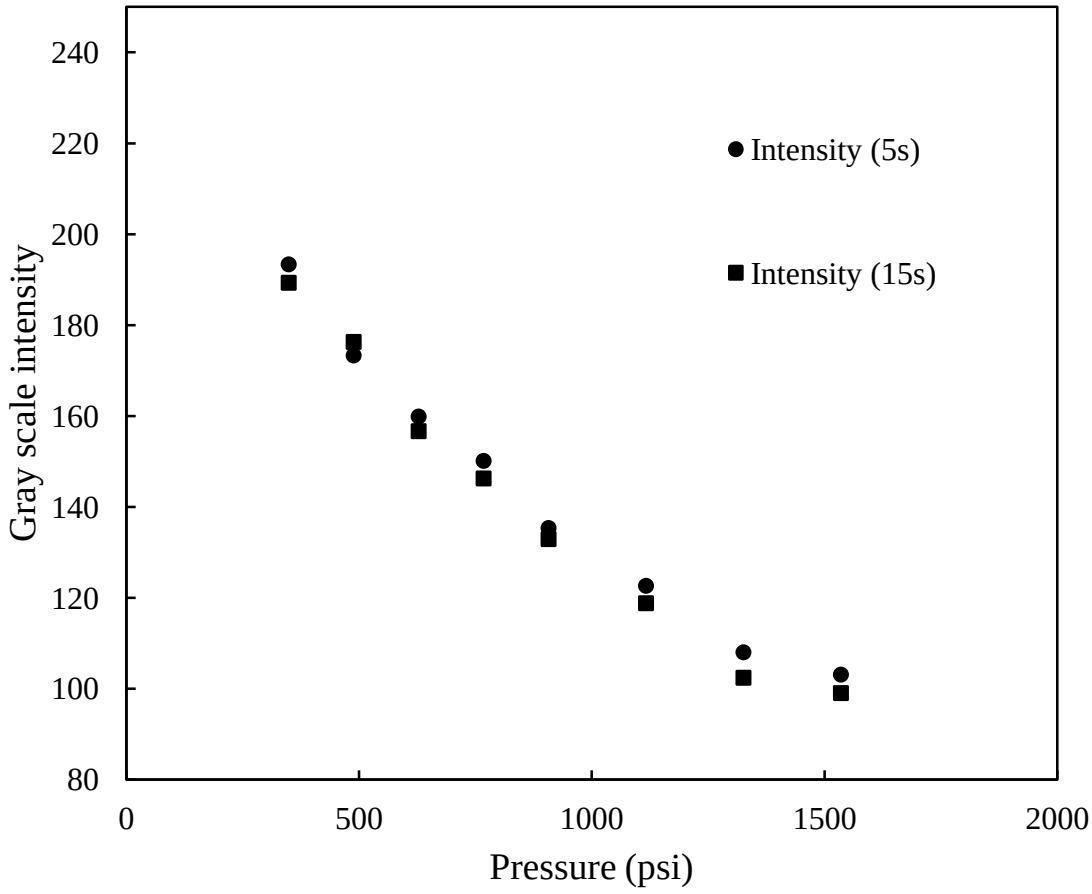

Figure A.1 Calibration Curve for RH=34.8% at 15s and 5s Press Time

To show procedure of calibration the result for calibration of low pressure-sensitive films is presented. Figure A.1 is a plot of gray scale intensity versus applied pressure for a relative humidity of 34.8% for low pressure-sensitive film. The 15s curve is consistently below the 5s curve. This means that it is a darker shade of red. The color scale ranges from 255 (pure white) to 0 (pure black).However, it should be noted that time press time makes little difference in the intensity of the film at a given pressure. For pressure higher than 1200 psi, the two curves flatten out, and there is a much larger difference in measured pressure at a given intensity. That the slope of the curve flattens out and appears to approach zero as the pressure increases. This means that the there is an

ultimate intensity at which the pressure film no longer changes in color no matter how much pressure is applied. The data for three films showed that for the majority of pressures, the press time makes little difference in the measured gray scale intensity and thus little difference in the corresponding pressure at a measured intensity on the other hand humidity was found to have a significant effect on the measured intensity.

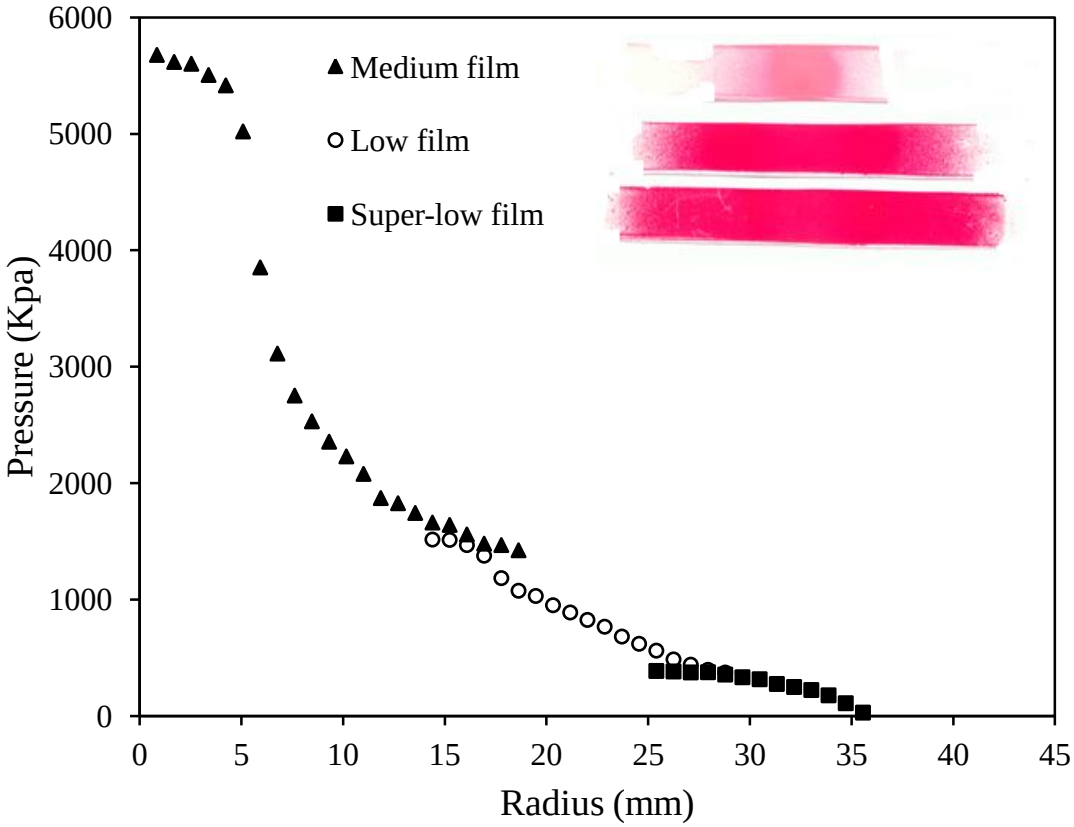

Figure A.2 Measured normal stress distribution of suspensions with volume fraction of 0.586 squeezed for 35 s with constant force of 13.3 kN using three different pressure sensitive films

For each squeeze test of suspensions, the calibration with the same temperature and time and the closest humidity used to convert the gray scale to pressure values. Figure A.2 shows the result of measuring the normal stress distribution of suspension with volume fraction of 0.586 squeezed for 35 s using three calibrated pressure sensitive films.